

Combining Observational and Randomized Data for Estimating Heterogeneous Treatment Effects

Tobias Hatt

ETH Zurich

THATT@ETHZ.CH

Jeroen Berrevoets

Alicia Curth

University of Cambridge

JEROEN.BERREVOETS@DAMTP.CAM.AC.UK

AMC253@DAMTP.CAM.AC.UK

Stefan Feuerriegel

ETH Zurich & LMU Munich

FEUERRIEGEL@LMU.DE

Mihaela van der Schaar

University of Cambridge & The Alan Turing Institute & UCLA

MV472@DAMTP.CAM.AC.UK

Abstract

Estimating heterogeneous treatment effects is an important problem across many domains. In order to accurately estimate such treatment effects, one typically relies on data from observational studies *or* randomized experiments. Currently, most existing works rely *exclusively* on observational data, which is often confounded and, hence, yields biased estimates. While observational data is confounded, randomized data is unconfounded, but its sample size is usually too small to learn heterogeneous treatment effects. In this paper, we propose to estimate heterogeneous treatment effects by combining large amounts of observational data *and* small amounts of randomized data via representation learning. In particular, we introduce a two-step framework: first, we use observational data to learn a shared structure (in form of a representation); and then, we use randomized data to learn the data-specific structures. We analyze the finite sample properties of our framework and compare them to several natural baselines. As such, we derive conditions for when combining observational and randomized data is beneficial, and for when it is not. Based on this, we introduce a sample-efficient algorithm, called CorNet. We use extensive simulation studies to verify the theoretical properties of CorNet and multiple real-world datasets to demonstrate our method’s superiority compared to existing methods.

Keywords: Heterogeneous treatment effects, randomized controlled trial, observational data, representation learning, neural networks

1. Introduction

Estimating heterogeneous treatment effects is of great importance in many domains such as marketing (Brodersen et al., 2015), economics (Heckman et al., 1997), and epidemiology (Robins et al., 2000). For instance, in the medical domain, clinicians must know the effect a drug (treatment) has on an individual patient in order to personalize treatment decisions.

When estimating heterogeneous treatment effects, most works rely on data from observational studies (OSs), since it is available in large quantities. This allows to estimate individual-level heterogeneity of treatment effects (e.g., Johansson et al., 2016; Shalit et al., 2017; Wager and Athey, 2018). However, data from OSs is often subject to unobserved confounding. That is, some confounders (i.e., variables that affect both treatment assignment

and outcome) are not measured and, hence, not available in the data. Therefore, we are unable to control for these unobserved confounders, which results in biased estimates of the treatment effect.

In order to circumvent the problem of unobserved confounding, existing methods assume that data from OSs is unconfounded, i. e., all confounders are observed (e. g., [Johansson et al., 2016](#); [Shalit et al., 2017](#)), or rely on other assumptions (e. g., [Wang and Blei, 2019](#); [Hatt and Feuerriegel, 2021b](#)). However, these assumptions are strong, since they are not testable and often do not hold true in practice (e. g., [Rosenbaum, 2010](#); [Kallus et al., 2018](#); [Kallus and Zhou, 2018](#); [Kallus et al., 2019](#); [Wang and Blei, 2019](#); [Zhao et al., 2019](#); [Rosenman et al., 2020](#); [Hatt and Feuerriegel, 2021b](#)). As a consequence, without making strong assumptions, the use of observational data for estimating heterogeneous treatment effect is prohibited in practice.

An alternative data source stems from randomized experiments. For instance, randomized controlled trials (RCTs) are widely recognized as the gold standard for estimating treatment effects ([Robins et al., 2000](#)). The reason for this is that, in RCTs, the treatment assignment is controlled by an investigator, and, hence, all variables that affect the treatment assignment are known (i. e., observed). As a result, data from RCTs is *unconfounded*, and, therefore, using such data for estimating treatment effects yields unbiased estimates. However, randomized data has been predominantly used to estimate average treatment effects rather than heterogeneous treatment effects. There are two major reasons for this: (i) The size of randomized data is often too small to estimate treatment effect heterogeneity across patients. This is due to the large cost of RCTs as well as the difficulties of recruiting enough eligible subjects. (ii) Subjects in RCTs are, by design, highly selected and, therefore, regularly not representative of the population of interest ([Downs and Black, 1998](#); [Norris et al., 2001](#); [Willan et al., 2004](#); [Rothwell, 2005](#); [Cole and Stuart, 2010](#); [Stuart et al., 2011](#); [Buchanan et al., 2018](#); [Hatt et al., 2021](#); [Flores et al., 2021](#)). For instance, a review of HIV/AIDS clinical trials found that women are largely underrepresented in these trials ([Gandhi et al., 2005](#); [Greenblatt, 2011](#)). Hence, findings from such trials can often not be generalized to the population of interest (i. e., the population of HIV-positive patients). In sum, relying *exclusively* on either observational *or* randomized data may not yield reliable estimates of heterogeneous treatment effects.

In this paper, we investigate how to combine: (i) large but possibly confounded observational data; *and* (ii) unconfounded but small randomized data, to estimate heterogeneous treatment effects. This is in contrast to most previous works, which rely on one data type exclusively. Combining *both* data types allows us to leverage randomized data to overcome the untestable unconfoundedness assumption *and* observational data to discover effect heterogeneity. This is particularly relevant for medical and pharmaceutical sciences, where both types of data coexist. That is, RCTs are required for a drug’s approval and, once approved and used in practice, observational data is routinely collected during post-drug monitoring. Furthermore, the 21st Century Cures Act ([21c, 2015](#)) places additional focus on the use of observational and randomized data to support healthcare decision-making. Most importantly, it enhances the U.S. Food and Drug Administration’s ability to modernize RCTs by authorizing the use of OSs.

We propose a two-step framework for combining observational and randomized data which relies on a shared structure between both data types. In the first step, observational

data is used to learn a shared structure (in the form of a representation). In the second step, randomized data is used to learn the data-specific structures. We theoretically and empirically compare our proposal to natural baselines making use of either one or both data types. This allows us to derive conditions indicating when it is useful to combine observational and randomized data, and when it is not. In particular, we prove finite sample (i. e., non-asymptotic) learning bounds. A finite sample view is particularly important in our setting, since it offers insights into which factors drive the estimation error when the size of randomized data is small. Our theoretical analysis reveals three driving factors of relative performance: (i) the size of the observational data; (ii) the discrepancy between the RCT population and the population of interest; and (iii) the complexity of the bias function due to unobserved confounding. Guided by the insights obtained through this finite sample view, we design a sample-efficient algorithm of our two-step framework for combining observational and randomized data. The specific instantiation is based on neural networks; hence, we call this algorithm **CorNet**. We then verify the finite sample properties of our algorithm empirically using simulation studies. Moreover, we use multiple real-world randomized experiments to demonstrate that, compared to existing baselines, our CorNet yields superior performance. A summary of our findings is outlined in Table 1.

We summarize our main **contributions**¹ as follows:

1. We study how to combine observational and randomized data for estimating heterogeneous treatment effects. For this, we propose a two-step framework which relies on a shared structure between both data types.
2. We derive finite sample learning bounds for our two-step framework and, moreover, for several natural baselines. This yields theoretical insights into the drivers of the estimation error and allows us to derive conditions for when observational and randomized data should be combined and when not.
3. Guided by these theoretical insights, we propose **CorNet**, a sample-efficient algorithm of our two-step framework. We verify its finite sample properties empirically using extensive simulation studies and compare to baselines which use one data type exclusively. Moreover, we use multiple real-world randomized experiments to demonstrate that our CorNet outperforms the state-of-the-art by a substantial margin.

2. Related Work

In this section, we give an overview of (i) methods for estimating heterogeneous treatment effects that rely on observational data whilst making strong assumptions and (ii) methods that combine observational and randomized data, but which are mostly for estimating average treatment effects. In addition, (iii) we review related approaches from multi-task and transfer learning.

(i) Estimating heterogeneous treatment effects using observational data. Many machine learning methods have been adapted for estimating heterogeneous treatment effects. These methods range across random forest-based methods (e. g., [Wager and Athey, 2018](#)),

1. Code available at <https://github.com/tobhatt/CorNet>.

Table 1: Summary of the questions raised and answered in this paper and where to find the details. We use “obs.” as abbreviation for “observational” and “rand.” as abbreviation for “randomized”.

Question	Answer	Details in
<i>How to combine obs. and rand. data?</i>	Our two-step framework	Section 4
<i>What factors drive the finite sample error?</i>	<ul style="list-style-type: none"> • Size of obs. data • Distributional discrepancy between obs. and rand. data • Complexity of the bias function 	Section 5, Theorem 2
<i>When to combine obs. and rand. data?</i>	<ul style="list-style-type: none"> • Large obs., but small rand. data • Large discrepancy between obs. and rand. data 	Section 5.3, Prop. 11
<i>How to efficiently combine obs. and rand. data?</i>	Our CorNet , which can: <ul style="list-style-type: none"> • balance the covariate distributions • regularize the bias function 	Section 6, Algorithm 1

Bayesian algorithms due to their ability to quantify uncertainty (e. g., Alaa and van der Schaar, 2017; Alaa and van der Schaar, 2018; Zhang et al., 2020), and deep learning algorithms due to their strong predictive performance (e. g., Johansson et al., 2016; Yoon et al., 2018; Hatt and Feuerriegel, 2021a). Especially deep learning has been used to learned a shared representation and treatment-specific hypotheses for each outcome (e. g., Shalit et al., 2017; Yao et al., 2018; Curth and van der Schaar, 2021b,a). However, all these methods are based on the assumption that the observational data is unconfounded, which is not testable and usually fails to hold true in practice (e. g., Rosenbaum, 2010; Kallus and Zhou, 2018; Kallus et al., 2019; Wang and Blei, 2019; Zhao et al., 2019; Hatt and Feuerriegel, 2021b). Hence, this prohibits the above methods from being applied in practice.

Another stream of research aims towards using latent variable models to recover unobserved confounders. For instance, some approaches try to recover the true confounders from noisy proxies of the true confounders (e. g., Louizos et al., 2017; Kuzmanovic et al., 2021). However, we do not know whether the covariates we observe are indeed proxies of the true confounders. Other attempts try recover unobserved confounders using the treatment assignment of either multiple treatments (Wang and Blei, 2019; Bica et al., 2019) or sequential treatments (Hatt and Feuerriegel, 2021b). However, these approaches again assume variants of no unmeasured confounders, so-called single strong ignorability and time-invariant confounders. Neither of the assumptions can be tested in practice, thereby limiting the usefulness of these methods in practice.

Difference to our work: We accept the presence of unobserved confounders in observational data, but recognize the potential use of randomized data. Therefore, we proposed a two-step framework for combine observational *and* randomized data.

(ii) Combining observational and randomized data. There exist only a few recent methods for combining observational and randomized data. For instance, [Kallus et al. \(2018\)](#) use observational data to estimate a flexible, but biased function for the heterogeneous treatment effect and then aim to remove the bias using the randomized data. However, they makes strong parametric assumptions on the form of the bias due to the small sample size of randomized data. This restricts their method in its applicability to biases which are linear in the covariates. A recently proposed approach is to estimate two separate estimators: one estimator on observational data, which is biased, and one estimator on randomized data, which is unbiased. Then, a weighted average of these two estimators is used. For estimating average treatment effects, the weight can be chosen by a shrinkage factor determined by Stein’s unbiased risk estimate ([Rosenman et al., 2020](#)) or by minimizing the asymptotic variance ([Yang and Ding, 2020](#)). Concurrent to our work, this averaging approach has been extended to heterogeneous treatment effects. [Cheng and Cai \(2021\)](#) propose to estimate one estimator on observational data and one on randomized data. Then, a weighted average of the two estimators is used. However, in order to tune the averaging weight, a large validation set of randomized data is required. We observe in our experiments that this stands in conflict with the small sample size of randomized data.

Several further approaches have been proposed recently, but for different settings than ours. [Ilse et al. \(2021\)](#) propose a causal reduction method for combining interventional and observational data. However, they consider a discrete treatment *and* discrete outcome and rely on linear-Gaussian models. This is different from our setting, since we consider a discrete treatment and a continuous outcome. Other approaches rely on outcomes from different time-steps such as before and after the treatment assignment ([Strobl and Lasko, 2021](#)) or short- and long-term outcomes ([Athey et al., 2020](#); [Imbens et al., 2022](#)). This renders both approaches inapplicable to the standard causal inference setting, which is the focus of our work.

Difference to our work: We propose to combine observational and randomized data via representation learning. For this, we leverage observational data to learn a shared representation and, then, use the randomized data to learn the data-specific structures. By leveraging a shared representation, we can learn complex and non-linear biases even though the size of the randomized data is small. Moreover, we can leverage representation learning to account for the distributional discrepancy between observational and randomized data.

(iii) Multi-task and transfer learning. Combining observational and randomized data can be seen as an instance of multi-task learning (MTL) or transfer learning (TL). MTL leverages data from multiple different, but related prediction tasks to estimate similar predictive models for these tasks. To this end, MTL assumes some similarity across the predictive tasks (e. g., [Caruana, 1997](#); [Argyriou et al., 2006](#)). For instance, such similarity can be enforcing the same covariate support (for linear regression) or the same kernel ([Caruana, 1997](#); [Meier et al., 2008](#); [Jalali et al., 2010](#)) for all tasks. A similarity can also be achieved by intermediate (neural network) representations (i. e., the same weights are used for intermediate layers for all tasks) ([Collobert and Weston, 2008](#); [Maurer et al., 2016](#)). While MTL estimates a model that works well on multiple related tasks, TL focuses on

learning a single new task by transferring information from an already learned related task (Pan and Yang, 2009; Tripuraneni et al., 2020; Du et al., 2020).

Difference to our work: Similar to MTL and TL, we leverage a shared representation between observational and randomized data to transfer information from observational data to (different, but related) randomized data for which we have far fewer samples. However, our setting is distinctly different for two reasons. First, MTL and TL usually do not focus on possible covariate distribution mismatches between tasks. However, in practice, the subjects in an RCT are often not representative for the population of interest, which yields such a distribution mismatch (e.g., Rothwell, 2005; Cole and Stuart, 2010; Stuart et al., 2011; Buchanan et al., 2018; Hatt et al., 2021). Second, in MTL and TL, task-specific functions are used, since the data types considered are usually not closely related. For instance, Bayati et al. (2018) simultaneously estimate logistic regressions with the aim to predict *different* diseases (heart failure, diabetes, dementia, cancer, pulmonary disorder, etc.). In contrast, observational and randomized data are closely related, since both concern the same treatment, but biased due to unobserved confounding. This goes as far as practitioners ignoring randomized data and relying only on observational data (e.g., Shalit et al., 2017; Berrevoets et al., 2020, 2021; Hatt and Feuerriegel, 2021a). This allows us to learn the bias more efficiently by exploiting structural similarities.

3. Preliminaries

3.1 Problem Setup

We consider the standard causal inference setting in which our objective is to estimate the effect of a binary treatment. For this, let $T \in \{0, 1\}$ be a treatment, $X \in \mathbb{R}^d$ patient covariates, and $Y \in \mathbb{R}$ an outcome. Then, our objective is to estimate the conditional average treatment effect (CATE) defined as

$$\tau(x) = \mathbb{E}[Y(1) - Y(0) \mid X = x], \quad (1)$$

where $Y(1), Y(0) \in \mathbb{R}$ are the potential outcomes for treatment and control (Robins et al., 2000). Estimating the CATE in (1) is non-trivial, since we never observe both potential outcomes, but only the outcome under treatment *or* control.

When estimating the CATE, two types of data can be considered: (i) observational data, which originates from an OS, and (ii) randomized data, which originates from an RCT. Formally, let $R \in \{0, 1\}$ be an indicator of participation in the RCT ($R = 1$) or OS ($R = 0$). Then, randomized data is drawn from $(X^{\text{Unc}}, T^{\text{Unc}}, Y^{\text{Unc}}) \sim (X, T, Y \mid R = 1)$ and observational data is drawn from $(X^{\text{Conf}}, T^{\text{Conf}}, Y^{\text{Conf}}) \sim (X, T, Y \mid R = 0)$.² When estimating the CATE from solely (i) observational data *or* (ii) randomized data, there may occur the following problems:

(i) Problems with observational data: unobserved confounders. Observational data, $(X^{\text{Conf}}, T^{\text{Conf}}, Y^{\text{Conf}})$, is likely to be confounded (e.g., Rosenbaum, 2010; Kallus et al., 2018; Kallus and Zhou, 2018; Wang and Blei, 2019; Zhao et al., 2019). That is, some confounders, i.e., variables that affect treatment assignment and outcome, are unobserved

2. We use the superscript “Unc” for the unconfounded randomized data and “Conf” for the confounded observational data.

and, therefore, not contained in the observational data. Hence, when conditioning on the observed covariates, the potential outcomes and the treatment assignment are *not* independent, i. e., $Y(1), Y(0) \not\perp\!\!\!\perp T^{\text{Conf}} \mid X^{\text{Conf}}$. Because of this, in general,

$$\mathbb{E}[Y^{\text{Conf}} \mid X^{\text{Conf}} = x, T^{\text{Conf}} = t] \neq \mathbb{E}[Y(t) \mid X^{\text{Conf}} = x], \quad (2)$$

and, therefore, using $\mathbb{E}[Y^{\text{Conf}} \mid X^{\text{Conf}} = x, T^{\text{Conf}} = t]$ as an estimate for $\mathbb{E}[Y(t) \mid X^{\text{Conf}} = x]$ may yield biased estimates of the CATE.

On the other hand, randomized data, which originated from an RCT, is unconfounded, since the treatment assignment was randomized. Hence, $Y(1), Y(0) \perp\!\!\!\perp T^{\text{Unc}} \mid X^{\text{Unc}}$ holds true for randomized data. As such, different to observational data, we can obtain reliable estimates of $\mathbb{E}[Y(t) \mid X^{\text{Unc}} = x]$, since

$$\mathbb{E}[Y^{\text{Unc}} \mid T^{\text{Unc}} = t, X^{\text{Unc}} = x] = \mathbb{E}[Y(t) \mid X^{\text{Unc}} = x]. \quad (3)$$

(ii) Problems with randomized data: sample size and generalizability. RCTs are costly to conduct and the patient recruitment is a tedious undertaking. As a consequence, randomized data admits two different problems than observational data. First, due to the costs of RCTs, the sample size of randomized data is usually very small. This is limiting its usefulness for estimating treatment heterogeneity. Second, due to the difficulty of patient recruitment, many RCTs lack generalizability (also known as external validity) (e. g., [Rothwell, 2005](#); [Cole and Stuart, 2010](#); [Buchanan et al., 2018](#); [Hatt et al., 2021](#)). This means that the covariate distribution in the randomized data, may differ from the actual covariate distribution of the population of interest, i. e.,

$$p(X^{\text{Unc}}) \neq p(X). \quad (4)$$

Fortunately, observational data is usually available in large quantities and, hence, can be used to estimate treatment effect heterogeneity. Moreover, observational data shares the covariate distribution of the population of interest, i. e., $p(X^{\text{Conf}}) = p(X)$. This is due to the nature of OSs, in which information about treatment outcomes is collected in the actual population of interest.

In this paper, we argue that these two data types are complementary and study how to combine observational data, $(X^{\text{Conf}}, T^{\text{Conf}}, Y^{\text{Conf}})$, and randomized data, $(X^{\text{Unc}}, T^{\text{Unc}}, Y^{\text{Unc}})$, to estimate the CATE, $\tau(x)$. Moreover, we study the influence of the different properties of observational and randomized data when estimating the CATE.

3.2 Assumptions for Identification

Identification of the CATE, $\tau(x)$, requires assumptions, which relate the potential outcomes to the observed data. For this, we first state the standard assumptions for causal inference (e. g., [Rosenbaum, 2010](#)) that hold globally and then consider additional assumptions that hold for either randomized or observational data.

Assumption 1 (*Standard Assumptions*)

- (i) *Consistency*, i. e., $Y = TY(1) + (1 - T)Y(0)$,

(ii) *Treatment overlap*, i. e., $0 < \mathbb{P}(T = t \mid X = x, R = r) < 1$, for all t, x , and r ,

(iii) *Population overlap*, i. e., $0 < \mathbb{P}(R = r \mid X = x) < 1$, for all x and r .

Consistency states that if a patient receives treatment t , then the observed outcome is the corresponding potential outcome $Y(t)$. In particular, this holds true for both observational and randomized data, since $Y^{\text{Unc}} \sim (Y \mid R = 1)$ and, thus, $Y^{\text{Unc}} = T^{\text{Unc}} Y(1) + (1 - T^{\text{Unc}}) Y(0)$ (analogously for Y^{Conf}). Treatment overlap requires that the treatment assignment is non-deterministic in both the RCT and OS. These are standard assumptions in causal inference (e. g., [Rosenbaum, 2010](#)). Population overlap requires that the covariates in the randomized and observational data (i. e., X^{Unc} and X^{Conf}) to have common support. However, it allows the covariates to follow different distributions, since the subjects in the RCT may not be representative for the population of interest.

Further, in order to make the CATE identifiable from the randomized data and generalizable to the population of interest, we make the following assumptions on the RCT and OS separately.

Assumption 2 (*Unconfoundedness, no outcome modification, and generalizability*)

(i) *Unconfounded RCT*, i. e., $Y(1), Y(0) \perp\!\!\!\perp T \mid X, R = 1$,

(ii) *No outcome modification*, i. e., $Y(1), Y(0) \perp\!\!\!\perp R \mid X$,

(iii) *Generalizable OS*, i. e., $\mathbb{P}(R = 0 \mid X = x) = \mathbb{P}(R = 0)$.

Assumption (i) ensures that the data we obtained from the RCT is unconfounded, and, hence, the expected potential outcomes can be estimated from this data. Assumption (ii) means that being in the RCT or OS does not affect the potential outcomes.³ This is a very weak assumption and merely ensures that the functional relationship between covariates and potential outcomes is the same across data sources. Assumption (iii) implies that the covariate distribution in the OS is the same as in the population of interest.⁴ While (i) and (ii) are made explicitly in previous work for combining RCT and OS data ([Kallus et al., 2018](#); [Rosenman et al., 2020](#); [Cheng and Cai, 2021](#)), (iii) has been implicitly used, but not explicitly stated.

These assumptions ensure that the treatment effect is identifiable only within the small RCT. However, the estimation of CATE is hindered by the small sample size of RCTs and their lack of generalizability. We overcome these obstacles by combining observational data and randomized.

3.3 Notation

Throughout this paper, we use the following notations. We use upper-case letters (i. e., X) for random variables and lower-case letters (i. e., x) for realizations of these random

3. In practice, it can happen that the potential outcomes are different in an OS due to non-compliance. However, this problem is orthogonal to our work. For works on non-compliance, see [Robins \(1994\)](#); [Cuzick et al. \(1997\)](#); [Ye et al. \(2014\)](#).

4. Assumption (iii) implies the same covariate distributions, since $p(X^{\text{Conf}}) = p(X \mid R = 0) = \mathbb{P}(R = 0 \mid X)p(X)/\mathbb{P}(R = 0) = p(X)$.

variables. Further, we use bold upper-case letters (i. e., \mathbf{W}) for matrices and bold lower-case letters (i. e., \mathbf{v}) for vectors. Generically, we use “hatted” functions, vectors, and matrices (e. g., $\hat{\mathbf{f}}$, $\hat{\mathbf{v}}$, and $\hat{\mathbf{W}}$) to refer to their (random) estimators. We use Φ to refer to a function class of representations $\phi : \mathbb{R}^d \rightarrow \mathbb{R}^{d_\phi}$ and \mathcal{H} to refer to a function class of hypotheses $h : \mathbb{R}^{d_\phi} \rightarrow \mathbb{R}$. Further, we use \mathcal{B} to refer to a function class of bias functions $\delta : \mathbb{R}^{d_\phi} \rightarrow \mathbb{R}$. For the hypothesis class \mathcal{H} , we use $\mathcal{H}^{\otimes 2}$ to refer to the 2-fold Cartesian product, i. e., $\mathcal{H}^{\otimes 2} = \{\mathbf{h} = (h_1, h_0) : h_1 \in \mathcal{H}, h_0 \in \mathcal{H}\}$. Similarly, $\mathcal{B}^{\otimes 2}$ refers to the 2-fold Cartesian product of the bias function class \mathcal{B} . We use ‘ \circ ’ to denote composition of functions. That is, for two functions $\phi \in \Phi$ and $h \in \mathcal{H}$, their composition is given by $h \circ \phi(x) = h(\phi(x))$. In particular, for $h \in \mathcal{H}$ and $\delta \in \mathcal{B}$, we also use ‘ \circ ’ to refer to addition of h and δ using the same representation, i. e., $(h + \delta) \circ \phi(x) = h(\phi(x)) + \delta(\phi(x))$. We use $\tilde{\mathcal{O}}$ to denote an expression that hides polylogarithmic factors.

4. Combining Observational and Randomized Data by Learning a Shared Representation

In this section, we discuss how to estimate the CATE using both observational and randomized data. For this, we build upon a long-standing history in machine learning of assuming a shared structure between learning tasks. This is particularly prominent in multi-task learning, transfer learning, and, most relevant to our work, in causal inference (e. g., Caruana, 1997; Argyriou et al., 2006; Maurer et al., 2016; Shalit et al., 2017; Du et al., 2020; Zhang and Yang, 2021) and has been proven useful in machine learning across general learning tasks (e. g., Ruder, 2017; Radford et al., 2019; Liu et al., 2019; Li et al., 2020; Brown et al., 2020). In particular, we first formalize the difference in observational and randomized outcomes using a shared representation and connect it to the bias due to unobserved confounding (Section 4.1). Motivated by this, we introduce our two-step procedure for combining observational and randomized data (Section 4.2).

4.1 Formalizing the Bias due to Unobserved Confounding

Here, we assume the shared structure between observational and randomized data to be the *representation*, which is a function $\phi^* : \mathbb{R}^d \rightarrow \mathbb{R}^{d_\phi}$ that maps the covariates $X \in \mathbb{R}^d$ to some representation of the covariates $Z \in \mathbb{R}^{d_\phi}$. This representation captures the shared structure between observational and randomized data and, hence, is the same function for both types of data. On top of the representation, we consider hypotheses for both treatment and control. These hypotheses are “data-specific” and, thus, can vary across observational and randomized data. That is, we consider, for $t \in \{0, 1\}$, separate hypotheses $h_t^u, h_t^c : \mathbb{R}^{d_\phi} \rightarrow \mathbb{R}$ for randomized and observational data.⁵

Then, we recognize that the difference between observational and randomized outcomes can be connected to the bias due to unobserved confounding by the following:

$$\mathbb{E}[Y(t) \mid X^{\text{Conf}} = x] - \mathbb{E}[Y^{\text{Conf}} \mid T^{\text{Conf}} = t, X^{\text{Conf}} = x] = \quad (5)$$

$$\mathbb{E}[Y^{\text{Unc}} \mid T^{\text{Unc}} = t, X^{\text{Unc}} = x] - \mathbb{E}[Y^{\text{Conf}} \mid T^{\text{Conf}} = t, X^{\text{Conf}} = x] = \quad (6)$$

$$(h_t^u - h_t^c) \circ \phi^*(x), \quad (7)$$

5. The superscripts “u” and “c” denote “unconfounded” and “confounded” hypotheses.

where (5) is the bias due to unobserved confounding and (6) follows directly from (i) and (ii) in Assumption 2. As such, the bias due to unobserved confounding is connected to the difference in the “data-specific” hypotheses.

Formally, the observational and randomized outcomes, $Y^{\text{Conf}}, Y^{\text{Unc}}$, are generated by

$$Y^{\text{Conf}} \sim h_{T^{\text{Conf}}}^c \circ \phi^*(X^{\text{Conf}}) + \varepsilon^c, \quad (8)$$

$$Y^{\text{Unc}} \sim h_{T^{\text{Unc}}}^u \circ \phi^*(X^{\text{Unc}}) + \varepsilon^u, \quad (9)$$

where $\varepsilon^c, \varepsilon^u \sim \mathcal{N}(0, \sigma_{c,u}^2)$. The representation, ϕ^* , is shared and, hence, encodes the common structure between the observational and randomized data. The confounded and unconfounded hypotheses, h_t^c, h_t^u may differ and, hence, capture the bias due to unobserved confounding as in (7).

Moreover, the covariates, i. e., $X^{\text{Conf}}, X^{\text{Unc}} \sim p_x^{\text{Conf}}, p_x^{\text{Unc}}$, and the treatment assignment, i. e., $T^{\text{Conf}}, T^{\text{Unc}} \sim p_t^{\text{Conf}}, p_t^{\text{Unc}}$, can follow any distribution, which satisfies the assumptions from Section 3.2. In particular, the distributions p_x^{Conf} and p_x^{Unc} may differ across observational and randomized data.⁶ Moreover, the treatment assignment may depend on unobserved confounders. However, as we have seen earlier in this section, the bias due to unobserved confounding can be formulated as the difference between of the observational and randomized outcomes.

Motivated by these insights, we propose an intuitive two-step procedure, which exploits the shared structure of observational and randomized data for estimating the CATE.

4.2 Two-Step Procedure for Combining Observational and Ranomized Data

We introduce our two-step procedure for estimating the CATE that combines observational and randomized data. In the first step, we use observational data to learn a representation $\hat{\phi}$ and confounded hypotheses \hat{h}_t^c for each $t \in \{0, 1\}$. Since the representation is shared across observational and randomized data, we can use it in the second step, together with the randomized data, to debias the confounded hypotheses. Note that we do not propose to learn the unconfounded hypothesis, \hat{h}_t^u . Rather, we use the fact that the bias due to unobserved confounding can be expressed by the difference in the “data-specific” hypotheses, as in (7), and learn the bias function, i. e., $\delta_t = h_t^u - h_t^c$. We do so, since learning \hat{h}_t^u may be statistically inefficient due to the small sample size of the randomized data. As such, structural restrictions on the form of \hat{h}_t^u would have to be made upfront. However, to improve upon this, we seek to learning δ_t directly. Specifically, we recognize that, while \hat{h}_t^c and \hat{h}_t^u are different, they are likely to be related (i. e., structurally similar), because they both concern the same drug and partially overlapping populations. Hence, this allows us to make structural restrictions on δ_t , which plays an important role later, when we derive a finite sample learning bound. An illustration of our two-step procedure can be found in Figure 1.

Formally, we consider a two-step empirical risk minimization procedure that leverages observational data $\{(x_i^{\text{Conf}}, t_i^{\text{Conf}}, y_i^{\text{Conf}})\}_{i=1}^{n^{\text{Conf}}}$ and randomized data $\{(x_i^{\text{Unc}}, t_i^{\text{Unc}}, y_i^{\text{Unc}})\}_{i=1}^{n^{\text{Unc}}}$. For this, we consider the function classes Φ, \mathcal{H} , and \mathcal{B} for the representation ϕ , the con-

6. This is due to the fact that the subjects in RCTs are often not representative of the population of interest. See discussion in Section 3.1 for details.

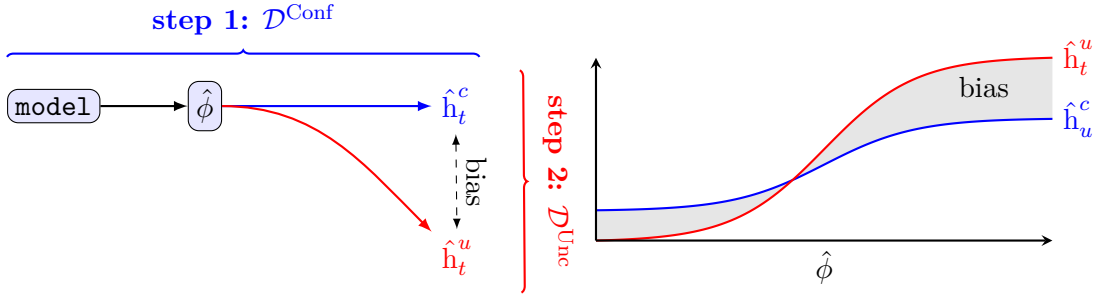


Figure 1: **Conceptual overview of our procedure.** Given a confounded dataset ($\mathcal{D}^{\text{Conf}}$), and an unconfounded dataset (\mathcal{D}^{Unc}), our procedure learns an unconfounded estimate using both datasets. We propose to do this in two steps: in step 1, we learn a shared representation $\hat{\phi}$ and *confounded* hypotheses, and in step 2 we *correct* for the bias in these confounded hypotheses such that we have *unconfounded* hypotheses (\hat{h}_t^u). Left, we depict a conceptual overview of our procedure, and right we show the potential impact on the actual hypotheses.

founded hypotheses h_t^c , and the bias function δ_t .

Step 1. In the first step, we learn the shared representation and the confounded hypotheses by minimizing the empirical loss of the observational data

$$\hat{\phi}, \hat{\mathbf{h}}^c = \arg \min_{\phi \in \Phi, \mathbf{h}^c \in \mathcal{H}^{\otimes 2}} \hat{\epsilon}_{\text{Conf}}(\mathbf{h}^c, \phi), \quad (10)$$

where the empirical loss of the observational data is defined as

$$\hat{\epsilon}_{\text{Conf}}(\mathbf{h}^c, \phi) = \frac{1}{n^{\text{Conf}}} \sum_{i=1}^{n^{\text{Conf}}} \left(h_{t_i^{\text{Conf}}}^c \circ \phi(x_i^{\text{Conf}}) - y_i^{\text{Conf}} \right)^2, \quad (11)$$

and $\mathbf{h}^c = (h_1^c, h_0^c) \in \mathcal{H}^{\otimes 2}$.

Step 2. In the second step, we use randomized data together with the estimates from the first step, $\hat{\phi}$ and $\hat{\mathbf{h}}^c$, to learn the bias in the confounded hypothesis by minimizing the empirical loss of the randomized data

$$\hat{\boldsymbol{\delta}} = \arg \min_{\boldsymbol{\delta} \in \mathcal{B}^{\otimes 2}} \hat{\epsilon}_{\text{Unc}}(\boldsymbol{\delta}, \hat{\mathbf{h}}^c, \hat{\phi}), \quad (12)$$

where the empirical loss of the randomized data is defined as

$$\hat{\epsilon}_{\text{Unc}}(\boldsymbol{\delta}, \hat{\mathbf{h}}^c, \hat{\phi}) = \frac{1}{n^{\text{Unc}}} \sum_{i=1}^{n^{\text{Unc}}} \left((\hat{h}_{t_i^{\text{Unc}}}^c + \delta_{t_i^{\text{Unc}}}) \circ \hat{\phi}(x_i^{\text{Unc}}) - y_i^{\text{Unc}} \right)^2, \quad (13)$$

and $\boldsymbol{\delta} = (\delta_1, \delta_0) \in \mathcal{B}^{\otimes 2}$.

Once we obtained the representation $\hat{\phi}$, the confounded hypothesis $\hat{\mathbf{h}}^c$, and the bias function $\hat{\boldsymbol{\delta}}$, the unconfounded hypothesis is then obtained by

$$\hat{h}_t^u = \hat{h}_t^c + \hat{\delta}_t. \quad (14)$$

Finally, the unconfounded hypotheses yield our estimator for combining observational and randomized data

$$\hat{\tau}_{\text{Cor}}(x) = (\hat{\mathbf{h}}_1^u - \hat{\mathbf{h}}_0^u) \circ \hat{\phi}(x). \quad (15)$$

Remark 1 *Note that the first step only requires observational data, whereas the second step only requires randomized data. As a result, observational and randomized data do not need to be simultaneously available during training. This is very useful if the two data sources cannot be easily merged, for instance, due to regulatory issues, which is common in medical practice. Our two-step procedure only requires to share the estimated functions, $\hat{\phi}$ and $\hat{\mathbf{h}}^c$.*

The efficacy of an estimator $\hat{\tau}$ is gauged by the precision of estimating heterogeneous effects (PEHE), which is defined as

$$\epsilon_{\text{PEHE}}(\hat{\tau}) = \int_{\mathbb{R}^d} (\hat{\tau}(x) - \tau(x))^2 p_x^{\text{Conf}}(x) dx. \quad (16)$$

The density $p_x^{\text{Conf}}(x)$ occurs, since the covariate distribution in the observational data is representative of (i. e., the same as) the covariate distribution in the population of interest. In order to study the efficacy of our two-step procedure, we need to make a connection between our two-step procedure and the quantity $\epsilon_{\text{PEHE}}(\hat{\tau}_{\text{Cor}})$. In particular, we derive a finite sample bound on $\epsilon_{\text{PEHE}}(\hat{\tau}_{\text{Cor}})$. This finite sample view provides useful insights into which components influence the convergence of $\epsilon_{\text{PEHE}}(\hat{\tau}_{\text{Cor}})$ and, based on this, how algorithms for combining observational and randomized data should be designed.

5. Finite Sample Learning Bounds

In this section, we derive finite sample learning bounds for our two-step procedure. Based on this, we further derive conditions for when it is useful to combine confounded and unconfounded data and for when it is not. In particular, we derive finite sample bounds on $\epsilon_{\text{PEHE}}(\hat{\tau}_{\text{Cor}})$, where $\hat{\tau}_{\text{Cor}}$ is the CATE estimator obtained by our two-step procedure (see Theorem 2). The finite sample view offers insights into which factors impact the estimation error when the sample size is *not* infinite; in particular, when sample the size is small as in our setting. We find three driving factors of the error: (i) the size of observational data, (ii) the distributional discrepancy between the covariate distributions in observational data and randomized data, and (iii) the complexity of the bias in the confounded hypotheses. Moreover, we derive conditions for when our two-step procedure should be used over standard algorithms, but also when our procedure should not be used (see Section 5.3). This gives a complete picture of the disadvantages and advantages of our two-step procedure.

5.1 Preliminaries

Throughout this section, we assume that the true shared representation, hypotheses, and bias functions are contained in the function classes Φ , \mathcal{H} , and \mathcal{B} over which the two-step procedure optimizes. For this, we make the following standard realizability assumption.

Assumption 3 (Realizability). *The true shared representation ϕ^* is contained in the functions class Φ . Further, the true hypotheses and bias functions, $\mathbf{h}^c = (\mathbf{h}_1^c, \mathbf{h}_0^c)$ and $\delta = (\delta_1, \delta_0)$, are contained in $\mathcal{H}^{\otimes 2}$ and $\mathcal{B}^{\otimes 2}$, respectively.*

We first introduce an appropriate distance measure in order to measure the difference between the learned representation $\hat{\phi}$ and the true representation ϕ^* on the confounded data. For this, we introduce the *representation difference*, which measures the extent to which two representation functions ϕ and ϕ' differ in aggregation across treatment and control group. For a function class \mathcal{H} and hypotheses $\mathbf{h} = (h_1, h_0) \in \mathcal{H}^{\otimes 2}$, the *representation difference* between two representations $\phi, \phi' \in \Phi$ is defined as

$$d_{\mathcal{H}, \mathbf{h}}(\phi'; \phi) = \inf_{\mathbf{h}' \in \mathcal{H}^{\otimes 2}} \sum_{t=0}^1 \mathbb{E} \left[\left(h'_t \circ \phi'(X^{\text{Conf}}) - h_t \circ \phi(X^{\text{Conf}}) \right)^2 \right]. \quad (17)$$

The representation difference $d_{\mathcal{B}, \delta}(\phi'; \phi)$ for the function class \mathcal{B} and bias functions $\delta = (\delta_1, \delta_0) \in \mathcal{B}^{\otimes 2}$ is defined analogously.

The representation difference measures the estimation error due to not exactly learning the true representation. The following conditions ensures that the estimation error due to not exactly learning the true shared representation ϕ^* is, up to a constant, larger in the hypotheses than in the bias functions.

Condition 1 $d_{\mathcal{B}, \delta}(\hat{\phi}; \phi^*) \leq \gamma d_{\mathcal{H}, \mathbf{h}^c}(\hat{\phi}; \phi^*)$, for some $\gamma > 0$.

Note that this only requires that the two representation differences can be set into relation to each other; $d_{\mathcal{H}, \mathbf{h}^c}(\hat{\phi}; \phi^*)$ itself does not need to be larger than $d_{\mathcal{B}, \delta}(\hat{\phi}; \phi^*)$, only up to a constant $\gamma > 0$. In particular, we show later that this conditions holds true for the specific instantiation of the two-step procedure that we propose.

While our procedure works with arbitrary function classes, we consider feedforward neural networks for our representation class Φ , hypothesis class \mathcal{H} , and bias function class \mathcal{B} . We provide a mathematical definition of feedforward neural networks and an architecture illustration of our two-step procedure using neural networks in Appendix B. We also provide the theoretical results proven in this section for general function classes in Appendix C.1.

5.2 Main Result

We can now present the main result of this section: the finite sample learning bound for our two-step procedure.

Theorem 2 (*Finite sample learning bound.*) *Let $(\hat{\phi}, \hat{\mathbf{h}}^c)$ be the empirical loss minimizer of $\hat{\epsilon}_{\text{Conf}}(\cdot, \cdot)$ from (10) over the function classes Φ and \mathcal{H} , and let $\hat{\delta}$ be the empirical loss minimizer of $\hat{\epsilon}_{\text{Unc}}(\cdot, \hat{\mathbf{h}}^c, \hat{\phi})$ from (12) over the function class \mathcal{B} . Further, let $\hat{\tau}_{\text{Cor}}$ be the resulting CATE estimator from (15). Then, if Assumption 3 and Condition 1 hold true, we have that, with probability at least $1 - p$,*

$$\epsilon_{\text{PEHE}}(\hat{\tau}_{\text{Cor}}) \leq \tilde{\mathcal{O}} \left(\frac{\mathcal{C}_{\Phi} + \mathcal{C}_{\mathcal{H}}}{\sqrt{n^{\text{Conf}}}} + \frac{d_{\infty}(p_{\phi}^{\text{Conf}} | p_{\phi}^{\text{Unc}}) \mathcal{C}_{\mathcal{B}}}{\sqrt{n^{\text{Unc}}}} \right), \quad (18)$$

where \mathcal{C}_Φ , $\mathcal{C}_\mathcal{H}$, and $\mathcal{C}_\mathcal{B}$ are constants depending on the complexity of the neural networks and $d_\infty(p_\phi^{\text{Conf}} | p_\phi^{\text{Unc}}) = \sup_{z \in \mathcal{Z}} \frac{p_\phi^{\text{Conf}}(z)}{p_\phi^{\text{Unc}}(z)}$ is a measure for the distributional discrepancy between p_ϕ^{Conf} and p_ϕ^{Unc} .^{7,8}

Proof See Appendix C.1. ■

From Theorem 2, we can derive three major insights about the factors that impact the error of our two-step procedure. In particular, we gain insights into how (i) the size of observational data, (ii) the distributional discrepancy, and (iii) the complexity of the bias function impact the error. This is only possible, since we take a finite sample (i. e., non-asymptotic) point of view. In contrast to an infinite sample view, which considers infinitely many samples, a finite sample view allows to study what happens when n^{Conf} and n^{Unc} are varied (i. e., small or large). In particular, an finite sample view allows to study what happens when n^{Unc} is small, which is our setting of interest. We elaborate more on each of the above points in the following. An illustration of the three factors can be found in Section 5.2.

(i) The size of the observational data. Leveraging observational data is beneficial, since the error bound in Theorem 2 decreases with the size of observational data, i. e., n^{Conf} . This is not obvious, since the observational data is biased, and, hence, it is a priori not clear that using biased data improves the estimation error. Moreover, the more observational data we have, the better, since this decreases the error bound in Theorem 2. This is particularly favorable in our setting, in which we usually have large amounts of observational data.

(ii) The distributional discrepancy between observational and randomized data. The distributional discrepancy, $\bar{d}_\infty(p_\phi^{\text{Conf}} | p_\phi^{\text{Unc}})$, arises since the randomized data does not have the same covariate distribution as the observational data (which coincides with the target distribution). Therefore, since the bias function is learned from randomized data, distributional discrepancy between observational and randomized data impacts the error. In particular, the discrepancy between the observational and randomized data, $d_\infty(p_\phi^{\text{Conf}} | p_\phi^{\text{Unc}})$, increases the error bound (since, by definition, $d_\infty(p_\phi^{\text{Conf}} | p_\phi^{\text{Unc}}) \geq 1$). This, itself, is an interesting result, since most works on covariate shift derive an additive impact of the distributional discrepancy. This leads to the intuition that we *have to* minimize the discrepancy in order for the error to converge to zero. However, this is not true as we can see in Theorem 2. As long as the discrepancy is finite, the error converges to zero in any case, but the discrepancy slows down the convergence. Thus, in a data-rich environment (i. e., where n^{Unc} is large), the impact of the discrepancy may not be substantial. However, and more importantly for our setting, the discrepancy may have a large impact in data-scarce environments (i. e., when n^{Unc} is small as in our setting). Hence, while the discrepancy may be negligible when n^{Unc} is large, it is certainly important to consider it when n^{Unc} is small. As a direct consequence, when designing algorithms to integrate observational data into randomized data, we should bear this in mind and account for the discrepancy.

7. The terms p_ϕ^{Conf} and p_ϕ^{Unc} are the push-forwards of p_x^{Conf} and p_x^{Unc} through the representation ϕ . Moreover, $d_\infty(p_\phi^{\text{Conf}} | p_\phi^{\text{Unc}})$ is the exponential in base 2 of the Rényi divergence $D_\infty(p_\phi^{\text{Conf}} | p_\phi^{\text{Unc}})$. Note that $d_\infty(p_\phi^{\text{Conf}} | p_\phi^{\text{Unc}})$ is well-defined, since we assume population overlap in Assumption 1.

8. In Theorem 2 and throughout this section, we use $\tilde{\mathcal{O}}$ to hide polylogarithmic factors. In particular, in the error bounds, we hide factor such as $\log(n^{\text{Conf}})$ and $\log(n^{\text{Unc}})$. We do so, since $\mathcal{O}(\log(n^{\text{Conf}})) = \mathcal{O}(\sqrt{n^{\text{Conf}}})$, but not vice versa. Similar holds true for $\mathcal{O}(\log(n^{\text{Unc}}))$. Moreover, using L'Hôpital's rule, $\mathcal{O}(\log(n^{\text{Conf}})^2) = \mathcal{O}(\sqrt{n^{\text{Conf}}})$.

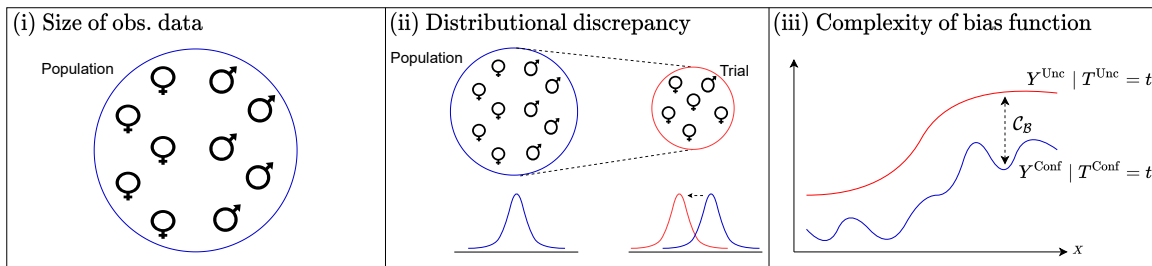


Figure 2: Illustration of the three factors driving the error bound of ϵ_{PEHE} . We increase the number of observational samples. All other parameters are fixed. The solid blue line represent the error for the unregularized two-step procedure. The dashed blue line represent the error for $\hat{\tau}_{\text{Cor}}$. We observe that, for both algorithms, ϵ_{PEHE} decreases in the number of observational samples.

(iii) The complexity of the bias function. Based on Theorem 2, we gain insight into impact of the complexity of the bias function (i. e., the larger $\mathcal{C}_{\mathcal{B}}$), the larger the error. This again is crucial, since in a data-scarce regime, such as in RCTs, this term can substantially impact the error. Hence, while the bias may be negligible when n^{Unc} is large, it is certainly important to consider it when n^{Unc} is small. Again, this insight should guide the design of algorithms for combining observational and randomized data.

Remark 3 *Note that, in Theorem 2, we do not consider selection bias in the observational data. That is, we consider the case in which treatment and control group in the observational data possess the same covariate distribution. There is a large body of research addressing selection bias in observational data (e. g., Johansson et al., 2016; Shalit et al., 2017; Yao et al., 2018; Zhang et al., 2020), which is orthogonal to our work. However, since selection bias can arise in observational data, we provide a detailed discussion in Appendix D. In particular, we prove a version of Theorem 2 which considers selection bias. We find that selection bias has a similar impact as the distributional discrepancy between observational and randomized data. However, if the size of observational data is large, i. e., n^{Conf} is large, selection bias may play a less important role. For more details, see the discussion in Appendix D.*

Guided by the above theoretical insights, we design sample-efficient algorithms of our two-step procedure in Section 6.

5.3 Theoretical Comparison with Baseline Alternatives

In this section, we compare multiple natural baseline alternatives for combining observational and randomized data and theoretically compare them to our two-step procedure. In particular, we consider four baselines approaches: The estimators trained on (i) only randomized data, denoted as τ_{Unc} , and (ii) only observational data, denoted as τ_{Conf} , as well as two alternatives, (iii) the averaging estimators, denoted as τ_{Avg} , and (iv) the weighted risk estimator, denoted as τ_{Weight} . For each of these approaches, we derive corresponding finite sample learning bounds similar to Theorem 2. Based on these results, we can then compare the baselines to our two-step procedure and derive conditions for when combining observational and randomized data is beneficial and for when it is not.

5.3.1 ESTIMATOR ON RANDOMIZED DATA (τ_{Unc})

We introduce an approach that only uses randomized data. In order to allow appropriate comparison, we rely again on neural networks for the function classes for the representation, Φ , and hypotheses, \mathcal{H} . However, the representation and hypotheses are learned using only randomized data. This is equivalent to learning a neural network (such as TarNet from [Shalit et al. \(2017\)](#)) on the randomized data. Formally, the representation and the hypotheses are learned by minimizing the empirical loss of the randomized data, i. e.,

$$\hat{\phi}, \hat{\mathbf{h}} = \arg \min_{\phi \in \Phi, \mathbf{h} \in \mathcal{H}^2} \hat{\epsilon}_{\text{Unc}}(\mathbf{h}, \phi), \quad (19)$$

where the empirical loss of the randomized data is given by

$$\hat{\epsilon}_{\text{Unc}}(\mathbf{h}, \phi) = \frac{1}{n^{\text{Unc}}} \sum_{i=1}^{n^{\text{Unc}}} \left(\mathbf{h}_{t_i^{\text{Unc}}} \circ \phi(x_i^{\text{Unc}}) - y_i^{\text{Unc}} \right)^2. \quad (20)$$

This then yields the following CATE estimator

$$\hat{\tau}_{\text{Unc}} = (\hat{\mathbf{h}}_1 - \hat{\mathbf{h}}_0) \circ \hat{\phi}(x). \quad (21)$$

Then, we can derive a finite sample learning bound for $\hat{\tau}_{\text{Unc}}$ similar to our two-step procedure.

Theorem 4 (*Finite sample learning bound for τ_{Unc} .*) *Let $(\hat{\phi}, \hat{\mathbf{h}})$ be the empirical loss minimizer from (19) and $\hat{\tau}_{\text{Unc}}$ as in (21). Then, if Assumption 3 holds true, we have that, with probability at least $1 - p$,*

$$\epsilon_{\text{PEHE}}(\hat{\tau}_{\text{Unc}}) \leq \tilde{\mathcal{O}} \left(\bar{d}_{\infty}(p_{\phi}^{\text{Conf}} | p_{\phi}^{\text{Unc}}) \frac{\mathcal{C}_{\Phi} + \mathcal{C}_{\mathcal{H}}}{\sqrt{n^{\text{Unc}}}} \right), \quad (22)$$

where \mathcal{C}_{Φ} and $\mathcal{C}_{\mathcal{H}}$ are the same constants depending on the complexity of the neural networks as in Theorem 2 and $\bar{d}_{\infty}(p_{\phi}^{\text{Conf}} | p_{\phi}^{\text{Unc}}) = \sup_{\phi \in \Phi} d_{\infty}(p_{\phi}^{\text{Conf}} | p_{\phi}^{\text{Unc}})$.

Proof See Appendix C.2. ■

The distributional discrepancy, $\bar{d}_{\infty}(p_{\phi}^{\text{Conf}} | p_{\phi}^{\text{Unc}})$, arises since the representation and hypotheses are estimated on randomized data, which does not have the same covariate distribution as the observational data (which coincides with the target population). For details, we refer to the proof in the Appendix C.2.

5.3.2 ESTIMATOR ON OBSERVATIONAL DATA (τ_{Conf})

Another approach is to ignore any randomized data and simply rely on observational data to construct an estimator for the CATE (e. g., [Johansson et al., 2016](#); [Shalit et al., 2017](#); [Alaa and van der Schaar, 2017](#)). Again, for fair comparison, we rely on neural networks for the function classes. As such, an estimator that only relies on observational data is identical to the first step of our procedure, but not the second step. For this, let $(\hat{\phi}, \hat{\mathbf{h}}^c)$ be the empirical loss minimizer of $\hat{\epsilon}_{\text{Conf}}(\cdot, \cdot)$ from (10). Then, let the CATE estimator which only uses observational data be

$$\hat{\tau}_{\text{Conf}}(x) = (\hat{\mathbf{h}}_1^c - \hat{\mathbf{h}}_0^c) \circ \hat{\phi}(x). \quad (23)$$

Again, we derive finite sample error bounds for the estimator which only uses observational data, $\hat{\tau}_{\text{Conf}}$.

Theorem 5 (Finite sample learning bound for τ_{Conf} .) *Let $(\hat{\phi}, \hat{\mathbf{h}}^c)$ be the empirical loss minimizer from (10) and $\hat{\tau}_{\text{Conf}}$ as in (23). Then, if Assumption 3 holds true, we have that, with probability at least $1 - p$,*

$$\epsilon_{\text{PEHE}}(\hat{\tau}_{\text{Conf}}) \leq \tilde{\mathcal{O}}\left(\frac{\mathcal{C}_{\Phi} + \mathcal{C}_{\mathcal{H}}}{\sqrt{n^{\text{Conf}}}}\right) + 2\Delta, \quad (24)$$

where \mathcal{C}_{Φ} and $\mathcal{C}_{\mathcal{H}}$ are the same constants depending on the complexity of the neural networks as in Theorem 2 and $\Delta = \mathbb{E}[\left((\delta_1 - \delta_0) \circ \phi^*(X^{\text{Conf}})\right)^2]$ is the bias due to unobserved confounding.

Proof See Appendix C.3. ■

Since n^{Conf} is usually large, the first term in the error bound, $\frac{\mathcal{C}_{\Phi} + \mathcal{C}_{\mathcal{H}}}{\sqrt{n^{\text{Conf}}}}$, is small. Hence, the estimation error of $\hat{\tau}_{\text{Conf}}$, which only uses observational data, is dominated by the bias term Δ . When there is no bias due to unobserved confounding in the observational data, then Δ is zero. In this case, $\hat{\tau}_{\text{Conf}}$ may be more accurate than $\hat{\tau}_{\text{Unc}}$ from (21), which explains the widespread use of observational data in previous works. However, if the bias is non-zero, then relying on observational data can lead to an irreducible estimation error.

5.3.3 AVERAGING ESTIMATOR (τ_{Avg})

Another possible baseline alternative for combining observational and randomized data is to average the estimators from the randomized data, $\hat{\tau}_{\text{Unc}}$, and from the observational data, $\hat{\tau}_{\text{Conf}}$, i. e.,

$$\hat{\tau}_{\text{Avg}}(\lambda) = (1 - \lambda)\hat{\tau}_{\text{Unc}} + \lambda\hat{\tau}_{\text{Conf}}, \quad (25)$$

where $\lambda \in [0, 1]$ is a hyperparameter. For $\lambda = 0$, we recover $\hat{\tau}_{\text{Unc}}$, i. e., the estimator trained only on randomized data. Vice versa, for $\lambda = 1$, we obtain $\hat{\tau}_{\text{Conf}}$, i. e., the estimator trained only on observational data. For $\lambda \in (0, 1)$, this yields a weighted average of $\hat{\tau}_{\text{Unc}}$ and $\hat{\tau}_{\text{Conf}}$.

Remark 6 *Concurrent to our work, this approach was recently also proposed for combining observational and randomized data in Cheng and Cai (2021). In particular, the authors propose to estimate kernel regressions separately on the observational and randomized data, yielding $\hat{\tau}_{\text{Conf}}$ and $\hat{\tau}_{\text{Unc}}$. Then, both estimators are combined using the parameter λ via*

$$\hat{\tau} = \hat{\tau}_{\text{Unc}} + \lambda(\hat{\tau}_{\text{Conf}} - \hat{\tau}_{\text{Unc}}), \quad (26)$$

which is equivalent to the approach in (25). We show in the following that this baseline does (up to constants) not yield an improvement over best choice of $\hat{\tau}_{\text{Conf}}$ or $\hat{\tau}_{\text{Unc}}$. Moreover, in the experiments in Section 7, we show empirically that this approach does indeed not perform substantially better than the two standalone estimators.

The finite sample learning bound for the averaging estimator, $\hat{\tau}_{\text{Avg}}(\lambda)$, is give as follows.

Theorem 7 (Finite sample learning bound for τ_{Avg} .) *Let $\hat{\tau}_{\text{Avg}}(\lambda)$ be as in (25) and $\lambda \in [0, 1]$. Then, if Assumption 3 holds true, we have that, with probability at least $1 - p$,*

$$\epsilon_{\text{PEHE}}(\hat{\tau}_{\text{Avg}}(\lambda)) \leq \tilde{\mathcal{O}}\left((1 - \lambda)\bar{d}_{\infty}(p_{\phi}^{\text{Conf}} \mid p_{\phi}^{\text{Unc}}) \frac{\mathcal{C}_{\Phi} + \mathcal{C}_{\mathcal{H}}}{\sqrt{n^{\text{Unc}}}} + \lambda \frac{\mathcal{C}_{\Phi} + \mathcal{C}_{\mathcal{H}}}{\sqrt{n^{\text{Conf}}}}\right) + 2\lambda\Delta, \quad (27)$$

where \mathcal{C}_{Φ} and $\mathcal{C}_{\mathcal{H}}$ are the same constants depending on the complexity of the neural networks as in Theorem 2 and $\Delta = \mathbb{E}[\left((\delta_1 - \delta_0) \circ \phi^*(X^{\text{Conf}})\right)^2]$ is the bias due to unobserved confounding.

Proof See Appendix C.4. ■

The above error bound is dependent on the hyperparameter λ . If, hypothetically, we chose the optimal hyperparameter λ for every particular data instance, then we would obtain the following error bound, which is strictly smaller than the above result.

Corollary 8 (*Learning bound with optimal λ .*) Let $\hat{\tau}_{\text{Avg}}(\lambda)$ be as in (25). Then, if Assumption 3 holds true, we have that, with probability at least $1 - p$,

$$\min_{\lambda \in [0,1]} \epsilon_{\text{PEHE}}(\hat{\tau}_{\text{Avg}}(\lambda)) \leq \min \left(\tilde{\mathcal{O}} \left(\bar{d}_{\infty}(p_{\phi}^{\text{Conf}} | p_{\phi}^{\text{Unc}}) \frac{\mathcal{C}_{\Phi} + \mathcal{C}_{\mathcal{H}}}{\sqrt{n^{\text{Unc}}}} \right), \tilde{\mathcal{O}} \left(\frac{\mathcal{C}_{\Phi} + \mathcal{C}_{\mathcal{H}}}{\sqrt{n^{\text{Conf}}}} \right) + 2\Delta \right), \quad (28)$$

where \mathcal{C}_{Φ} and $\mathcal{C}_{\mathcal{H}}$ are the same constants depending on the complexity of the neural networks as in Theorem 2 and $\Delta = \mathbb{E} \left[((\delta_1 - \delta_0) \circ \phi^*(X^{\text{Conf}}))^2 \right]$ is the bias due to unobserved confounding.

Proof The proof follows immediately from Theorem 7 using $\lambda = \mathbf{1} \{ \bar{d}_{\infty}(p_{\phi}^{\text{Conf}} | p_{\phi}^{\text{Unc}}) \frac{\mathcal{C}_{\Phi} + \mathcal{C}_{\mathcal{H}}}{\sqrt{n^{\text{Unc}}}} \geq \frac{\mathcal{C}_{\Phi} + \mathcal{C}_{\mathcal{H}}}{\sqrt{n^{\text{Conf}}}} + 2\Delta \}$. ■

Corollary 8 shows that, even with the optimal hyperparameter λ , the averaging estimator does not achieve more than a constant factor improvement over the best of $\hat{\tau}_{\text{Unc}}$ or $\hat{\tau}_{\text{Conf}}$. In particular, the error bound in Corollary 8 is, up to constant factors, exactly the minimum of the error bounds of the estimator on randomized data (see Theorem 4) and the estimator on observational data (see Theorem 5). Because the averaging estimator spans both of these estimators (depending on the choice of λ), it is to be expected that the best possible averaging estimator does at least as well as either of these two estimators; surprisingly, it does no better.

5.3.4 WEIGHTED RISK ESTIMATOR (τ_{Weight})

In the last section, we studied an estimator that combines two separate estimators, and now we consider an estimator, which is directly learned on a combination of observational and randomized data. That is, we use a weighted regression combining observational and randomized data, but assign a higher weight to randomized data. Formally, again using neural networks for fair comparison, this yields the following weighted risk minimization procedure

$$\hat{\phi}, \hat{\mathbf{h}} = \arg \min_{\phi \in \Phi, \mathbf{h} \in \mathcal{H}^{\otimes 2}} \hat{\epsilon}_{\text{Weight}}(\mathbf{h}, \phi), \quad (29)$$

where the weighted empirical risk is given by

$$\hat{\epsilon}_{\text{Weight}}(\mathbf{h}, \phi) = \frac{1}{\Lambda n^{\text{Unc}} + n^{\text{Conf}}} \left(\Lambda \sum_{i=1}^{n^{\text{Unc}}} (\mathbf{h}_{i^{\text{Unc}}} \circ \phi(x_i^{\text{Unc}}) - y_i^{\text{Unc}})^2 + \sum_{i=1}^{n^{\text{Conf}}} (\mathbf{h}_{i^{\text{Conf}}} \circ \phi(x_i^{\text{Conf}}) - y_i^{\text{Conf}})^2 \right), \quad (30)$$

where $\Lambda \in [0, \infty)$ is a hyperparameter. For $\Lambda \rightarrow \infty$, we recover $\hat{\tau}_{\text{Unc}}$, i. e., the estimator which only uses randomized data. Vice versa, for $\Lambda = 0$, we obtain $\hat{\tau}_{\text{Conf}}$, i. e., the estimator which only uses observational data.

Then, the CATE estimator which weighted risk minimization procedure is given by

$$\hat{\tau}_{\text{Weight}}(\Lambda) = (\hat{\mathbf{h}}_1 - \hat{\mathbf{h}}_0) \circ \hat{\phi}(x). \quad (31)$$

We derive finite sample error bounds for $\hat{\tau}_{\text{Weight}}$ as follows.

Theorem 9 (*Finite sample learning bound for τ_{Weight} .*) *Let $(\hat{\mathbf{h}}, \hat{\phi})$ be the empirical loss minimizer from (29) and $\hat{\tau}_{\text{Weight}}(\Lambda)$ as in (31). Then, if Assumption 3 holds true, we have that, with probability at least $1 - p$,*

$$\epsilon_{\text{PEHE}}(\hat{\tau}_{\text{Weight}}(\Lambda)) \leq \tilde{\mathcal{O}}\left((1 - \lambda)\bar{d}_{\infty}(p_{\phi}^{\text{Conf}} | p_{\phi}^{\text{Unc}}) \frac{\mathcal{C}_{\Phi} + \mathcal{C}_{\mathcal{H}}}{\sqrt{n^{\text{Unc}}}} + \lambda \frac{\mathcal{C}_{\Phi} + \mathcal{C}_{\mathcal{H}}}{\sqrt{n^{\text{Conf}}}}\right) + 2\lambda\Delta, \quad (32)$$

where $\lambda = \frac{n^{\text{Conf}}}{\Lambda n^{\text{Unc}} + n^{\text{Conf}}} \in [0, 1]$. Moreover, \mathcal{C}_{Φ} and $\mathcal{C}_{\mathcal{H}}$ are the same constants depending on the complexity of the neural networks as in Theorem 2 and $\Delta = \mathbb{E}\left[\left((\delta_1 - \delta_0) \circ \phi^*(X^{\text{Conf}})\right)^2\right]$ is the bias due to unobserved confounding.

Proof See Appendix C.5. ■

The above error bound depends on the constant $\lambda = \frac{n^{\text{Conf}}}{\Lambda n^{\text{Unc}} + n^{\text{Conf}}}$. If, hypothetically, we could choose the optimal λ (via the hyperparameter Λ) for every particular data instance, we would obtain the following, strictly smaller, error bound.

Corollary 10 (*Learning bound with optimal λ .*) *Let $\hat{\tau}_{\text{Weight}}(\Lambda)$ be as in (31). Then, if Assumption 3 holds true, we have that, with probability at least $1 - p$,*

$$\min_{\Lambda \in [0, \infty)} \epsilon_{\text{PEHE}}(\hat{\tau}_{\text{Weight}}(\Lambda)) \leq \min\left(\tilde{\mathcal{O}}\left(\bar{d}_{\infty}(p_{\phi}^{\text{Conf}} | p_{\phi}^{\text{Unc}}) \frac{\mathcal{C}_{\Phi} + \mathcal{C}_{\mathcal{H}}}{\sqrt{n^{\text{Unc}}}}\right), \tilde{\mathcal{O}}\left(\frac{\mathcal{C}_{\Phi} + \mathcal{C}_{\mathcal{H}}}{\sqrt{n^{\text{Conf}}}}\right) + 2\Delta\right), \quad (33)$$

where \mathcal{C}_{Φ} and $\mathcal{C}_{\mathcal{H}}$ are the same constants depending on the complexity of the neural networks as in Theorem 2 and $\Delta = \mathbb{E}\left[\left((\delta_1 - \delta_0) \circ \phi^*(X^{\text{Conf}})\right)^2\right]$ is the bias due to unobserved confounding.

Proof The proof immediately follows from Theorem 9 using $\lambda = \mathbf{1}\left\{\bar{d}_{\infty}(p_{\phi}^{\text{Conf}} | p_{\phi}^{\text{Unc}}) \frac{\mathcal{C}_{\Phi} + \mathcal{C}_{\mathcal{H}}}{\sqrt{n^{\text{Unc}}}} \geq \frac{\mathcal{C}_{\Phi} + \mathcal{C}_{\mathcal{H}}}{\sqrt{n^{\text{Conf}}}} + 2\Delta\right\}$. ■

Corollary 10 shows that the weighted risk minimization achieves exactly the same bound as the averaging estimator (Corollary 8). Thus, the weighted risk minimization also does not achieve more than a constant factor improvement over the best of $\hat{\tau}_{\text{Unc}}$ or $\hat{\tau}_{\text{Conf}}$. Similar to the averaging estimator, the weighted estimator spans both of these estimators (depending on the choice of λ) and we would expect that the best possible weighted estimator does at least as well as either of these two estimators; again, surprisingly, it does no better.

5.3.5 COMPARISON WITH BASELINES AND IMPROVEMENT CONDITIONS

In this section, we derive conditions for our two-step procedure should be used. In particular, we compare the error bounds of our estimator against the ones of the baseline alternatives. Based on this, we derive conditions for when our two-step procedure improves upon the baselines and when we should rely on one of the baseline estimators.

For ease of comparison, we tabulate the error bounds (up to constants) in Table 2. Recall that we are interested in the regime where n^{Conf} is large and n^{Unc} is small, since the latter originates from an RCT. Even with infinite observational samples, the error bound of $\hat{\tau}_{\text{Conf}}$ does not vanish due to its bias Δ . The error bound of $\hat{\tau}_{\text{Unc}}$ can also be very large, especially when $n^{\text{Unc}} < \bar{d}_{\infty}(p_{\phi}^{\text{Conf}} | p_{\phi}^{\text{Unc}})(\mathcal{C}_{\Phi} + \mathcal{C}_{\mathcal{H}})$. Moreover, since the number of randomized samples is small and fixed, the error bound of $\hat{\tau}_{\text{Unc}}$ does not converge to zero the more observational data is used. The estimators $\hat{\tau}_{\text{Avg}}$ and $\hat{\tau}_{\text{Weight}}$ do not improve upon this by more than a constant factor. Our estimator, $\hat{\tau}_{\text{Cor}}$, is the only approach which leverages observational data and enables its error bound to converge to zero the more data is used.

Table 2: Comparison of error bounds (up to constants and polylogarithmic factors) across estimators. We denote observational and randomized samples as $n = (n^{\text{Unc}}, n^{\text{Conf}})$.

Estimator	Error bound	$\epsilon_{\text{PEHE}}(\hat{\tau}) \xrightarrow{n \rightarrow \infty} 0$
$\hat{\tau}_{\text{Unc}}$	$\bar{d}_{\infty}(p_{\phi}^{\text{Conf}} p_{\phi}^{\text{Unc}}) \frac{\mathcal{C}_{\Phi} + \mathcal{C}_{\mathcal{H}}}{\sqrt{n^{\text{Unc}}}}$	✓
$\hat{\tau}_{\text{Conf}}$	$\frac{\mathcal{C}_{\Phi} + \mathcal{C}_{\mathcal{H}}}{\sqrt{n^{\text{Conf}}}} + 2\Delta$	✗
$\hat{\tau}_{\text{Avg}}(\lambda)$	$(1 - \lambda) \bar{d}_{\infty}(p_{\phi}^{\text{Conf}} p_{\phi}^{\text{Unc}}) \frac{\mathcal{C}_{\Phi} + \mathcal{C}_{\mathcal{H}}}{\sqrt{n^{\text{Unc}}}} + \lambda \frac{\mathcal{C}_{\Phi} + \mathcal{C}_{\mathcal{H}}}{\sqrt{n^{\text{Conf}}}} + 2\lambda\Delta$	✗
$\hat{\tau}_{\text{Weight}}(\Lambda)$	$(1 - \lambda) \bar{d}_{\infty}(p_{\phi}^{\text{Conf}} p_{\phi}^{\text{Unc}}) \frac{\mathcal{C}_{\Phi} + \mathcal{C}_{\mathcal{H}}}{\sqrt{n^{\text{Unc}}}} + 2\lambda \frac{\mathcal{C}_{\Phi} + \mathcal{C}_{\mathcal{H}}}{\sqrt{n^{\text{Conf}}}} + 2\lambda\Delta$	✗
$\hat{\tau}_{\text{Cor}}$	$\frac{\mathcal{C}_{\Phi} + \mathcal{C}_{\mathcal{H}}}{\sqrt{n^{\text{Conf}}}} + \frac{d_{\infty}(p_{\phi}^{\text{Conf}} p_{\phi}^{\text{Unc}}) \mathcal{C}_{\mathcal{B}}}{\sqrt{n^{\text{Unc}}}}$	✓

Based on these finite sample error bounds, we now derive theoretical conditions for when our estimator yields superior performance compared to the baselines. We compare our estimator *empirically* against the above baseline estimators and further baselines in Section 7. For the theoretical conditions, we focus on $\hat{\tau}_{\text{Unc}}$ and $\hat{\tau}_{\text{Conf}}$. In the following proposition, we provide conditions for when the error of our estimator can improve upon the baseline estimators.

Proposition 11 (*Improvement conditions.*) *The error of our estimator, $\hat{\tau}_{\text{Cor}}$, can be substantially lower than the error of $\hat{\tau}_{\text{Unc}}$, if*

$$\frac{\mathcal{C}_{\Phi} + \mathcal{C}_{\mathcal{H}}}{\bar{d}_{\infty}(p_{\phi}^{\text{Conf}} | p_{\phi}^{\text{Unc}})(\mathcal{C}_{\Phi} + \mathcal{C}_{\mathcal{H}}) - d_{\infty}(p_{\phi}^{\text{Conf}} | p_{\phi}^{\text{Unc}})\mathcal{C}_{\mathcal{B}}} < \sqrt{\frac{n^{\text{Conf}}}{n^{\text{Unc}}}}, \quad (\text{C1})$$

and substantially lower than the error of $\hat{\tau}_{\text{Conf}}$, if

$$\frac{d_{\infty}(p_{\phi}^{\text{Conf}} | p_{\phi}^{\text{Unc}})\mathcal{C}_{\mathcal{B}}}{\sqrt{n^{\text{Unc}}}} < 2\Delta. \quad (\text{C2})$$

Proof See Appendix D.1. ■

In the following, we will discuss both conditions.

Condition (C1): The benefit of combining observational and randomized data (i. e., $\hat{\tau}_{\text{Cor}}$) over only using *randomized data* (i. e., $\hat{\tau}_{\text{Unc}}$) hinges again on three factors: (i) the distributional discrepancy, $d_\infty(p_\phi^{\text{Conf}} | p_\phi^{\text{Unc}})$, (ii) the size of observational data, n^{Conf} , and (iii) the complexity of the bias function, $\mathcal{C}_\mathcal{B}$:

- (i) A large distributional discrepancy acts in favor of satisfying the condition. This may sound counterintuitive at first. However, the larger the distributional discrepancy between observational and randomized data, the more useful observational data becomes for learning the representation, because the covariates in the observational data follow the distribution of interest, while the randomized data does not. In particular, if $\bar{d}_\infty(p_\phi^{\text{Conf}} | p_\phi^{\text{Unc}})$ and $d_\infty(p_\phi^{\text{Conf}} | p_\phi^{\text{Unc}})$ increases (but $\bar{d}_\infty(p_\phi^{\text{Conf}} | p_\phi^{\text{Unc}}) > d_\infty(p_\phi^{\text{Conf}} | p_\phi^{\text{Unc}})$ and, usually, $\mathcal{C}_\Phi + \mathcal{C}_\mathcal{H} > \mathcal{C}_\mathcal{B}$), a larger distributional discrepancy results in a larger denominator in the left-hand side of (C1). This makes it easier to satisfy condition.
- (ii) When n^{Conf} is sufficiently large, but n^{Unc} is relatively small (i. e., precisely our setting), it is also very likely that the condition is satisfied. This is because the representation and the confounded hypotheses can be learned with the observational data and then debiased with the randomized data. In particular, a larger n^{Conf} implies a larger $\sqrt{\frac{n^{\text{Conf}}}{n^{\text{Unc}}}}$, which makes it easier to satisfy the condition in (C1). This justifies the use of large amounts of observational data in our procedure.
- (iii) A complex bias function does not act in favor of satisfying the condition. This is because a complex bias function would increase also the left-hand side of (C1) via $\mathcal{C}_\mathcal{B}$ and, hence, would make it less likely for the condition to be satisfied. If the complexity of the bias function is very large, we are better off only using randomized data.

Condition (C2): The benefit of combining observational with randomized data (i. e., $\hat{\tau}_{\text{Cor}}$) over only using *observational data* (i. e., $\hat{\tau}_{\text{Conf}}$) hinges on the bias due to unobserved confounding, Δ . In other words, if there is substantial unobserved confounding, which results in a large bias and, thus a large Δ , then combining observational and randomized data in our estimator can yield substantially lower errors. Conversely, when the bias is small, using only observational data can be better.

In sum, in our regime of interest, i. e., there exist unobserved confounding, n^{Conf} is large, and n^{Unc} is small, the above conditions are likely be satisfied, and, hence, it is beneficial to combine observational data *and* randomized data using our two-procedure.

5.3.6 SAMPLE COMPLEXITY

The above results can also be interpreted in terms of sample complexity. That is, how many samples are required to ensure an estimation error below a particular threshold with high probability. To this end, let us consider a decision-maker that aims at a non-trivial estimation error of $\eta < \Delta$. First, note that $\hat{\tau}_{\text{Conf}}$ cannot achieve this error even with infinitely many observational samples, since it is lower bounded by Δ . Based on the bounds in Table 2, it is straightforward to show that the estimator on randomized data, $\hat{\tau}_{\text{Unc}}$, requires at least $\sqrt{n^{\text{Unc}}} = \tilde{O}(\bar{d}_\infty(p_\phi^{\text{Conf}} | p_\phi^{\text{Unc}}) \frac{\mathcal{C}_\Phi + \mathcal{C}_\mathcal{H}}{\eta})$ regardless of the size of observational data. In contrast, if n^{Conf} is large enough such that $\frac{\mathcal{C}_\Phi + \mathcal{C}_\mathcal{H}}{\sqrt{n^{\text{Conf}}}} \leq d_\infty(p_\phi^{\text{Conf}} | p_\phi^{\text{Unc}}) \frac{\mathcal{C}_\mathcal{B}}{\sqrt{n^{\text{Unc}}}}$, our two-step

procedure only requires $\sqrt{n^{\text{Unc}}} = \tilde{O}(d_\infty(p_\phi^{\text{Conf}} | p_\phi^{\text{Unc}}) \frac{2\mathcal{C}_B}{\eta})$. In other words, if sufficient observational data is available and the bias function is less complex than the representation and hypotheses, i. e., $2\mathcal{C}_B < \mathcal{C}_\Phi + \mathcal{C}_H$, then the number of randomized samples required to achieve η is substantially smaller. This is particularly interesting, since in order to achieve the same error as τ_{Unc} , we need less randomized data. As a directly implication, less costly randomized data needs to be acquired and less subjects enrolled in an RCT, which could substantially accelerate drug safety and evaluation.

6. CorNet: an Algorithm for Combining Observational and Randomized Data

We propose an instantiation of our two-step procedure for estimating CATE. Our algorithm for **C**ombining **O**bservational and **R**andomized data is based on neural **N**etworks, and, thus, we call it **CorNet**. Guided by the theoretical insights from Section 5, we propose a sample-efficient algorithm of CorNet, which first learns a *balanced*⁹ shared representation and confounded hypothesis using observational data and, then, debiases the confounded hypotheses by learning the bias functions while regularizing its complexity. In particular, we let Φ be parametrized by neural networks, while \mathcal{H} and \mathcal{B} are parametrized by linear functions, i. e., $h_t^c \circ \phi^*(x) = \phi^*(x) \mathbf{w}_t^c$ and $h_t^u \circ \phi^*(x) = \phi^*(x)(\mathbf{w}_t^c + \boldsymbol{\delta}_t)$, where $\mathbf{w}_t^c, \boldsymbol{\delta}_t \in \mathbb{R}^{d_\phi}$. Moreover, we prove that this instantiation satisfies Condition 1.

6.1 Learning a Balanced Representation

In the first step, we learn a shared representation and the confounded hypotheses using observational data as proposed in Section 4.2. As discussed in Section 5.2, the distributional discrepancy between observational and randomized covariate distributions is an important factor in the finite sample error bound (Theorem 2), which should be accounted for. For this, we seek a representation ϕ and a confounded hypothesis \mathbf{h}^c which minimize the trade-off between predictive accuracy and distributional discrepancy. That is, ϕ (together with \mathbf{h}^c) should be predictive of the confounded outcome Y^{Conf} , and the distribution of X^{Unc} and X^{Conf} in the representation space should be balanced.¹⁰ Balancing of the distributions is achieved by regularizing for a distributional metric (either by directly computing the metric, or by using adversarial learning) in the learning procedure. However, since we only observe a small sample from the randomized data, standard approaches are not directly applicable. That is because estimating the distributional metric based on scarce data is difficult. While any approach for balancing the distributions can be chosen, we propose to combine adversarial learning with data augmentation similar to Wang et al. (2019). We refer to Section 6.4.2 for an in-depth discussion.

9. A balanced representation is a representation in which the distribution of $\phi(X^{\text{Conf}})$ and $\phi(X^{\text{Unc}})$ are similar with respect to some distributional discrepancy measure.

10. In particular, this means that the push-forwards of the covariate distributions p_x^{Unc} and p_x^{Conf} through ϕ should be similar.

6.2 Regularizing the Complexity of the Bias Function Class

In the second step, we use the shared representation and confounded hypothesis from in the first step together with randomized data to debias the confounded hypotheses. That is, we learn the bias function δ .

As discussed in Section 5.2, the complexity of the bias function class is an important factor in the finite sample error bound (Theorem 2) and, thus, should be accounted for in our algorithm. For this, we regularize the bias function, which imposes structure on the bias function. Regularizing the bias has two advantages: (i) it decreases the error bound in Theorem 2, since we decrease the complexity of the bias function, $\mathcal{C}_{\mathcal{B}}$. As such, we may achieve faster lower error with less data, which is particularly favorable in our setting. (ii) The second step of our procedure is a high-dimensional inference problem, since the representation is often high-dimensional and the randomized sample size is small. As such, the inference of the parameters δ requires regularization, since the small sample size prohibits inference otherwise (Meinshausen and Bühlmann, 2006; Bühlmann and van de Geer, 2011). In particular, we use the L_1 -norm to regularize the bias function, which imposes sparsity on the bias function (in the representation) and renders the second step as a Lasso regression.

Two questions arise: (i) why not directly learning the unconfounded hypotheses \mathbf{w}^u and (ii) why not using L_2 -regularization to circumvent the high-dimensional inference problem? Both are discussed in the following.

- (i) Directly learning the unconfounded hypotheses (without further structural restrictions) is prohibited by the small sample size of the randomized data. Therefore, some structural restrictions via a regularization have to be imposed. However, imposing such restrictions (e. g., sparsity) on the hypotheses directly may be more restrictive than imposing restrictions on the difference between the confounded and unconfounded hypotheses (i. e., the bias). That is since observational and randomized data are closely related, which may allow to impose more structure on the bias function.
- (ii) While L_2 -regularization would also circumvent the high-dimensional inference problem, the choice of regularization (i. e., L_1 - or L_2 -regularization) depends on the implicit assumptions we make on the data-generating process. That is, whether we implicitly assume that unobserved confounding in the observational data affects a subset of entries of δ (i. e., δ is sparse in $\phi(X)$), and, hence, we use a L_1 -regularization. On the contrary, the L_2 -regularization implicitly assumes that all covariates in the representation $\phi(X)$ influence the bias function δ . However, we argue that there are often unobserved confounders that systematically affect a subset of the features, creating a bias between the observational and randomized data. For instance, the difference in the patient records from different hospitals (such as hospitals from the RCT and hospitals from the OS) may arise in the difference of how some diagnoses are recorded, but likely not how all diagnoses are recorded (Bastani, 2021). Therefore, the bias induces by these differences can be explained by the few covariates corresponding to the subset of diagnoses where differences arise. Note that both regularizations are feasible and the decision which one is used has to be made by the user. In the experiments in Section 7, we conduct an ablation study on the type of regularization and find that, indeed, for most datasets, an L_1 -regularization yields better results, but in some cases, an L_2 -regularization works better.

6.3 CorNet Algorithm

In this section, we present the actual algorithm for CorNet and discuss some of its theoretical properties. We defer a in-depth theoretical discussion to Appendix E. We present the algorithm of CorNet in Algorithm 1.

Algorithm 1: CorNet algorithm

Input: Observational data $\{(x_i^{\text{Conf}}, t_i^{\text{Conf}}, y_i^{\text{Conf}})\}_{i=1}^{n^{\text{Conf}}}$ and randomized data $\{(x_i^{\text{Unc}}, t_i^{\text{Unc}})y_i^{\text{Unc}}\}_{i=1}^{n^{\text{Unc}}}$

Output: $\hat{\phi}, \hat{\mathbf{w}}^c = (\hat{\mathbf{w}}_1^c, \hat{\mathbf{w}}_0^c), \hat{\boldsymbol{\delta}} = (\hat{\boldsymbol{\delta}}_1, \hat{\boldsymbol{\delta}}_0)$

Step 1. Compute

$$\hat{\phi}, \hat{\mathbf{w}}^c = \arg \min_{\phi \in \Phi, \mathbf{w}^c \in \mathbb{R}^{d_\phi \otimes 2}} \frac{1}{n^{\text{Conf}}} \sum_{i=1}^{n^{\text{Conf}}} (\phi(x_i^{\text{Conf}}) \mathbf{w}_{t_i^{\text{Conf}}}^c - y_i^{\text{Conf}})^2 \quad (34)$$

$$+ \lambda_d \mathcal{D}(\{\phi(x_i^{\text{Conf}})\}_{i=1}^{n^{\text{Conf}}}, \{\phi(x_i^{\text{Unc}})\}_{i=1}^{n^{\text{Unc}}}) \quad (35)$$

Step 2. Compute

$$\hat{\boldsymbol{\delta}} = \arg \min_{\boldsymbol{\delta} \in \mathbb{R}^{d_\phi \otimes 2}} \frac{1}{n^{\text{Unc}}} \sum_{i=1}^{n^{\text{Unc}}} (\hat{\phi}(x_i^{\text{Unc}}) (\hat{\mathbf{w}}_{t_i^{\text{Unc}}}^c + \boldsymbol{\delta}_{t_i^{\text{Unc}}}) - y_i^{\text{Unc}})^2 + \lambda_\delta \|\boldsymbol{\delta}\|_1 \quad (36)$$

Most theoretical results from Section 5 remain in tact, since only the complexities of the function classes change (see Appendix E for details). Here, we prove that Condition 1 is satisfied for CorNet.

Proposition 12 *For the function classes as in Algorithm 1, i. e., neural networks for Φ and linear functions for \mathcal{H} and \mathcal{B} , the condition $d_{\mathcal{B}, \boldsymbol{\delta}}(\hat{\phi}; \phi^*) \leq \gamma d_{\mathcal{H}, \mathbf{h}^c}(\hat{\phi}; \phi^*)$, for some $\gamma > 0$ is satisfied.*

Proof See Appendix E.4. ■

Once we obtain $\hat{\phi}$, $\hat{\mathbf{w}}^c$, and $\hat{\boldsymbol{\delta}}$, the estimator for the CATE is given by

$$\hat{\tau}_{\text{CorNet}}(x) = \hat{\phi}(x) (\hat{\mathbf{w}}_1^c + \hat{\boldsymbol{\delta}}_1 - \hat{\mathbf{w}}_0^c - \hat{\boldsymbol{\delta}}_0). \quad (37)$$

In Algorithm 1, \mathcal{D} denotes the distributional discrepancy between observational and randomized data. The specific expression depends on the method for balancing and can be chosen by the user. We detail our choice in Section 6.4.2. Further, the hyperparameter λ_d trades off the predictive accuracy and the distributional discrepancy in the first step, and λ_δ regularizes the complexity of the bias function in the second step.

Remark 13 *Note that, when $\lambda_\delta \rightarrow \infty$, we recover the estimator that only uses observational data. This can be seen by recognizing that $\hat{\mathbf{w}}^u = \hat{\mathbf{w}}^c + \boldsymbol{\delta}$ and $\boldsymbol{\delta} \rightarrow \mathbf{0}$ for $\lambda_\delta \rightarrow \infty$.*

Remark 14 In Algorithm 1, the hyperparameter λ_d and λ_δ must be chosen. This can be done by hyperparameter optimization (e. g., grid search) using a validation set. However, since n^{Unc} is small, we do not want to sacrifice any randomized samples for the hyperparameter optimization of λ_d and λ_δ . For the choice of λ_δ , we recognize that the second step is a Lasso regression and, based on high-dimensional statistics theory, the optimal choice of the regularization parameter is $\lambda_\delta = \sqrt{c_0 \log(d_\phi) / \log(n^{\text{Unc}})}$ (e. g., Bühlmann and van de Geer, 2011). In particular, in our experiments, the constant c_0 is set to $1/d_\phi$. Moreover, we choose $\lambda_d = \lambda_\delta$, since the distributional discrepancy has the same impact on the finite sample error as the complexity of the bias functions. Hence, we attribute the same importance to both factors.

6.4 Practical Considerations

In this section, we discuss two practical considerations of our algorithm. First, we need to ensure that the bias function is identifiable from the randomized data, and, second, we detail how a balanced representation can be learned with only few randomized samples.

6.4.1 IDENTIFIABILITY OF THE BIAS FUNCTION

Here, we discuss the identifiability of the bias function δ in the second step. For this, we assume that the so-called ‘‘compatibility conditions’’, a condition from the theory of high-dimensional statistics (e. g., Bühlmann and van de Geer, 2011), is satisfied. We discuss this condition in the following.

In the second step of our Algorithm 1, we are given an estimate of the representation function $\hat{\phi}$. Based on this, we have to ensure that δ_t can be identified from $\hat{\phi}(\mathbf{X}_t^{\text{Unc}})$, where $\mathbf{X}_t^{\text{Unc}}$ is the (unconfounded) design matrix for all samples with $T = t$ for $t \in \{0, 1\}$. For this, we define the (unconfounded) sample covariance matrix

$$\Sigma_t^{\text{Unc}}(\hat{\phi}) = \frac{1}{n^{\text{Unc}}} \hat{\phi}(\mathbf{X}_t^{\text{Unc}})^\top \hat{\phi}(\mathbf{X}_t^{\text{Unc}}). \quad (38)$$

In order to ensure that δ_t is identifiable from $\hat{\phi}(\mathbf{X}_t^{\text{Unc}})$, we could assume that $\hat{\phi}(\mathbf{X}_t^{\text{Unc}})$ is positive-definite, i. e., for any vector $\mathbf{v} \in \mathbb{R}^{d_\phi}$, $\mathbf{v}^\top \hat{\phi}(\mathbf{X}_t^{\text{Unc}}) \mathbf{v} > 0$. This, however, is infeasible in our setting, since n^{Unc} is small and, hence, $n^{\text{Unc}} < d_\phi$. Therefore, there exists collinearity in features. The compatibility condition is a strictly weaker condition, since, for instance, it allows for collinearity in features outside of the index set¹¹ $S_t = \text{supp}(\delta_t)$ ¹², which is often the case in a high-dimensional setting such as ours.

We assume that the following compatibility condition holds for the (unconfounded) sample covariance matrix, $\Sigma_t^{\text{Unc}}(\hat{\phi})$, and the index set $S_t = \text{supp}(\delta_t)$, for each $t \in \{0, 1\}$.

Compatibility Condition. The compatibility condition is satisfied if for an index set $S \subseteq \{1, \dots, d\}$ and a matrix $\Sigma \in \mathbb{R}^{d \times d}$, there exists $\rho > 0$ such that, for all $\mathbf{v} \in \mathbb{R}^d$ satisfying

-
11. An index set S is a set $S \subseteq \{1, \dots, d\}$. Then, for any vector $\mathbf{v} \in \mathbb{R}^d$, the vector $\mathbf{v}_S \in \mathbb{R}^d$ is obtained by setting the entries in \mathbf{v} which are not in S to zero. Furthermore, S^c denotes the complement of the index set.
 12. The support of a vector $\mathbf{v} \in \mathbb{R}^d$, denoted as $\text{supp}(\mathbf{v}) \subseteq \{1, \dots, d\}$, is the set of indices corresponding to nonzero entries of \mathbf{v} .

$\|\mathbf{v}_{S^c}\|_1 \leq 3\|\mathbf{v}_S\|_1$, it holds that

$$\|\mathbf{v}_S\|_1^2 \leq \frac{|S|}{\rho^2} \mathbf{v}^\top \mathbf{v}. \quad (39)$$

This assumption is standard in the high-dimensional statistics literature to ensure the convergence of high-dimensional estimators such as the Dantzig selector or Lasso (Candes and Tao, 2007; Bickel et al., 2009; Bühlmann and van de Geer, 2011).

Note that we make this assumption for the bias function $\boldsymbol{\delta}_t$ and not the unconfounded hypothesis \mathbf{w}_t^u directly. We do so, since we only need to estimate the bias vector $\boldsymbol{\delta}_t$ in the second step of our algorithm. In particular, if the bias is sparse enough, i. e., $\|\boldsymbol{\delta}_t\|_1$ is small, the compatibility condition in (39) is satisfied.

Furthermore, the compatibility condition is always satisfied if $\boldsymbol{\Sigma}_t^{\text{Unc}}(\hat{\phi})$ is positive-definite. This can be seen by letting $\psi > 0$ the minimum eigenvalue of $\boldsymbol{\Sigma}_t^{\text{Unc}}(\hat{\phi})$. Then, the compatibility condition is satisfied with the constant $\rho_0 = \sqrt{\psi}$ for an index set. Hence, the compatibility condition is strictly weaker than positive definiteness. This is particularly relevant, since positive definiteness for the unconfounded covariance matrix might not hold true due to the small samples size of the randomized data. As such, even if \mathbf{w}_t^u is not identifiable, we may be able to identify the bias function $\boldsymbol{\delta}_t$.

6.4.2 BALANCING REPRESENTATION VIA AUGMENTED DISTRIBUTION ALIGNMENT

In Algorithm 1, we regularize for the distributional discrepancy between the covariate distributions in the representation space, $\mathcal{D}(\{\phi(x_i^{\text{Conf}})\}_{i=1}^{n^{\text{Conf}}}, \{\phi(x_i^{\text{Unc}})\}_{i=1}^{n^{\text{Unc}}})$. We do this, since the distributional discrepancy is a driving factor in the learning bound from Theorem 2. Regularizing for the distributional discrepancy, so-called balancing, is not straightforward in our setting, since the small sample size of the randomized data may cause instability in optimization and leads to performance degradation. While several approaches for balancing exist from the fields of domain adaptation (Ganin and Lempitsky, 2015; Ganin et al., 2016) and causal inference (e. g., Shalit et al., 2017; Zhang et al., 2020), these approaches assume large sample sizes and, therefore, are not directly applicable in our setting.

As a remedy, we adopt an adversarial distribution alignment approach using augmented data (Wang et al., 2019). For this, Wang et al. (2019) propose to iteratively generate new samples by interpolating between the observational and the randomized samples similar to the *mixup* approach for supervised learning (Zhang et al., 2018). This has two advantages: First, the new samples enlarge the training data set, which leads to a more stable optimization (particularly for neural networks). Second, since the new samples are generated by interpolating between observational and randomized samples, the distribution of the interpolated samples is expected to be closer to the observational distribution as proven in Wang et al. (2019). We use these new samples to augment the existing randomized samples and, based on this, minimize the distributional discrepancy using adversarial learning.

Mathematically, let x^{Unc} and x^{Conf} be observational and randomized covariate samples. Then, we sample from the following density function

$$p_\mu(x | x^{\text{Unc}}, x^{\text{Conf}}) = \mathbf{1}_{\{\mu x^{\text{Unc}} + (1-\mu)x^{\text{Conf}}\}}(x), \quad (40)$$

where $\mathbf{1}_{\{\cdot\}}(\cdot)$ is the indicator function and $\mu \sim \text{Beta}(\alpha, \alpha)$, with $\alpha > 0$. Sampling from this density is equivalent to linearly interpolating between x^{Unc} and x^{Conf} via

$$\tilde{x} = \mu x^{\text{Unc}} + (1 - \mu) x^{\text{Conf}}, \quad (41)$$

where, for each sample x^{Conf} , a sample x^{Unc} is randomly chosen from all randomized samples and $\mu \sim \text{Beta}(\alpha, \alpha)$ determines the degree of interpolation. The interpolated sample is denoted by \tilde{x} .

Based on the samples from the above density, $\{\tilde{x}_i\}_{i=1}^m$, for large enough m , we balance the empirical distribution of $\tilde{\mathcal{U}} = \{\phi(\tilde{x}_i)\}_{i=1}^m$ and $\mathcal{U}^{\text{Conf}} = \{\phi(x_i^{\text{Conf}})\}_{i=1}^{n^{\text{Conf}}}$. Here, both m and n^{Conf} are large.¹³ In order to measure the distributional discrepancy, we use the H -divergence between interpolated and confounded samples as inspired by domain adaptation (Ben-David et al., 2010). We optimize the H -divergence, $\hat{d}_H(\tilde{\mathcal{U}}, \mathcal{U}^{\text{Conf}})$, using adversarial learning and a gradient reverse layer (GRL) (Ganin and Lempitsky, 2015).¹⁴ This renders step 1 in Algorithm 1 as

$$\arg \min_{\phi \in \Phi, \mathbf{w}^c \in \mathbb{R}^{d_\phi \otimes 2}} \frac{1}{n^{\text{Conf}}} \sum_{i=1}^{n^{\text{Conf}}} (\phi(x_i^{\text{Conf}}) \mathbf{w}_{t_i^{\text{Conf}}}^c - y_i^{\text{Conf}})^2 + \lambda_d \hat{d}_H(\tilde{\mathcal{U}}, \mathcal{U}^{\text{Conf}}), \quad (42)$$

where λ_d trades off the predictive accuracy and the distributional discrepancy. Therefore, augmented distribution alignment can be easily incorporated by appending a GRL and adding the proposed interpolated samples during the optimization.

7. Experiments

In this section, we perform extensive experiments which demonstrate the superior performance of our CorNet. For this, we conduct simulation studies in which we verify the theoretical properties of CorNet (see Section 7.1) and experiments using real-world data in which we compare the estimation performance against a variety of baselines (see Section 7.2). During this section, we refer to the estimator yield by the unregularized variant of CorNet (i. e., $\lambda_d = \lambda_\delta = 0$) by τ_{CorNet} and to its regularized variant (i. e., $\lambda_d, \lambda_\delta > 0$) by τ_{CorNet^+} .

7.1 Simulation Studies: Empirical Verification of Theoretical Properties

Here, we empirically verify the theoretical properties of our procedure derived in Section 5. For this, we use simulated data, since this allows to manipulate the data-generating processes. In particular, we need to manipulate the data-generating process in order to study the impact of different factors as in Section 5. Note that for this, we use the *unregularized* variant, τ_{CorNet} , since regularizations may avoid observing the effect of certain factors.

We conduct the following three simulation studies. In Section 7.1.1, we empirically the finite sample properties derived in Theorem 2, i. e., the impact of the size of observational data, the distributional discrepancy, and the complexity of the bias on the error of our algorithm. In Section 7.1.2, we empirically verify the conditions derived in Theorem 11 for when our algorithm should be used and when is should not. In Section 7.1.3, we study the

13. In the experiments, m is set to n^{Conf} .

14. For details on the optimization of the H -divergence, see Appendix G.

robustness of our algorithm against alterations of our setup (i. e., the representation is not shared, the observational data is unconfounded, and no population overlap). We find that our algorithm yields robust results even when the underlying setup is altered.

7.1.1 FINITE SAMPLE PROPERTIES

Here, we empirically investigate the finite sample properties of our algorithm CorNet. As we discussed in Section 5.2, there are three driving factors of interest in the finite sample error bound: (i) the size of observational data, n^{Conf} , (ii) the distributional discrepancy between observational and randomized data, $d_\infty(p_\phi^{\text{Conf}} | p_\phi^{\text{Unc}})$, and (iii) the complexity of the bias, $\mathcal{C}_\mathcal{B}$. In particular, we have seen that from a theoretical point of view: more observational data is beneficial and large distributional discrepancy and large complexity of the bias function are not beneficial for the error of our algorithm. Therefore, we conduct three simulation studies to show the impact of these three factors on the finite sample error. Note that, in order to control the bias due to unobserved confounding, we do not introduce an unobserved confounder that affects treatment assignment and outcome. Instead, we directly manipulate the data-generating processes of the randomized and observational outcomes, $Y^{\text{Unc}}, Y^{\text{Conf}}$. This is permitted, since the unobserved confounding leads to a difference in $Y^{\text{Unc}}, Y^{\text{Conf}}$ (see Section 4.1), which gives direct access to controlling the bias.

We generate observational and randomized data following the data-generating process from Section 4.1. In particular, let $X^{\text{Unc}} \sim \mathcal{N}(\mathbf{0}, \sigma_u^2 \mathbf{1})$ and $X^{\text{Conf}} \sim \mathcal{N}(\mathbf{0}, \mathbf{1})$, where σ_u^2 controls the distributional discrepancy between the observational and randomized data. Furthermore, let the treatment assignment^{15,16} be $T^{\text{Unc}}, T^{\text{Conf}} \sim \text{Bernoulli}(\frac{1}{2})$ and the outcomes be

$$Y^{\text{Conf}} \sim \phi^*(X^{\text{Conf}}) \mathbf{w}_{T^{\text{Conf}}}^c + \epsilon, \quad (43)$$

$$Y^{\text{Unc}} \sim \phi^*(X^{\text{Unc}}) \mathbf{w}_{T^{\text{Unc}}}^u + \epsilon, \quad (44)$$

where $\epsilon \sim \mathcal{N}(0, \sigma_\epsilon^2)$. We use randomly chosen weights for ϕ^* and \mathbf{w}_t^c and control the bias between observational and randomized data via $\mathbf{w}_t^u = \mathbf{w}_t^c + \boldsymbol{\delta}_t$, by changing $\|\boldsymbol{\delta}_t\| = \beta$.

- (i) **Impact of size of observational data.** Here, we study the impact of the size of observational data on the finite sample error of our algorithm. In order to isolate the impact of the observational data, we fix all parameters and vary n^{Conf} . In particular, we set $n^{\text{Unc}} \in \{25, 50, 100\}$ and $d_\infty(p^{\text{Conf}} | p^{\text{Unc}}) = 1$ (i. e., $\sigma_u^2 = 1$). Although we are interested in the error across different values for n^{Conf} , we show the result across difference values for n^{Unc} as a sensitivity check. The parameter β is chosen such that the bias in the observational data is constant across the different settings, i. e., $\sqrt{\epsilon_{\text{PEHE}}(\tau_{\text{Conf}})} = 2$.

In Figure 3, we present the error of our method (i. e., τ_{CorNet}), the estimator which only uses randomized data (i. e., τ_{Unc}), and the estimator which only uses observational

15. Note that T^{Conf} does not depend on the covariates X^{Conf} , since the impact of selection bias (i. e., the covariate shift between treatment and control group) is orthogonal to this work. See discussion in Theorem 3 and Appendix D for details.

16. Note that we do not introduce bias due to unobserved confounding by conditioning T^{Conf} on the potential outcomes or an unobserved confounder. Instead we introduced bias by directly manipulating the DGP of $Y^{\text{Unc}}, Y^{\text{Conf}}$ (see discussion at beginning of Section 7.1).

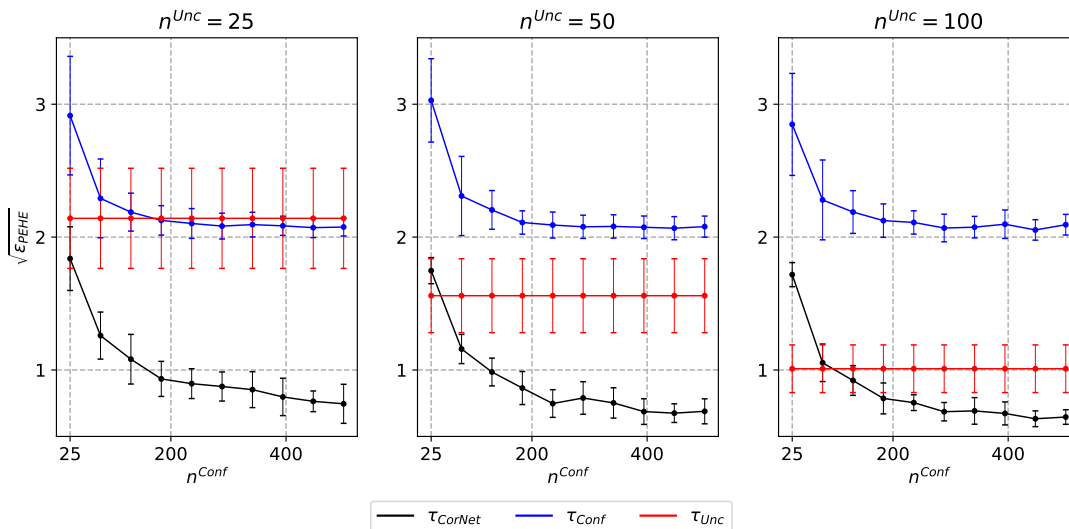


Figure 3: Simulation study on the impact of the size of observational data on the error, $\sqrt{\epsilon^{PEHE}}$. We compare our algorithm, τ_{CorNet} , against the algorithm that only uses randomized data, τ_{Unc} , and the algorithm that only uses observational data, τ_{Conf} . The size of observational data is increased (x -axis). All other parameters are fixed. The mean and standard deviation (over 10 samples of the data-generating process) are shown. We observe that, for τ_{CorNet} , $\sqrt{\epsilon^{PEHE}}$ decreases in the number of observational samples, i. e., n^{Conf} .

data (i. e., τ_{Conf}) for increasing n^{Conf} . We are interested in whether more observational data (i. e., larger n^{Conf}) is beneficial for our algorithm.

We make the following three observations. (1) The insight derived from the result in Theorem 2 holds true empirically: using observational data is beneficial, since the error decreases the more observational data is used (i. e., larger n^{Conf}). This is not obvious, since the observational data is biased. (2) Compared to τ_{Unc} , our method achieves smaller error for large enough n^{Conf} . Moreover, the standard deviation of our method, τ_{CorNet} , is much smaller than the standard deviation of τ_{Unc} . This is because the sample size of the randomized data (i. e., n^{Unc}) is small. Our method achieves much smaller standard deviation, since we incorporate observational data, which is available in larger quantities and, hence, reduce the variance. If the sample size of the randomized data is increased, for instance, from the far left plot (with $n^{Unc} = 25$) to the far right plot (with $n^{Unc} = 100$), the benefit of observational data remains. However, the error of τ_{Unc} decreases (due to more data) and, in order to outperform τ_{Unc} , our method requires more observational data. Hence, since observational data is usually available in large quantities, it remains beneficial to combine observational and randomized data, even when more randomized data is acquired. However, this effect may diminish at some point when the size of randomized data becomes very large. (3) Compared to τ_{Conf} , our method achieves smaller error independent of n^{Conf} . Moreover, the error of τ_{Conf} stagnates at $\sqrt{\epsilon^{PEHE}(\tau_{Conf})} = 2$, which is exactly the square root of the bias in the observational data (see earlier in this section). If the sample size of the randomized data is increased (far left plot to far right plot), the error of τ_{Conf} does not change, since τ_{Conf} ignores any randomized data.

- (ii) **Impact of distributional discrepancy.** Here, we study the impact of the distributional discrepancy, $d_\infty(p^{\text{Conf}} | p^{\text{Unc}})$, on the finite sample error. Such a setting arises in practice when the covariate distribution of the subjects in the RCT does not fit the covariate distribution of the subject in the target population. For this, again, we fix all parameters (i. e., $n^{\text{Unc}} = 50$ and β such that $\sqrt{\epsilon_{\text{PEHE}}(\tau_{\text{Conf}})} = 2$). Then, we compare the error in the case in which there is no distributional discrepancy (i. e., $d_\infty(p^{\text{Conf}} | p^{\text{Unc}}) = 1$) to the case in which there is distributional discrepancy (i. e., $d_\infty(p^{\text{Conf}} | p^{\text{Unc}}) > 1$). For the former case, we set $\sigma_u = 1$, i. e., $X^{\text{Unc}} \sim \mathcal{N}(0, 1 \cdot \mathbf{1})$, and, for the latter case, we set $\sigma_u = 0.1$, i. e., $X^{\text{Unc}} \sim \mathcal{N}(0, 0.1^2 \cdot \mathbf{1})$.

The results are presented in Figure 4. We make the following three observations. (1) If $d_\infty(p^{\text{Conf}} | p^{\text{Unc}}) > 1$ (i. e., $\sigma_u = 0.1$), the error converges slower for our algorithm compared to when $d_\infty(p^{\text{Conf}} | p^{\text{Unc}}) = 1$. This is expected from the finite sample error bound, as the distributional discrepancy is a driving factor in Theorem 2. Hence, as our theory suggests, we observe that there is a negative impact of the distributional discrepancy between observational and randomized covariate distributions on the error. (2) If $d_\infty(p^{\text{Conf}} | p^{\text{Unc}}) > 1$, the performance of the estimator which only uses randomized data, τ_{Unc} , worsens. This is expected from the finite sample error bound of τ_{Unc} (see Theorem 4), in which the distributional discrepancy is a driving factor. In particular, we observe that the impact of distributional discrepancy is more pronounced for τ_{Unc} than for our algorithm, τ_{CorNet} (the error of τ_{Unc} worsens more than the error of τ_{CorNet}). This is because the distributional discrepancy impact the whole finite sample error bound of τ_{Unc} (see Theorem 4), but only parts of the finite sample error bound of τ_{CorNet} (see Theorem 2). (3) The error of τ_{Conf} is not affected by the distributional discrepancy. Again, this is suggested by our theory (see Theorem 5), since the term $d_\infty(p^{\text{Conf}} | p^{\text{Unc}})$ does not occur in the finite sample error bound.

- (iii) **Impact of the complexity of bias.** Finally, we study the impact of the complexity of the bias function, $\mathcal{C}_{\mathcal{B}}$, on the finite sample error. For this, we fix all parameters (i. e., $n^{\text{Unc}} = 50$ and $d_\infty(p^{\text{Conf}} | p^{\text{Unc}}) = 1$, i. e., no distributional discrepancy). Then, we compare the error in the case in which the complexity is small (i. e., $\mathcal{C}_{\mathcal{B}}$ small) to the case in which the complexity is large (i. e., $\mathcal{C}_{\mathcal{B}}$ large). The complexity of the bias function is measured in terms of its Gaussian complexity and, hence, can be controlled by varying $\|\delta_t\| = \beta$ (i. e., larger β corresponds to larger Gaussian complexity).

The results are presented in Figure 5. We make the following three observations. (1) The error of our algorithm, τ_{CorNet} , increases in the complexity of the bias function (from the left to the right plot). This is in line with our theoretical results in Theorem 2, in which the complexity of the bias function, $\mathcal{C}_{\mathcal{B}}$, is one of the driving factors. Moreover, the convergence of the error is substantially slower the more complex the bias function is. In particular, for large bias complexity, the error remains substantially larger than in the case with smaller bias complexity. This observation is, again, expected by our finite sample error bound in Theorem 2. For both settings, our method improves upon the estimators τ_{Unc} and τ_{Conf} . (2) The estimator which only uses randomized data, i. e., τ_{Unc} , is not impacted by the complexity of the bias, since it is trained on only randomized (i. e., unbiased) data. It, therefore, remains identical across the two plots. (3) The estimator which only uses observational data, i. e., τ_{Conf} , achieves smaller error

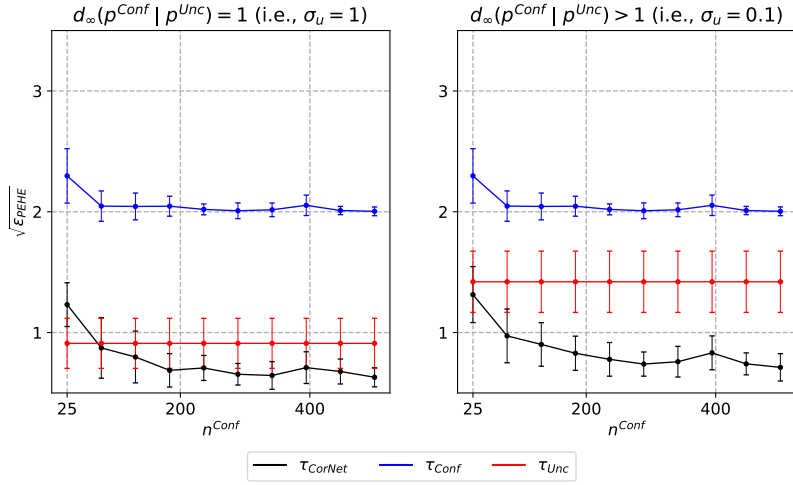


Figure 4: Simulation study on the impact of the distributional discrepancy on the error, $\sqrt{\epsilon_{PEHE}}$ (left plot: no discrepancy, right plot: discrepancy). We compare our algorithm, τ_{CorNet} , against the algorithm that only uses randomized data, τ_{Unc} , and the algorithm that only uses observational data, τ_{Conf} . The size of observational data is increased (x -axis). All other parameters are fixed. The mean and standard deviation (over 10 samples of the data-generating process) are shown. We observe that, for τ_{CorNet} and τ_{Unc} , the distributional discrepancy negatively impacts the convergence of $\sqrt{\epsilon_{PEHE}}$.

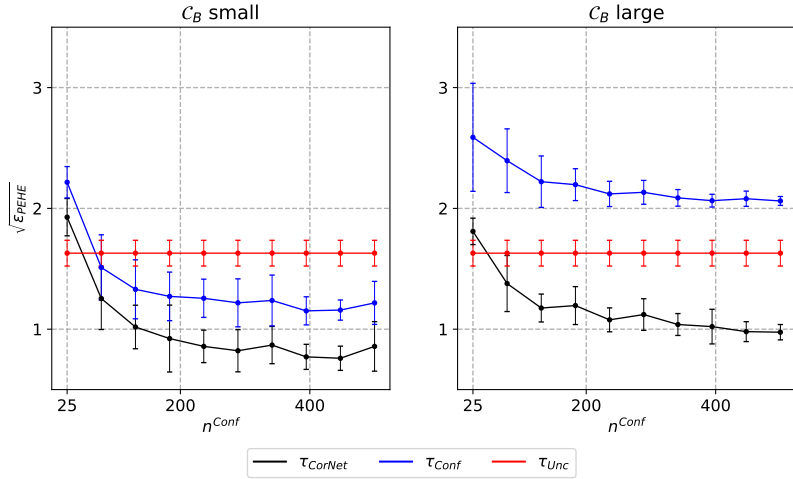


Figure 5: Simulation study on the impact of the complexity of the bias function on the error, $\sqrt{\epsilon_{PEHE}}$ (left plot: small complexity, right plot: large complexity). We compare our algorithm, τ_{CorNet} , against the algorithm that only uses randomized data, τ_{Unc} , and the algorithm that only uses observational data, τ_{Conf} . The size of observational data is increased (x -axis). All other parameters are fixed. The mean and standard deviation (over 10 samples of the data-generating process) are shown. We observe that the complexity of the bias negatively impacts the convergence of $\sqrt{\epsilon_{PEHE}}$.

in the case in which the bias complexity is small compared to the case in which bias complexity is large. This is due to the fact that, when the complexity of the bias is increased (by scaling β), the bias itself also becomes larger.

7.1.2 IMPROVEMENT CONDITIONS FOR OUR ALGORITHM

In this section, we empirically verify the theoretical conditions derived in Proposition 11 in Section 5.3.5 for when our method, τ_{CorNet} , should be used over τ_{Unc} and τ_{Conf} and when it should not. For this, we compare $\epsilon_{\text{PEHE}}(\tau_{\text{CorNet}})$ against $\epsilon_{\text{PEHE}}(\tau_{\text{Unc}})$ and $\epsilon_{\text{PEHE}}(\tau_{\text{CorNet}})$ against $\epsilon_{\text{PEHE}}(\tau_{\text{Conf}})$ across different settings.

For the comparison against $\epsilon_{\text{PEHE}}(\tau_{\text{Unc}})$, we are interested in when our method is more beneficial than $\hat{\tau}_{\text{Unc}}$ and how the size of the observational data, the distributional discrepancy, and the complexity of the bias affect this. For this, we compare across three settings: (1) no distributional discrepancy and small bias complexity (i. e., $d_{\infty}(p^{\text{Conf}} | p^{\text{Unc}}) = 1$, $\mathcal{C}_{\mathcal{B}}$ small), (2) distributional discrepancy and small bias complexity (i. e., $d_{\infty}(p^{\text{Conf}} | p^{\text{Unc}}) > 1$, $\mathcal{C}_{\mathcal{B}}$ small), and (3) no distributional discrepancy and large bias complexity (i. e., $d_{\infty}(p^{\text{Conf}} | p^{\text{Unc}}) = 1$, $\mathcal{C}_{\mathcal{B}}$ large). The distributional discrepancy and the complexity of the bias are controlled similarly as in the simulation studies conducted earlier in this section.

In Figure 6, we present the results. We note that we observe empirically what we found theoretically in Section 5.3.5. We make the following three observations. First, the larger the size of the observational data (and, therefore, the larger the ratio $\sqrt{\frac{n^{\text{Conf}}}{n^{\text{Unc}}}}$), the more beneficial (in terms of error) our method is. We can observe this in Figure 6 (top), where the vertical dashed line indicates the point when our method, τ_{CorNet} , improve upon τ_{Unc} . Second, the larger the distributional discrepancy, the more beneficial our method is. We can observe this in Figure 6 (middle), where the vertical dashed line moves to the left compared to the plot in the first row (i. e., less data required). Third, the larger the complexity of the bias function, the more observational data our algorithm needs to offset its negative effect and to be beneficial over τ_{Unc} . We can observe this in Figure 6 (bottom), where the vertical dashed line moves to the right (i. e., more data required).

For the comparison against $\epsilon_{\text{PEHE}}(\tau_{\text{Conf}})$, we are interested in when our method, τ_{CorNet} , is more beneficial than τ_{Conf} and how the size of the randomized data, the distributional discrepancy, and the bias affect this. Similar to before, we compare across three settings: (1) no distributional discrepancy and small bias (i. e., $d_{\infty}(p^{\text{Conf}} | p^{\text{Unc}}) = 1$, $\Delta = 1$), (2) distributional discrepancy and small bias (i. e., $d_{\infty}(p^{\text{Conf}} | p^{\text{Unc}}) > 1$, $\Delta = 1$), and (3) no distributional discrepancy and larger bias (i. e., $d_{\infty}(p^{\text{Conf}} | p^{\text{Unc}}) = 1$, $\Delta = 1.5$). The distributional discrepancy and the bias are controlled similarly as in the simulation studies conducted earlier in this section.

In Figure 7, we present the results. We note that we again observe empirically what we found theoretically in Section 5.3.5. First, the larger the size of the randomized data (and, therefore, the smaller the ratio $\sqrt{1/n^{\text{Unc}}}$), the more beneficial (in terms of error) our method becomes. We can observe this in Figure 7 (top), where the vertical dashed line indicates the point when our method, τ_{CorNet} , improves upon τ_{Conf} . Second, the larger the distributional discrepancy, the more randomized data is required to offset the negative effect from the distributional discrepancy and to be beneficial over τ_{Conf} . We can observe this in the Figure 7 (middle), where the vertical dashed line moves to the right compared to the plot at the top (i. e., more data required). Third, the larger the bias, the more beneficial our algorithm becomes over τ_{Conf} . We can observe this in Figure 7 (bottom), where the vertical dashed line moves to the left (i. e., less data required).

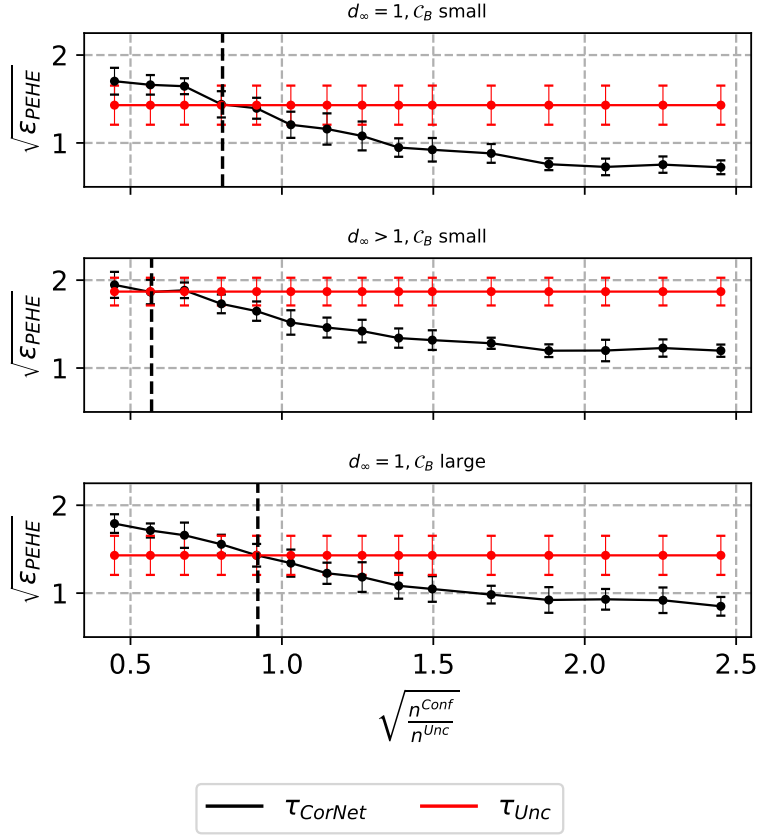


Figure 6: Simulation study on the conditions for when our algorithm, τ_{CorNet} , is beneficial over the algorithm which only uses randomized data, τ_{Unc} . Top: $d_\infty(p^{\text{Conf}} | p^{\text{Unc}}) = 1$ and \mathcal{C}_B small. Middle: $d_\infty(p^{\text{Conf}} | p^{\text{Unc}}) > 1$ and \mathcal{C}_B small. Bottom: $d_\infty(p^{\text{Conf}} | p^{\text{Unc}}) = 1$ and \mathcal{C}_B large. The ratio $\sqrt{\frac{n^{\text{Conf}}}{n^{\text{Unc}}}}$ is increased. All other parameters are fixed. We observe that: (1) the larger the size of the observational data, the more beneficial our algorithm becomes. (2) The larger the distributional discrepancy, the fewer observational samples are needed to improve upon τ_{Unc} . (3) The larger the bias, the more observational data is required to improve upon τ_{Unc} .

7.1.3 ROBUSTNESS AGAINST ALTERATIONS OF OUR SETUP

In this section, we study the robustness of our algorithm against alteration of the underlying setup. In particular, we investigate three different settings, in which our setup is altered: (i) the representation between observational and randomized data is *not* shared, (ii) the observational data is unconfounded, and (iii) the observational and randomized covariate distributions do not fully overlap.

(i) No shared representation: Here, we generate a observational and randomized dataset, whose data-generating processes do *not* possess a shared representation.

For this, we generate observational and randomized samples as follows: $X^{\text{Conf}}, X^{\text{Unc}} \sim \mathcal{N}(\mathbf{0}, \mathbf{1})$, $T^{\text{Conf}}, T^{\text{Unc}} \sim \text{Bernoulli}(\frac{1}{2})$. The outcomes are sampled from two different distribu-

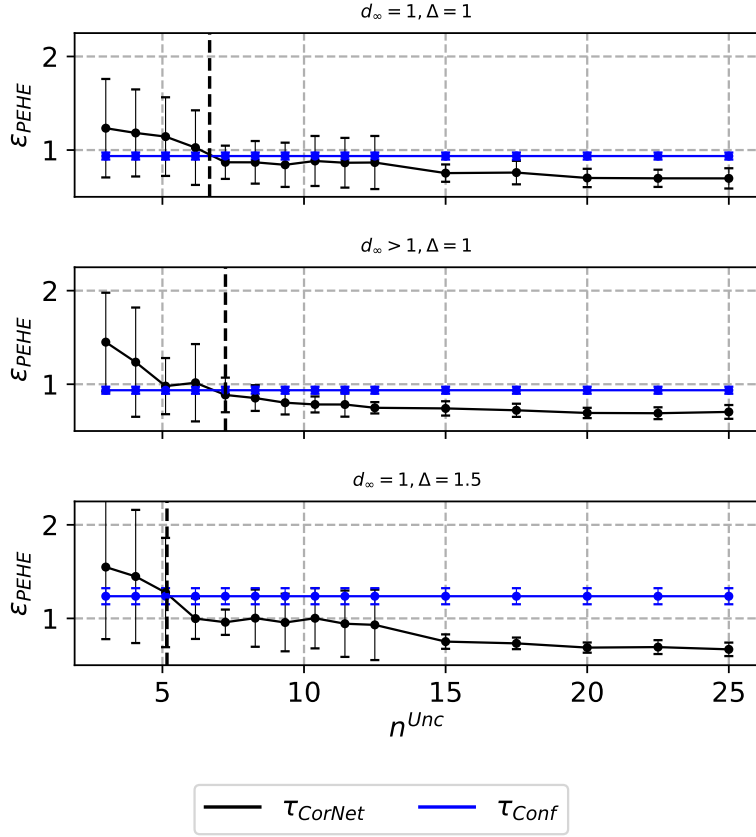


Figure 7: Simulation study on the conditions for when our algorithm, τ_{CorNet} , is beneficial over the algorithm which only uses observational data, τ_{Conf} . Top: $d_\infty(p^{\text{Conf}} | p^{\text{Unc}}) = 1$ and $\Delta = 1$ Middle: $d_\infty(p^{\text{Conf}} | p^{\text{Unc}}) > 1$ and $\Delta = 1$. Bottom: $d_\infty(p^{\text{Conf}} | p^{\text{Unc}}) = 1$ and $\Delta = 1.5$. The number of randomized samples n^{Unc} is increased. All other parameters are fixed. We observe that: (1) the larger the size of the randomized data, the more beneficial our algorithm becomes (2) The larger the distributional discrepancy, the more randomized samples are needed to improve upon τ_{Conf} . (3) The larger the bias, the fewer randomized data is required to improve upon τ_{Conf} .

tions, with two different representations ϕ^c and ϕ^u :

$$Y^{\text{Conf}} \sim \phi^c(X^{\text{Conf}}) \mathbf{w}_{T^{\text{Conf}}}^c + \epsilon, \quad (45)$$

$$Y^{\text{Unc}} \sim \phi^u(X^{\text{Unc}}) \mathbf{w}_{T^{\text{Unc}}}^u + \epsilon, \quad (46)$$

where $\epsilon \sim \mathcal{N}(0, \sigma_\epsilon^2)$. If both observational and randomized data share the representation, then $\phi^* = \phi^c = \phi^u$. We break the shared representation assumption by choosing $\phi^c \neq \phi^u$. In particular, we use randomly chosen weights for ϕ^c . Then, we vary by how much ϕ^u differs from ϕ^c using $\|\mathbf{W}_K^u - \mathbf{W}_K^c\|_{1,\infty} = \beta_\phi$, where \mathbf{W}_K^u and \mathbf{W}_K^c are the last weight matrices of the corresponding representations. For $\beta_\phi = 0$, the representation is shared, i. e., $\phi^* = \phi^c = \phi^u$ and the larger β_ϕ , the larger the difference between ϕ^c and ϕ^u . We sample three different settings for β_ϕ : (1) $\beta_\phi = 0$, i. e., the representation is shared, (2) β_ϕ small, i. e., there is a small difference between ϕ^c and ϕ^u , and (3) β_ϕ large, i. e., there is a large difference between ϕ^c and ϕ^u .

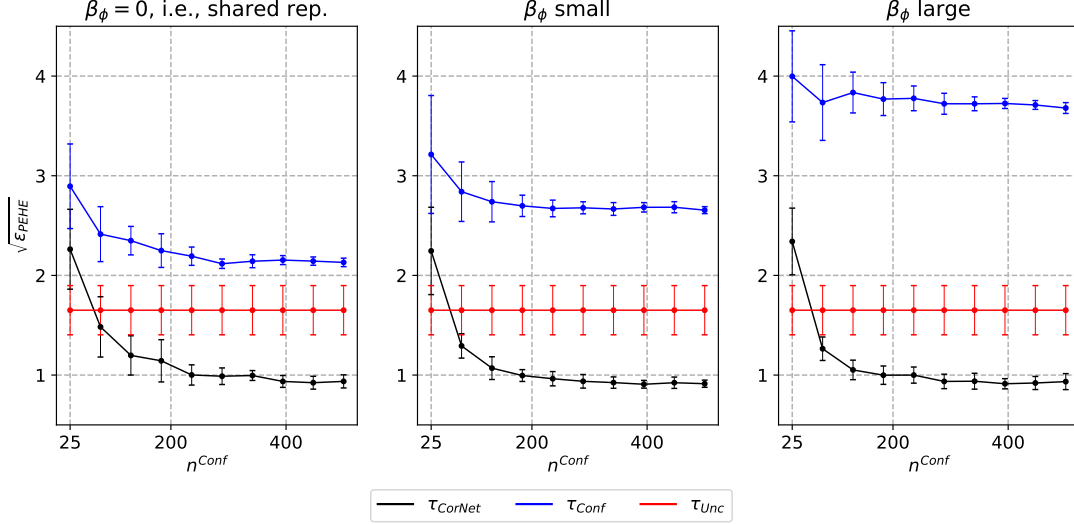


Figure 8: Simulation study for the robustness of our algorithm, if data does not possess a shared representation. The difference to the true representation is measured by $\|\mathbf{W}_K^u - \mathbf{W}_K^c\|_{1,\infty} = \beta_\phi$, where β_ϕ is increased in order to study the impact on the estimation error. We observe that our algorithm, τ_{CorNet} , remains robust with respect to violation of the shared representation assumption.

In Figure 8, we compare the estimation error of τ_{CorNet} against τ_{Unc} and τ_{Conf} for all three settings as described above. We make the following three observations. (1) When there is a shared representation, i.e., $\beta_\phi = 0$, our method substantially improves upon τ_{Unc} and τ_{Conf} . (2) When we break the assumption of a shared representation (i.e., β_ϕ small and β_ϕ large), the error of τ_{Conf} increases, which is due to a larger bias. At the same time, the error of τ_{Unc} remains unchanged across the different settings, since τ_{Unc} only uses randomized (i.e., unbiased) data. (3) When we break the assumption of a shared representation (i.e., β_ϕ small and β_ϕ large), the error of our method, τ_{CorNet} , remains consistent across the different settings. That means, our method is robust to violations of the “shared representation” assumption. This may be the case, since the bias function is directly learned in the second step of our CorNet. As such, any difference between the representations that has not been correctly learned in the first step, may be learned in the second step as part of the bias function.

(ii) Unconfounded observational data: In this setting, we generate an observational dataset which is unconfounded, i.e., it does not yield biased estimates. We are interested in whether, in this case, it would be more beneficial to rely only on observational data.

For this, we generate observational and randomized samples as follows: $X^{\text{Conf}}, X^{\text{Unc}} \sim \mathcal{N}(\mathbf{0}, \mathbf{1})$, $T^{\text{Conf}}, T^{\text{Unc}} \sim \text{Bernoulli}(\frac{1}{2})$. Then, the outcomes are sampled from two different distributions:

$$Y^{\text{Conf}} \sim \phi^*(X^{\text{Conf}}) \mathbf{w}_{T^{\text{Conf}}}^c + \epsilon, \quad (47)$$

$$Y^{\text{Unc}} \sim \phi^*(X^{\text{Unc}}) \mathbf{w}_{T^{\text{Unc}}}^u + \epsilon, \quad (48)$$

where $\epsilon \sim \mathcal{N}(0, \sigma_\epsilon^2)$. Then, the overall bias due to unobserved confounding can be controlled via $\delta_t = \mathbf{w}_t^u - \mathbf{w}_t^c$, since $\Delta = \mathbb{E} \left[(\phi^*(X^{\text{Conf}}) (\delta_1 - \delta_0))^2 \right]$. Hence, by varying δ_t , we vary the

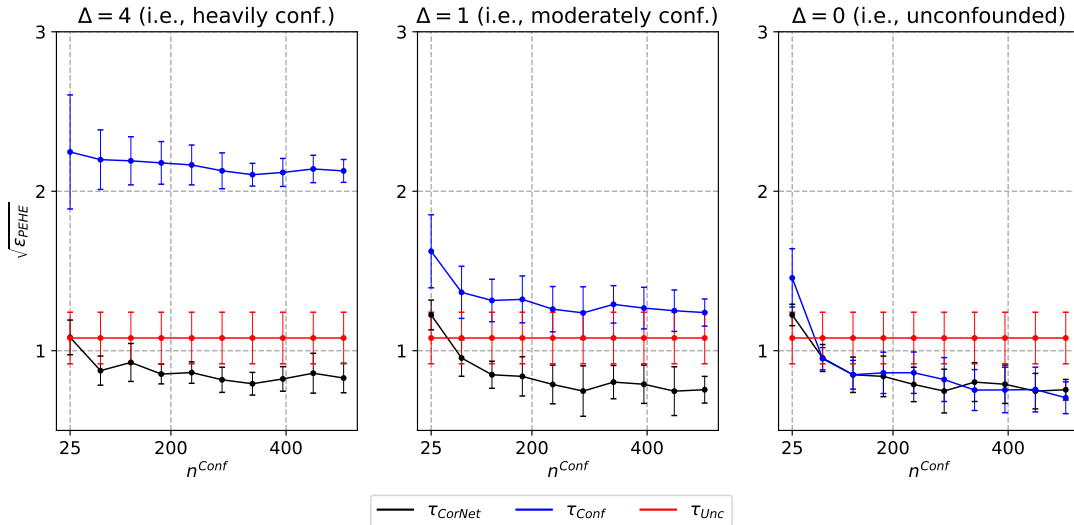


Figure 9: Simulation study for robustness of our algorithm if the observational data is unconfounded. The amount of bias due to unobserved confounding is measured by Δ , which is decreased in order to study the impact of no unobserved confounding on the estimation error. We observe that our algorithm, τ_{CorNet} , remains superior even if the observational data is confounded.

bias due to unobserved confounding. In particular, we use randomly chosen weights for \mathbf{w}_t^u and, then, we vary by how much \mathbf{w}_t^c differs from \mathbf{w}_t^u using $\|\delta_t\|_1 = \beta$. Hence, for $\beta = 0$, the observational data is unconfounded (i. e., $\mathbf{w}_t^c = \mathbf{w}_t^u$ and, therefore, $\Delta = 0$). The larger β , the larger the difference between \mathbf{w}_t^c and \mathbf{w}_t^u , and, therefore, the larger Δ . We sample three different settings for Δ : (1) $\Delta = 4$, i. e., the observational data is heavily confounded, (2) $\Delta = 1$, i. e., the observational data is moderately confounded, and (3) $\Delta = 0$, i. e., the observational data is unconfounded.

In Figure 9, we compare the estimation error of τ_{CorNet} against τ_{Unc} and τ_{Conf} for all three settings as described above. We make the following two observations. First, when there is confounding in the observational data, i. e., $\Delta = 4$ or $\Delta = 1$, our method consistently improves upon the τ_{Unc} and, especially, upon τ_{Conf} , where the latter estimator only uses observational data. Second, when the observational data is unconfounded (i. e., $\Delta = 0$), the error of τ_{Conf} decreases below the error of τ_{Unc} and to a similar level as the error of our method, τ_{CorNet} . Notably, the error of τ_{Conf} does not decrease below the error of our method. This is particularly important, since this implies that there is no drawback from using our method, since it yields superior results even if the observational data is unconfounded. That is, even if the observational data is unconfounded, our method, τ_{CorNet} , is on par with methods that only use observational data. The reason for this is that our method uses observational data in the first step and randomized data in the second step. If both types of data are unconfounded, then, our method uses unconfounded data in every step. On the other hand, τ_{Conf} only uses observational data. Hence, if the observational data is unconfounded, then, τ_{Conf} uses unconfounded data in every “step” as well, which explains the similar, but not superior, error of τ_{Conf} .

(iii) Limited overlap between observational and randomized data: Here, we investigate whether our method yields robust results if the population overlap assumption (see (iii) in Assumption 1) is violated. In particular, this assumption implies that p_x^{Unc} and p_x^{Conf} fully overlap, which ensures that the distributional discrepancy, $d_\infty(p_\phi^{\text{Conf}} | p_\phi^{\text{Unc}})$, in Theorem 2 is well-defined. Here, we study the impact on our method if this is not satisfied.

For this, we generate observational and randomized samples as follows: $X^{\text{Conf}} \sim \mathcal{N}(\mathbf{0}, \mathbf{1})$ and $T^{\text{Conf}}, T^{\text{Unc}} \sim \text{Bernoulli}(\frac{1}{2})$. The outcomes are sampled from two different distributions:

$$Y^{\text{Conf}} \sim \phi^*(X^{\text{Conf}}) \mathbf{w}_{T^{\text{Conf}}}^c + \epsilon, \quad (49)$$

$$Y^{\text{Unc}} \sim \phi^*(X^{\text{Unc}}) \mathbf{w}_{T^{\text{Unc}}}^u + \epsilon, \quad (50)$$

where $\epsilon \sim \mathcal{N}(0, \sigma_\epsilon^2)$. In order to study what happens if p_x^{Unc} and p_x^{Conf} do not fully overlap, we sample the randomized covariates as follows: $X^{\text{Unc}} \sim \mathcal{U}([-a, a]^d)$. As such, p_x^{Unc} is zero outside of the hypercube $[-a, a]^d$ and, therefore, violates the overlap assumption. By varying ‘a’, we control by how much the population overlap assumption is violated. In particular, we study three different settings for $X^{\text{Unc}} \sim \mathcal{U}([-a, a]^d)$: $a = 3$, $a = 1$, and $a = \frac{1}{2}$.

In Figure 10 (top), we compare the estimation error of τ_{CorNet} against τ_{Unc} and τ_{Conf} for all three settings for $X^{\text{Unc}} \sim \mathcal{U}([-a, a]^d)$ as described above. We also display the covariate distribution of the observational (in blue) and randomized (in red) data for one dimension, which illustrates the violation of the overlap.

We make the following three observations. (1) We observe that the error of τ_{Conf} remains constant across the settings, since it uses only observational data. (2) The error of τ_{Unc} increases the less the two distributions overlap. (3) The error of τ_{CorNet} also increases when the overlap becomes less, but, it increases substantially less than the error of τ_{Unc} . Moreover, the error of τ_{CorNet} remains substantially below τ_{Unc} and τ_{Conf} across all settings. However, we cannot conclude from this that the violation of the population overlap assumption harms the performance of our method, since, by varying a in $\mathcal{U}([-a, a]^d)$, we also vary the distributional discrepancy. And, as seen in Theorem 2 and Figure 4, varying the distributional discrepancy also impacts the error.

In order to isolate the impact of the violation of the population overlap assumption, we sample randomized data, which fulfills the overlap assumption, but has a similar distribution as $X^{\text{Unc}} \sim \mathcal{U}([-a, a]^d)$ (i. e., a sample is with high probability in $[-a, a]^d$). This means, we sample randomized data with similar distributional discrepancy, but without violating the population overlap assumption. As such, we can distinguish the contribution of the overlap violations and the distributional discrepancy to the error.

For this, for each of the above settings, we sample $X^{\text{Unc}} \sim \mathcal{N}(\mathbf{0}, \sigma_u^2 \mathbf{1})$, which satisfies the overlap assumption. Moreover, we choose σ_u for each setting such that X^{Unc} is, with high probability,¹⁷ in $[-a, a]^d$. This yields, for each of the above settings, the following choices: for $a = 3$, we choose $\sigma_u = 1$; for $a = 1$, we choose, $\sigma_u = \frac{1}{3}$; and, for $a = \frac{1}{2}$, we choose $\sigma_u = \frac{1}{6}$.

In Figure 10 (bottom), we present the same results as in the first row, but for $X^{\text{Unc}} \sim \mathcal{N}(\mathbf{0}, \sigma_u^2 \mathbf{1})$ with $\sigma_u \in \{1, \frac{1}{3}, \frac{1}{6}\}$.

By comparing the results at the top against the results at the bottom in Figure 10, we see how much of the changes in error are contributed to the violation of the population

17. To be precise, with high probability, we mean that we choose σ_u such that $\mathbb{P}(X^{\text{Unc}} \in [-a, a]^d) = 0.9973$ in *all* settings.

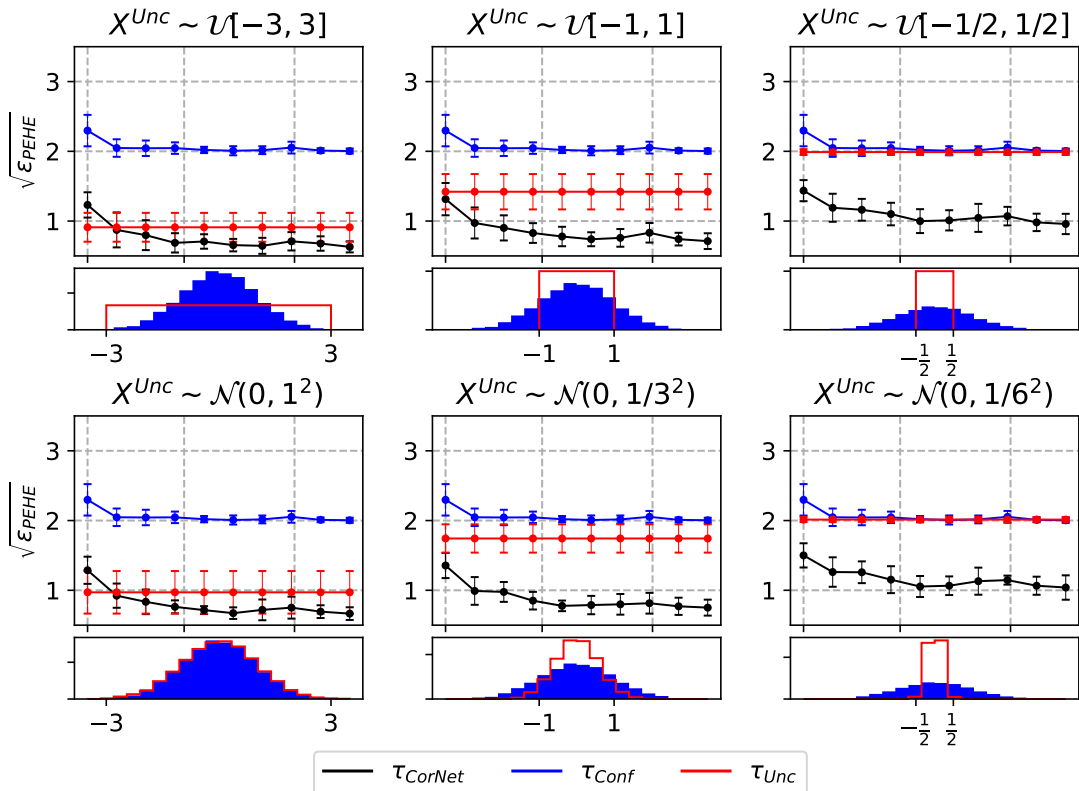


Figure 10: Simulation study for the violation of the population overlap assumption. The degree of overlap is measured by the hypercube $[-a, a]^d$, which is decreased in order to study the impact of assumption violation on the estimation error. Top: the error for τ_{CorNet} , τ_{Conf} , and τ_{Unc} for different hypercubes and for different values of n^{Conf} (x -axis). The distribution of the covariates, X^{Conf} and X^{Unc} , and their limited overlap is illustrated below the error plot. Bottom: the errors for the same methods, but without violating the overlap assumption in order to distinguish the contribution of the overlap violations and the distributional discrepancy to the error. The distribution of the covariates, X^{Conf} and X^{Unc} , are presented below the error plot. Since the errors increase across the settings similarly in both rows, we can conclude that our algorithm, τ_{CorNet} , remains robust with respect to violation of the population overlap assumption.

overlap assumption and how much to the distributional discrepancy. We find that the errors change similarly across the settings for our method, τ_{CorNet} , at the top *and* at the bottom in Figure 10. As such, the errors at the bottom change similarly (from left to right) as at the top. However, at the bottom, the population overlap assumption is *not* violated. Hence, we can conclude that, also at the top, the change in the errors is coming from the distributional discrepancy and *not* from the violation of the population overlap assumption. As a consequence, our method remains robust against violations of the population overlap assumptions.

7.2 Real-World Data

In this section, we validate our method against an extensive set of baselines on real-world data. Validating causal inference method on real-world data is challenging, since we do

not have access to the true potential outcomes. We circumvent this challenge by using real-world data from three large experiments: the Tennessee Student/Teacher Achievement Ratio (STAR) experiment (Word et al., 1990; Krueger, 1999), the AIDS Clinical Trial Group (ACTG) study 175 (Hammer et al., 1996), and the National Supported Work Demonstration (LaLonde, 1986; Smith and Todd, 2005). We discuss in Section 7.2.2 how a ground truth can be constructed from this real-world data.

7.2.1 SUMMARY OF THE REAL-WORLD DATA

We briefly describe all three real-world datasets that we used for our experiments in the following. More details on each of the datasets can be found in Appendix H.

Tennessee Student/Teacher Achievement Ratio (STAR) experiment: The Tennessee Student/Teacher Achievement Ratio (STAR) experiment is a randomized randomized experiment, which started in 1985 with the objective to study the effect of class size (i. e., treatment) on students’ standardized test scores (i. e., outcome). This dataset was previously also used in Kallus et al. (2018) for removing bias due to unmeasured confounding in observational data. Following their setup yields a randomized samples of 8 covariates and 4,139 students: 1,774 students assigned to treatment (i. e., small class, $T = 1$) and 2,365 students assigned to control (i. e., regular class, $T = 0$).

AIDS Clinical Trial Group (ACTG) study 175: The AIDS Clinical Trial Group (ACTG) study 175 is a clinical trial with the goal of studying the effect of different treatments on subjects with human immunodeficiency virus type 1 (HIV-1), whose CD4 counts were 200–500 cells/mm³ (Hammer et al., 1996). The ACTG study was used in Hatt et al. (2021) for learning policies that generalize to the target population. Even though this is a different aim, the study is particularly suited for evaluating our method since HIV-positive females tend to be underrepresented in clinical trials, which makes these studies not representative of the target population (i. e., the HIV-positive population) (Gandhi et al., 2005; Greenblatt, 2011). The outcome Y is defined as the difference between the cluster of differentiation 4 (CD4) cell counts at the beginning of the study and the CD4 counts after 20 ± 5 weeks. The average treatment effects on the male and female subgroups are -8.97 and -1.39 , respectively (Hatt et al., 2021), which suggests a large discrepancy in the treatment effects between both subgroups. Following the setup in Hatt et al. (2021) yields a total of 1,056 patients and 12 covariates, which are detailed in Appendix H.

National Supported Work (NSW) Demonstration: The National Supported Work (NSW) Demonstration was a randomized experiment investigating the effect of job training on income (LaLonde, 1986).¹⁸ Following Smith and Todd (2005), we combine randomized samples of 465 subjects (297 treated, 425 control) with the 2,490 PSID observational controls to create an observational dataset and include 8 covariates, which are detailed in Appendix H.

7.2.2 ESTIMATING GROUND TRUTH TREATMENT EFFECTS

Evaluating causal inference methods is generally challenging, since observational data is often confounded and the size of randomized data is usually too small. Fortunately, our datasets,

18. The study by LaLonde (1986) is a widely used dataset in the causal inference literature and is also known as the “Jobs” dataset (e. g., Shalit et al., 2017; Hatt and Feuerriegel, 2021a).

STAR, ACTG, and NSW, originated from large-scale experiment. As such, these datasets are unconfounded, since the treatment assignment was controlled by the investigator of the experiment. Moreover, these experiments have the appropriate size to estimate treatment effect heterogeneity. As a result, the CATE is identifiable in all three datasets via standard causal inference methods.

Therefore, we can estimate the potential outcomes $\mathbb{E}[Y(t) | X = x]$ for each $t \in \{0, 1\}$. Note, that is possible, since the data is unconfounded and, therefore, $\mathbb{E}[Y(t) | X = x] = \mathbb{E}[Y | X = x, T = t]$. In addition, since we have access to large-scale experiments, we have enough data to estimate treatment effect heterogeneity. For this, we use neural networks; in particular, we use an architecture as proposed for TarNet (Shalit et al., 2017), which uses a shared representation across potential outcomes and two independent hypotheses. We use neural networks is two-fold. First, we implemented all methods¹⁹ using neural networks and, therefore, a consistent use of the same underlying method enables fair comparisons across all baselines. Second, we require a function class with sufficiently capacity such that the true functions are contained in this function class with high confidence. Due to their large capacity, neural networks are a favorable choice for this.²⁰ Based on this, we estimate the ground truth CATE by $\hat{\tau}_{GT}(x) = \hat{\mathbb{E}}[Y(1) | X = x] - \hat{\mathbb{E}}[Y(0) | X = x]$. Note that this is only feasible, since we have access to the data of uncommonly large experiments, which allows to estimate complex functions directly on the randomized data. This, however, is rarely the case in practice, but enables us to evaluate our proposed method.

7.2.3 GENERATING SMALL RANDOMIZED AND LARGE OBSERVATIONAL DATA

Following the same procedure as in Kallus et al. (2018), we artificially generate a large, but confounded observational dataset and an unconfounded, but small randomized datasets using the real-world data described in Section 7.2.1. In particular, the randomized data is generated over a different population than the observational data, which represents the limited capabilities of RCTs to generalize to the population of interest.

For this, we follow the same protocol for STAR, ACTG, and NSW: First, from the original dataset, we sample a unconfounded, but small randomized dataset. To do so, we sample $n^{\text{Unc}} = 2d$ samples. We introduce distributional discrepancy between the randomized and observational data by selecting subjects into the randomized dataset based on one of the covariates (“birthday” for STAR, “gender” for ACTG, and “age” for NSW). Second, we generate the observational dataset by introducing unobserved confounding, i. e., the treatment and control group must be systematically different in their potential outcomes. Similar to Kallus et al. (2018), we sample the following subjects from those who were not selected into the randomized dataset: we take the controls ($T = 0$) whose outcomes were particularly low (i. e., $y_i < \mathbb{E}[Y | T = 0] - c \cdot \sigma_{Y|T=0}$, where $\sigma_{Y|T=0}$ is the standard deviation of the outcomes in the control). Then, we take the treated (i. e., $T = 1$) whose outcomes were particularly high (i. e., $y_i > \mathbb{E}[Y | T = 1] + c \cdot \sigma_{Y|T=1}$, where $\sigma_{Y|T=1}$ is the standard

19. Strictly speaking, there are two baselines which are not based on neural networks. However, for these two baselines, we also implement a neural network-based version to guarantee fair comparison. See Section 7.2.4 for details.

20. As a sensitivity check, we also ran all experiments using random forest, tree-based methods, and kernel methods as estimators for the ground truth treatment effect, which did not alter the final outcome of our experiments.

deviation of the outcomes among treated). The constant c is used to control how many subjects are selected into the observational data (to ensure it remains large) and depends on the size of the original dataset (we choose $c = 1$, $c = 0$, $c = 0.25$ for STAR, ACTG, and NSW, respectively). This procedure yields confounding by including control subjects with lower outcomes and treated subjects with higher outcomes selectively into control and treatment group of the observational data. Hence, a naïve estimate which only uses observational data will be biased. Moreover, since this selection is based on the outcome variable, it makes it impossible to control for this confounding.

7.2.4 BASELINES

We compare our algorithm against seven baselines: (i) The estimator on randomized data, $\hat{\tau}_{\text{Unc}}$, as described in Section 5.3.1; (ii) the estimator on observational data, $\hat{\tau}_{\text{Conf}}$, as described in Section 5.3.2, which we have seen is biased; (iii) the averaging estimator, $\hat{\tau}_{\text{Avg}}$, as described in Section 5.3.3, which is a convex combination of $\hat{\tau}_{\text{Unc}}$ and $\hat{\tau}_{\text{Conf}}$. This is also the estimator that was proposed recently in Cheng and Cai (2021); (iv) the weighting estimator, $\hat{\tau}_{\text{Weight}}$, as described in Section 5.3.4, which joins both data sets, but assigns a larger weight to randomized samples. For all the above baselines, the chosen functions classes are neural networks, which allows for comparison between them. Moreover, we compare against the two-step approach proposed in Kallus et al. (2018), which first estimates a biased model and then tries to remove the bias using the randomized data (see Appendix I for a detailed description of the method). The authors use ridge regression and random forest (RF) for estimating the biased model. In addition, for fair comparison, we also use neural networks (NN) for estimating this biased model. Hence, this yields three further baselines from Kallus et al. (2018): (v) 2-step-ridge, (vi) 2-step-RF, (vii) 2-step-NN.

7.2.5 EVALUATION METRIC

Our method is evaluated against various baselines for predicting the CATE. We evaluate how well the CATE estimate matches the ground truth estimate (τ_{GT} from Section 7.2.2) in terms of the empirical version of the ϵ_{PEHE} . For this, an unconfounded version of the observational dataset, which is exactly the original dataset (as described in Section 7.2.1) minus the randomized dataset. In sum, the metric for evaluation is: $\hat{\epsilon}_{\text{PEHE}}(\hat{\tau}) = \frac{1}{n^{\text{test}}} \sum_{i=1}^{n^{\text{test}}} (\hat{\tau}(x_i^{\text{test}}) - \tau_{\text{GT}}(x_i^{\text{test}}))^2$.

7.2.6 RESULTS

We run extensive experiments across all three real-world datasets. We find that, across all datasets and compared to all baselines, our algorithms, i. e., τ_{CorNet} and its regularized variant, τ_{CorNet^+} , perform superior.

The results are presented in Table 3. We make the following five observations about the results presented in Table 3. (1) Our methods (i. e., τ_{CorNet} , τ_{CorNet^+}) outperform all other methods substantially. The regularized two-step procedure, τ_{CorNet^+} , improves upon the unregularized two-step procedure, τ_{CorNet} , on STAR and ACTG, but not on NSW. The reason for this may be that the bias function is not sparse for this dataset. We investigate this in more detail in the ablation study in Section 7.2.8. (2) The baselines “2-step-ridge”, “2-step-RF”, and “2-step-NN” from Kallus et al. (2018) perform comparatively poorly due

to the re-weighting of the outcomes. We discuss the reasons for this at length in Remark 15. (3) The error of τ_{Conf} , which only uses observational data, depends on the magnitude of the bias due to unobserved confounding and displays consistently high errors across all datasets. (4) The method τ_{Unc} , which only uses randomized data, displays also high errors across all datasets. Moreover, τ_{Unc} displays substantially higher variance than the other methods across all datasets. Both observations, the high error and high variance, are due to the small sample size of randomized data. (5) The averaging and weighted risk estimators, τ_{Avg} and τ_{Weight} , yield errors of a similar magnitude than τ_{Unc} and τ_{Conf} . This is expected from the theoretical comparison in Section 5.3.5, since these estimators are combinations of τ_{Unc} and τ_{Conf} . Between τ_{Avg} and τ_{Weight} , there is no clearly preference: On STAR and NSW, τ_{Avg} achieves lower error, whereas, on ACTG, τ_{Weight} achieves lower errors.

Table 3: Results for the experiments on the real-world datasets STAR, ACTG, and NSW. Results are obtained via 10 runs. Lower is better.

Results: Experiments on three real-world datasets				
		$\sqrt{\hat{\epsilon}_{\text{PEHE}}}$ (Mean \pm Std)		
Estimator \ Dataset	STAR	ACTG	NSW	
2-step ridge	3.01 \pm 0.01	1.51 \pm 0.01	2.82 \pm 0.02	
2-step RF	3.14 \pm 0.03	1.58 \pm 0.07	3.10 \pm 0.12	
2-step NN	3.03 \pm 0.02	1.60 \pm 0.02	2.82 \pm 0.02	
τ_{Conf}	2.66 \pm 0.01	1.08 \pm 0.04	0.85 \pm 0.04	
τ_{Unc}	1.33 \pm 0.22	1.10 \pm 0.11	0.52 \pm 0.15	
τ_{Avg}	1.68 \pm 0.35	0.91 \pm 0.29	0.51 \pm 0.20	
τ_{Weight}	2.26 \pm 0.09	0.80 \pm 0.10	0.76 \pm 0.07	
τ_{CorNet} (ours)	0.59 \pm 0.01	0.42 \pm 0.06	0.14 \pm 0.07	
τ_{CorNet^+} (ours)	0.38 \pm 0.07	0.27 \pm 0.03	0.21 \pm 0.08	

Remark 15 In Table 3, we observe that the baselines “2-step-ridge”, “2-step-RF”, and “2-step-NN” from Kallus et al. (2018) perform comparatively poorly. This is due to the re-weighting of the outcomes using the inverse propensity score.²¹ It is well-known that this yields high-variance estimates, particularly in higher dimensions. Hence, these baselines improve when n^{Unc} is increased, which can be observed in Figure 11. However, their performance remains inferior to naïve approaches such as τ_{Unc} and, in particular, inferior to our methods. In order to show that the poor performance originates from re-weighting, we modify these baselines to avoid re-weighting, which improves their performance by a substantial margin. For this, we apply their approach to both of the outcomes rather than the CATE directly. This circumvents the need of re-weighting with the inverse propensity score.

21. See Appendix I or Eq. (2) in Kallus et al. (2018) for more details.

Although these modifications improve the baselines, they remain inferior to our method. A detailed discussion on the modification and the numerical results for the modified baselines can be found in Appendix I.

In sum, we conclude that our methods, τ_{CorNet} and τ_{CorNet^+} , outperform a variety of baselines across different real-world datasets.

7.2.7 SENSITIVITY WITH RESPECT TO n^{Conf} AND n^{Unc}

In this section, we study the sensitivity of the previous results for different numbers of n^{Conf} and n^{Unc} . In the previous experiments, we chose an explicit size of the observational and randomized dataset. Specifically, we chose n^{Conf} to be the maximum available samples for the observational dataset after the processing described in Section 7.2.3. In particular, this yields $n^{\text{Conf}} \in \{643, 552, 482\}$ for the datasets STAR, ACTG, and NSW.²² Moreover, we chose $n^{\text{Unc}} = 2d$, where d is the number of covariates. We did so, since the randomized datasets are usually data-scarce. Here, we study the robustness of our results from the previous section when n^{Conf} and n^{Unc} are varied.

Sensitivity to n^{Conf} : We compare our method against the baselines across different numbers of observational samples used, i. e., we vary n^{Conf} . In particular, we choose $n^{\text{Conf}} \in \{300, 400, 500, 600, 643\}$ for STAR, $n^{\text{Conf}} \in \{200, 300, 400, 500, 552\}$ for ACTG, and $n^{\text{Conf}} \in \{100, 200, 300, 400, 482\}$ for NSW. The results are presented in Figure 11 (top). We observe that all results remain consistent across different numbers of observational samples. In particular, our methods, τ_{CorNet} and τ_{CorNet^+} , achieve consistently superior results.

Sensitivity to n^{Unc} : We compare our method against the baselines across different numbers of randomized samples used, i. e., we vary n^{Unc} . In particular, for $X^{\text{Unc}} \in \mathbb{R}^d$, we choose $n^{\text{Unc}} \in \{1 \cdot d, 2 \cdot d, 3 \cdot d, 4 \cdot d, 6 \cdot d, 8 \cdot d\}$ for all datasets. The results are presented in Figure 11 (bottom). We observe that the results remain consistent across different numbers of randomized samples. In particular, our methods, τ_{CorNet} and τ_{CorNet^+} , achieve the lowest error for any number of randomized samples. We make two further observations. First, the larger the number of randomized samples, the closer the error of τ_{Unc} becomes to the error of our methods. This is because, for a large randomized dataset, which is not data-scarce anymore, only using randomized data becomes a competitive alternative. However, notably, our method remains superior for any number of randomized samples across all real-world datasets. Second, turning to the baselines “2-step ridge”, “2-step RF”, and “2-step NN”, we observe that their error substantially decreases for increasing number of randomized samples. However, for any number of randomized samples, they remain inferior to the naïve approach τ_{Unc} and, in particular, to our methods.

7.2.8 ABLATION STUDY

In this section, we conduct an ablation study to investigate the contribution of the different components of our method, τ_{CorNet} , to its superior performance. We also investigate different

22. The sizes of the observational datasets, n^{Conf} , are smaller than the sizes of the original datasets used to construct the observational datasets. That is, since we introduce confounding by only including treated subjects with high outcomes and control subjects with low outcomes. As such, we exclude many of the subjects in the original dataset.

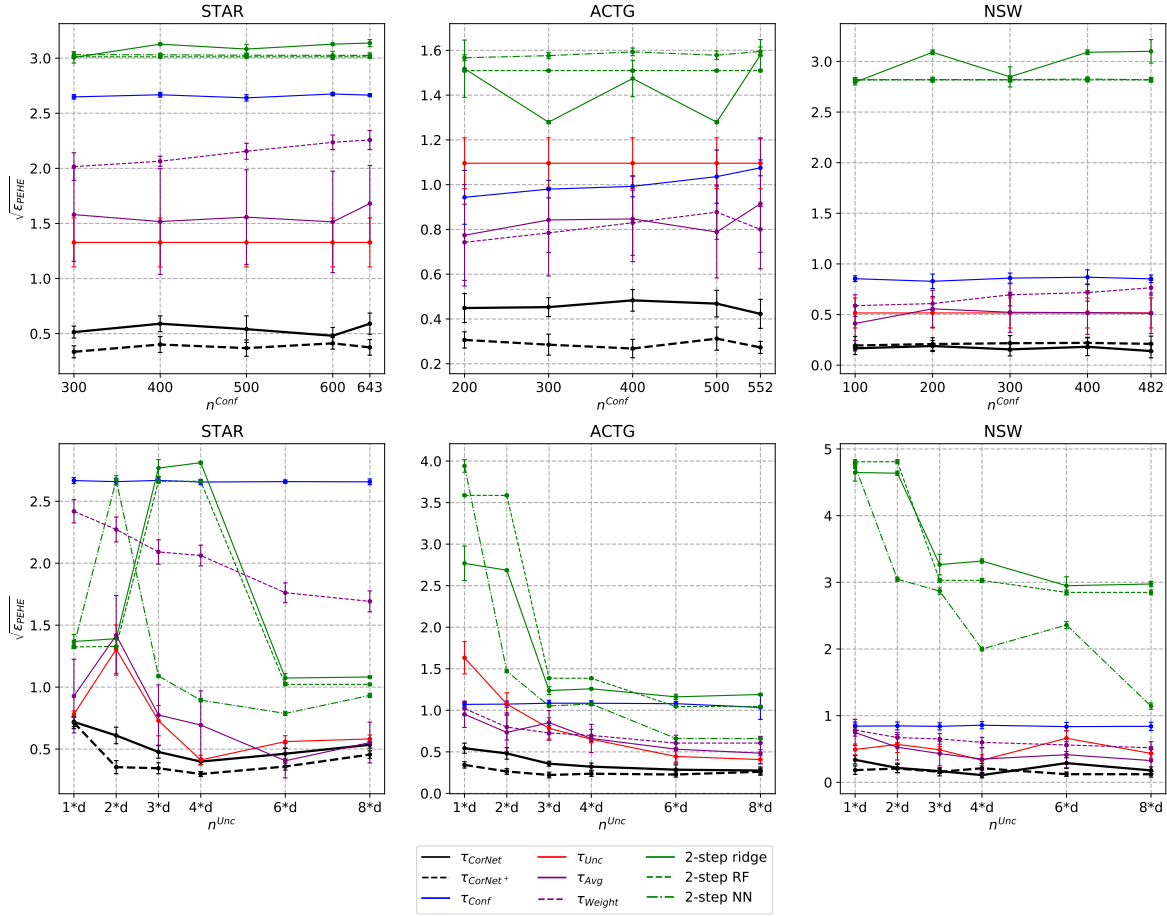


Figure 11: Sensitivity study of the results for different numbers of n^{Conf} (top row) and n^{Unc} (bottom row) across all real-world datasets STAR, ACTG, and NSW. The results are consistent across all numbers of observational (i. e., n^{Conf}) and randomized samples (i. e., n^{Unc}). For large number of randomized samples, the error of τ_{Unc} approaches the error of our methods, τ_{CorNet} and $\tau_{\text{CorNet}+}$. This is expected, since once the randomized dataset is not small anymore, only using randomized data may be a reasonable alternative. However, our methods remain superior across all numbers of observational and randomized samples.

extensions and variants of our method based on multi-task learning, which we discuss in depth in Appendix K.

For the ablation study, we take our τ_{CorNet} as a starting point. Then, we compare the performance of variants, for which we add different components as follows: τ_{CorNet} with (i) no regularizations, (ii) L_1 -regularization on the bias function δ , (iii) L_2 -regularization on δ , (iv) balancing the covariate distributions, i. e., $\lambda_d > 0$, and (v) L_1 -regularization on δ and balancing (which is $\tau_{\text{CorNet}+}$). In addition, we also compare to variants, which estimate the unconfounded hypotheses, \mathbf{w}^u , in the second step instead of the bias function. We denote this as $\tau_{\text{CorNet}} + \mathbf{w}^u$ and, then, add different components as follows: (vi) no regularization on \mathbf{w}^u , (vii) L_1 -regularization on \mathbf{w}^u , (viii) L_2 -regularization on \mathbf{w}^u , (ix) L_1 -regularization on \mathbf{w}^u and balancing, (x) L_2 -regularization on \mathbf{w}^u and balancing.

The results are presented in Table 4. We make the following observations. The L_1 -regularization on the bias improves the performance for STAR and ACTG, but not for NSW. This indicates that the bias function may not be sparse in the case of NSW. L_2 -regularization performs worse than L_1 -regularization for STAR and ACTG, but better for NSW. Again, this indicates that the bias functions may not be sparse on NSW. Learning the hypotheses, \mathbf{w}_t^u , (rather than the bias function) yields worse performance across all datasets. On top of this, regularizing the hypotheses (either L_1 or L_2) can yield improvement. Balancing the covariates can, but does not always lead to improvement compared to the unbalanced variants. Finally, L_1 -regularization on the bias function and balancing of the covariates (i.e., τ_{CorNet^+}) improves upon only regularizing the bias function for STAR and NSW, but not for ACTG. This may be due to extreme underrepresentation of women in these trials. Hence, counteracting this large discrepancy may cause the predictive accuracy to decrease by a substantial margin. Similarly to the sensitivity study for n^{Conf} and n^{Unc} in Section 7.2.7, we run the identical sensitivity study for the ablation study. The findings are consistent across different numbers of observational and randomized samples and can be found in Appendix J.

Table 4: Results for the ablation study on the real-world datasets STAR, ACTG, and NSW. L_1 , L_2 , and λ_d indicate whether L_1 -regularization, L_2 -regularization, or balancing was used. Results obtained via 10 runs. Lower is better.

Estimator		L_1 L_2 λ_d			$\sqrt{\hat{\epsilon}_{\text{PEHE}}}$ (Mean \pm Std)		
					STAR	ACTG	NSW
τ_{CorNet}	(i)	\times	\times	\times	0.59 \pm 0.10	0.42 \pm 0.06	0.14 \pm 0.07
	(ii)	\checkmark	\times	\times	0.41 \pm 0.07	0.25 \pm 0.04	0.23 \pm 0.04
	(iii)	\times	\checkmark	\times	0.57 \pm 0.09	0.40 \pm 0.06	0.10 \pm 0.05
	(iv)	\times	\times	\checkmark	0.54 \pm 0.09	0.47 \pm 0.04	0.19 \pm 0.05
	(v) τ_{CorNet^+}	\checkmark	\times	\checkmark	0.38 \pm 0.07	0.27 \pm 0.03	0.21 \pm 0.08
$\tau_{\text{CorNet}} + \mathbf{w}^u$	(vi)	\times	\times	\times	0.60 \pm 0.10	0.48 \pm 0.05	0.31 \pm 0.09
	(vii)	\checkmark	\times	\times	0.57 \pm 0.10	0.47 \pm 0.05	0.29 \pm 0.08
	(viii)	\times	\checkmark	\times	0.33 \pm 0.08	0.36 \pm 0.03	0.14 \pm 0.06
	(ix)	\checkmark	\times	\checkmark	0.31 \pm 0.04	0.39 \pm 0.04	0.14 \pm 0.04
	(x)	\times	\checkmark	\checkmark	0.53 \pm 0.07	0.51 \pm 0.06	0.33 \pm 0.06

8. Discussion

Individual-level decision-making is of great importance in many domains such as marketing (Hatt and Feuerriegel, 2020), economics (Heckman et al., 1997), or medicine (Ozyurt

et al., 2021). For this, heterogeneous treatment effects have to be estimated in order to personalize treatment decisions. In this paper, we propose a two-step procedure for estimating heterogeneous treatment effects, which combines observational and randomized data. In the first step, we use observational data to learn a shared representation and a confounded (i. e., biased) hypothesis. In the second step, we use the randomized data to debias the confounded hypothesis.

We prove finite sample learning bounds, which offer useful insights into which factors drive the estimation error when the size of randomized data is small. In particular, this reveals three driving factors affecting the error bound: (i) The size of observational data affects the error bound positively (i. e., the more observational data the better). (ii) The discrepancy between the covariate distributions in the observational and randomized data as well as (iii) the complexity of the bias function both negatively affect the error bound. We also prove finite sample learning bounds for several natural baselines which use either observational or randomized data or both. This allows us to compare our approach to these natural baselines and to derive conditions for when it is beneficial to combine observational and randomized data and when it is not. In particular, we find that the same factors as above affect these conditions. For instance, we reveal that if the distributional discrepancy is large, combining observational and randomized data is more beneficial than only using randomized data. This is particularly useful for pharmaceutical and medical sciences. If an RCT is poorly design in the sense that it may not generalize to the population of interest, combining the data from the RCT and observational data may substantially benefit the estimation of heterogeneous treatment effects. We also interpret these conditions in terms of sample complexity. This reveals that, under certain conditions, when combining observational and randomized data, we required less randomized data in order to achieve a predefined estimation error. This is particularly interesting, since RCTs are costly, and, hence, if we can reduce the required number of randomized samples, we can also reduce the costs of RCTs and accelerate drug approval. Based on these theoretical insights, we propose a sample-efficient algorithm based on our two-step procedure, called CorNet. We perform extensive simulation studies, which empirically verify the finite sample properties of CorNet as discussed above. Moreover, we study the robustness of CorNet against alterations of our setup. We find that even if observational and randomized data are generated from different representations (not a shared representation), CorNet yields robust results. Moreover, if observational data is unconfounded, CorNet yields similar results compared to only using observational data. This suggests that there is no drawback of using CorNet over method that only use observational data, even if observational data is unconfounded. Finally, if the population overlap assumption is violated, we find that the performance degradation of CorNet is due to the larger distributional discrepancy, but not the assumption violation itself. We further use multiple real-world datasets to compare CorNet against a variety of baseline methods. We find that CorNet outperforms all baseline methods by a substantial margin. This finding is consistent across different sizes of the observational data. Once we can acquire large amounts of randomized data, methods that only use randomized data perform similarly to CorNet. However, this means that we leave the setting for which CorNet was design (namely, small randomized data as in RCTs). Finally, in an ablation study, we find that the different components of CorNet (and extensions of it) improve upon the unregularized CorNet depending on the data at hand.

References

- 21st Century Cures Act, H.R. 34, 114th Congress, 2015.
- A. M. Alaa and M. van der Schaar. Bayesian inference of individualized treatment effects using multi-task Gaussian processes. In *Advances in Neural Information Processing Systems*, 2017.
- A. M. Alaa and M. van der Schaar. Limits of estimating heterogeneous treatment effects: Guidelines for practical algorithm design. In *International Conference on Machine Learning*, 2018.
- A. Argyriou, T. Evgeniou, and M. Pontil. Multi-task feature learning. *Advances in Neural Information Processing Systems*, 2006.
- S. Athey, R. Chetty, and G. Imbens. Combining experimental and observational data to estimate treatment effects on long term outcomes. *arXiv preprint arXiv:2006.09676*, 2020.
- H. Bastani. Predicting with proxies: Transfer learning in high dimension. *Management Science*, 67(5):2964–2984, 2021.
- M. Bayati, S. Bhaskar, and A. Montanari. Statistical analysis of a low cost method for multiple disease prediction. *Statistical Methods in Medical Research*, 27(8):2312–2328, 2018.
- S. Ben-David, J. Blitzer, K. Crammer, A. Kulesza, F. Pereira, and J. W. Vaughan. A theory of learning from different domains. *Machine Learning*, 79(1):151–175, 2010.
- J. Berrevoets, J. Jordon, I. Bica, A. Gimson, and M. van der Schaar. Organite: Optimal transplant donor organ offering using an individual treatment effect. *Advances in Neural Information Processing Systems*, 2020.
- J. Berrevoets, A. Alaa, Z. Qian, J. Jordon, A. Gimson, and M. van der Schaar. Learning queueing policies for organ transplantation allocation using interpretable counterfactual survival analysis. In *International Conference on Machine Learning*, 2021.
- I. Bica, A. M. Alaa, and M. van der Schaar. Time series deconfounder: Estimating treatment effects over time in the presence of hidden confounders. In *International Conference on Machine Learning*, 2019.
- P. J. Bickel, Y. Ritov, and A. B. Tsybakov. Simultaneous analysis of lasso and Dantzig selector. *The Annals of Statistics*, 37(4):1705–1732, 2009.
- S. Boyd, S. P. Boyd, and L. Vandenberghe. *Convex optimization*. Cambridge university press, 2004.
- K. Brodersen, F. Gallusser, J. Koehler, N. Remy, and S. Scott. Inferring causal impact using Bayesian structural time-series models. *Annals of Applied Statistics*, 9(1):247–274, 2015.
- T. Brown, B. Mann, N. Ryder, M. Subbiah, J. D. Kaplan, P. Dhariwal, et al. Language models are few-shot learners. *Advances in Neural Information Processing Systems*, 2020.

- A. L. Buchanan, M. G. Hudgens, S. R. Cole, K. R. Mollan, P. E. Sax, E. S. Daar, A. A. Adimora, J. J. Eron, and M. J. Mugavero. Generalizing evidence from randomized trials using inverse probability of sampling weights. *Journal of the Royal Statistical Society. Series A (Statistics in Society)*, 181(4):1193–1209, 2018.
- P. Bühlmann and S. van de Geer. *Statistics for high-dimensional data: methods, theory and applications*. Springer, 2011.
- E. Candes and T. Tao. The Dantzig selector: Statistical estimation when p is much larger than n . *The Annals of Statistics*, 35(6):2313–2351, 2007.
- R. Caruana. Multitask learning. *Machine Learning*, 28(1):41–75, 1997.
- D. Cheng and T. Cai. Adaptive combination of randomized and observational data. *arXiv preprint arXiv:2111.15012*, 2021.
- S. R. Cole and E. A. Stuart. Generalizing evidence from randomized clinical trials to target populations: the ACTG 320 trial. *American Journal of Epidemiology*, 172(1):107–115, 2010.
- R. Collobert and J. Weston. A unified architecture for natural language processing: Deep neural networks with multitask learning. In *International Conference on Machine Learning*, 2008.
- A. Curth and M. van der Schaar. On inductive biases for heterogeneous treatment effect estimation. *Advances in Neural Information Processing Systems*, 2021a.
- A. Curth and M. van der Schaar. Nonparametric estimation of heterogeneous treatment effects: From theory to learning algorithms. In *International Conference on Artificial Intelligence and Statistics*, 2021b.
- J. Cuzick, R. Edwards, and N. Segnan. Adjusting for non-compliance and contamination in randomized clinical trials. *Statistics in Medicine*, 16(9):1017–1029, 1997.
- S. H. Downs and N. Black. The feasibility of creating a checklist for the assessment of the methodological quality both of randomised and non-randomised studies of health care interventions. *Journal of Epidemiology & Community Health*, 52(6):377–384, 1998.
- S. S. Du, W. Hu, S. M. Kakade, J. D. Lee, and Q. Lei. Few-shot learning via learning the representation, provably. In *International Conference on Learning Representations*, 2020.
- L. E. Flores, W. R. Frontera, M. P. Andrasik, C. Del Rio, A. Mondríguez-González, S. A. Price, E. M. Krantz, S. A. Pergam, and J. K. Silver. Assessment of the inclusion of racial/ethnic minority, female, and older individuals in vaccine clinical trials. *JAMA Network Open*, 4(2):e2037640, 2021.
- M. Gandhi, N. Ameli, P. Bacchetti, G. B. Sharp, A. L. French, M. Young, S. J. Gange, K. Anastos, et al. Eligibility criteria for hiv clinical trials and generalizability of results: the gap between published reports and study protocols. *Aids*, 19(16):1885–1896, 2005.

- Y. Ganin and V. Lempitsky. Unsupervised domain adaptation by backpropagation. In *International Conference on Machine Learning*, 2015.
- Y. Ganin, E. Ustinova, H. Ajakan, P. Germain, H. Larochelle, F. Laviolette, M. Marchand, and V. Lempitsky. Domain-adversarial training of neural networks. *The Journal of Machine Learning Research*, 17(1):2096–2030, 2016.
- N. Golowich, A. Rakhlin, and O. Shamir. Size-independent sample complexity of neural networks. In *Conference On Learning Theory*, 2018.
- R. M. Greenblatt. Priority issues concerning hiv infection among women. *Women’s Health Issues*, 21(6):S266–S271, 2011.
- S. M. Hammer, D. A. Katzenstein, M. D. Hughes, H. Gundacker, R. T. Schooley, R. H. Haubrich, W. K. Henry, M. M. Lederman, et al. A trial comparing nucleoside monotherapy with combination therapy in hiv-infected adults with CD4 cell counts from 200 to 500 per cubic millimeter. *New England Journal of Medicine*, 335(15):1081–1090, 1996.
- T. Hatt and S. Feuerriegel. Early detection of user exits from clickstream data: A markov modulated marked point process model. In *The Web Conference 2020*, 2020.
- T. Hatt and S. Feuerriegel. Estimating average treatment effects via orthogonal regularization. In *International Conference on Information & Knowledge Management*, 2021a.
- T. Hatt and S. Feuerriegel. Sequential deconfounding for causal inference with unobserved confounders. *arXiv preprint arXiv:2101.08490*, 2021b.
- T. Hatt, D. Tschernutter, and S. Feuerriegel. Generalizing off-policy learning under sample selection bias. *arXiv preprint arXiv:2112.01387*, 2021.
- J. J. Heckman, H. Ichimura, and P. E. Todd. Matching as an econometric evaluation estimator: Evidence from evaluating a job training programme. *The Review of Economic Studies*, 64(4):605–654, 1997.
- M. Ilse, P. Forré, M. Welling, and J. M. Mooij. Combining interventional and observational data using causal reductions. *arXiv preprint arXiv:2103.04786*, 2021.
- G. Imbens, N. Kallus, X. Mao, and Y. Wang. Long-term causal inference under persistent confounding via data combination. *arXiv preprint arXiv:2202.07234*, 2022.
- C. Jackson, J. Stevens, S. Ren, N. Latimer, L. Bojke, A. Manca, and L. Sharples. Extrapolating survival from randomized trials using external data: a review of methods. *Medical Decision Making*, 37(4):377–390, 2017.
- A. Jalali, S. Sanghavi, C. Ruan, and P. Ravikumar. A dirty model for multi-task learning. *Advances in Neural Information Processing Systems*, 2010.
- F. D. Johansson, U. Shalit, and D. Sontag. Learning representations for counterfactual inference. In *International Conference on Machine Learning*, 2016.

- F. D. Johansson, N. Kallus, U. Shalit, and D. Sontag. Learning weighted representations for generalization across designs. *arXiv preprint arXiv:1802.08598*, 2018.
- Sham M Kakade, Karthik Sridharan, and Ambuj Tewari. On the complexity of linear prediction: Risk bounds, margin bounds, and regularization. In *Advances in Neural Information Processing Systems*, 2009.
- N. Kallus and A. Zhou. Confounding-robust policy improvement. In *Advances in Neural Information Processing Systems*, 2018.
- N. Kallus, A. M. Puli, and U. Shalit. Removing hidden confounding by experimental grounding. In *Advances in Neural Information Processing Systems*, 2018.
- N. Kallus, X. Mao, and A. Zhou. Interval estimation of individual-level causal effects under unobserved confounding. In *International Conference on Artificial Intelligence and Statistics*, 2019.
- E. H. Kennedy. Semiparametric theory and empirical processes in causal inference. In *Statistical causal inferences and their applications in public health research*, pages 141–167. Springer, 2016.
- A. B. Krueger. Experimental estimates of education production functions. *The Quarterly Journal of Economics*, 114(2):497–532, 1999.
- M. Kuzmanovic, T. Hatt, and S. Feuerriegel. Deconfounding temporal autoencoder: estimating treatment effects over time using noisy proxies. In *Machine Learning for Health*, 2021.
- R. J. LaLonde. Evaluating the econometric evaluations of training programs with experimental data. *The American Economic Review*, 76(4):604–620, 1986.
- M. Ledoux and M. Talagrand. *Probability in Banach Spaces: isoperimetry and processes*. Springer, 2013.
- T. Li, A. K. Sahu, A. Talwalkar, and V. Smith. Federated learning: Challenges, methods, and future directions. *IEEE Signal Processing Magazine*, 37(3):50–60, 2020.
- X. Liu, P. He, W. Chen, and J. Gao. Multi-task deep neural networks for natural language understanding. *arXiv preprint arXiv:1901.11504*, 2019.
- C. Louizos, U. Shalit, J. Mooij, D. Sontag, R. Zemel, and M. Welling. Causal effect inference with deep latent-variable models. In *Advances in Neural Information Processing Systems*, 2017.
- A. Maurer, M. Pontil, and B. Romera-Paredes. The benefit of multitask representation learning. *Journal of Machine Learning Research*, 17(81):1–32, 2016.
- L. Meier, S. van de Geer, and P. Bühlmann. The group lasso for logistic regression. *Journal of the Royal Statistical Society: Series B (Statistical Methodology)*, 70(1):53–71, 2008.

- N. Meinshausen and P. Bühlmann. High-dimensional graphs and variable selection with the lasso. *The Annals of Statistics*, 34(3):1436–1462, 2006.
- S. L. Norris, M. M. Engelgau, and K. V. Narayan. Effectiveness of self-management training in type 2 diabetes: a systematic review of randomized controlled trials. *Diabetes Care*, 24(3):561–587, 2001.
- Y. Ozyurt, M. Kraus, T. Hatt, and S. Feuerriegel. Attdmm: an attentive deep markov model for risk scoring in intensive care units. In *Conference on Knowledge Discovery & Data Mining*, 2021.
- S. J. Pan and Q. Yang. A survey on transfer learning. *IEEE Transactions on Knowledge and Data Engineering*, 22(10):1345–1359, 2009.
- A. Radford, J. Wu, R. Child, D. Luan, D. Amodei, I. Sutskever, et al. Language models are unsupervised multitask learners. *OpenAI blog*, 1(8):9, 2019.
- J. M. Robins. Correcting for non-compliance in randomized trials using structural nested mean models. *Communications in Statistics-Theory and Methods*, 23(8):2379–2412, 1994.
- J. M. Robins, M. A. Hernán, and B. Brumback. Marginal structural models and causal inference in epidemiology. *Epidemiology*, 11(5):550–560, 2000.
- P. R. Rosenbaum. *Design of observational studies*, volume 10. Springer, 2010.
- E. Rosenman, G. Basse, A. Owen, and M. Baiocchi. Combining observational and experimental datasets using shrinkage estimators. *arXiv preprint arXiv:2002.06708*, 2020.
- P. M. Rothwell. External validity of randomised controlled trials: “to whom do the results of this trial apply?”. *The Lancet*, 365(9453):82–93, 2005.
- S. Ruder. An overview of multi-task learning in deep neural networks. *arXiv preprint arXiv:1706.05098*, 2017.
- U. Shalit, F. D. Johansson, and D. Sontag. Estimating individual treatment effect: Generalization bounds and algorithms. In *International Conference on Machine Learning*, 2017.
- J. A. Smith and P. E. Todd. Does matching overcome lalonde’s critique of nonexperimental estimators? *Journal of Econometrics*, 125(1-2):305–353, 2005.
- E. V. Strobl and T. A. Lasko. Generalizing clinical trials with convex hulls. *arXiv preprint arXiv:2111.13229*, 2021.
- E. A. Stuart, S. R. Cole, C. P. Bradshaw, and P. J. Leaf. The use of propensity scores to assess the generalizability of results from randomized trials. *Journal of the Royal Statistical Society: Series A (Statistics in Society)*, 174(2):369–386, 2011.
- N. Tripuraneni, M. I. Jordan, and C. Jin. On the theory of transfer learning: The importance of task diversity. *Advances in Neural Information Processing Systems*, 2020.

- S. Wager and S. Athey. Estimation and inference of heterogeneous treatment effects using random forests. *Journal of the American Statistical Association*, 113(523):1228–1242, 2018.
- M. J. Wainwright. *High-dimensional statistics: A non-asymptotic viewpoint*, volume 48. Cambridge University Press, 2019.
- Q. Wang, W. Li, and L. Van Gool. Semi-supervised learning by augmented distribution alignment. In *International Conference on Computer Vision*, 2019.
- X. Wang, T.-K. Huang, and J. Schneider. Active transfer learning under model shift. In *International Conference on Machine Learning*, 2014.
- Y. Wang and D. M. Blei. The blessings of multiple causes. *Journal of the American Statistical Association*, 114(528):1574–1596, 2019.
- A. R. Willan, A. H. Briggs, and J. S. Hoch. Regression methods for covariate adjustment and subgroup analysis for non-censored cost-effectiveness data. *Health Economics*, 13(5):461–475, 2004.
- E. Word, J. Johnston, H. P. Bain, B. D. Fulton, J. B. Zaharias, C. M. Achilles, M. N. Lintz, J. Folger, and C. Breda. The state of tennessee’s student/teacher achievement ratio (star) project. *Tennessee Board of Education*, 1990.
- S. Yang and P. Ding. Combining multiple observational data sources to estimate causal effects. *Journal of the American Statistical Association*, 115(531):1540–1554, 2020.
- L. Yao, M. Huai, S. Li, J. Gao, Y. Li, and A. Zhang. Representation learning for treatment effect estimation from observational data. In *Advances in Neural Information Processing Systems*, 2018.
- C. Ye, J. Beyene, G. Browne, and L. Thabane. Estimating treatment effects in randomised controlled trials with non-compliance: a simulation study. *BMJ Open*, 4(6):e005362, 2014.
- J. Yoon, J. Jordon, and M. van der Schaar. Ganite: Estimation of individualized treatment effects using generative adversarial nets. In *International Conference on Learning Representations*, 2018.
- H. Zhang, M. Cisse, Y. N. Dauphin, and D. Lopez-Paz. mixup: Beyond empirical risk minimization. *International Conference on Learning Representations*, 2018.
- Y. Zhang and Q. Yang. A survey on multi-task learning. *IEEE Transactions on Knowledge and Data Engineering*, 2021.
- Y. Zhang, A. Bellot, and M. van der Schaar. Learning overlapping representations for the estimation of individualized treatment effects. In *International Conference on Artificial Intelligence and Statistics*, 2020.
- Q. Zhao, D. S. Small, and B. B. Bhattacharya. Sensitivity analysis for inverse probability weighting estimators via the percentile bootstrap. *Journal of the Royal Statistical Society: Series B (Statistical Methodology)*, 81(4):735–761, 2019.

Appendix A. Model Complexity

We first introduce measure for the complexity of function classes. We define the Gaussian complexity, which is used as a measure for the complexity of a function class. For a function class \mathcal{Q} with functions $q : \mathbb{R}^d \rightarrow \mathbb{R}^r$ and n data points, the empirical Gaussian complexity is defined as

$$\hat{\mathcal{G}}_{\bar{X}}(\mathcal{Q}) = \mathbb{E}_{\mathbf{g}} \left[\sup_{q \in \mathcal{Q}} \frac{1}{n} \sum_{k=1}^r \sum_{i=1}^n g_{ki} q_k(\mathbf{x}_i) \right], \quad (51)$$

where $g_{ki} \stackrel{\text{iid}}{\sim} \mathcal{N}(0, 1)$. The corresponding population quantity is defined as $\mathcal{G}_n(\mathcal{Q}) = \mathbb{E}_X[\hat{\mathcal{G}}_{\bar{X}}(\mathcal{Q})]$. The first expectation is taken over the distribution of the data samples, and the second expectation is taken over the Gaussian random variables. We further define the worst-case Gaussian complexity as

$$\bar{\mathcal{G}}_n(\mathcal{H}) = \max_{\mathcal{Z} \in \mathcal{Z}} \hat{\mathcal{G}}_{\bar{Z}}(\mathcal{H}), \quad \mathcal{Z} = \{(\phi(x_1), \dots, \phi(x_n)); \phi \in \Phi, x_i \in \mathcal{X} \text{ for all } i \in \{1, \dots, n\}\}. \quad (52)$$

Moreover, we define the empirical Rademacher complexity as

$$\hat{\mathcal{R}}_n(\mathcal{Q}) = \mathbb{E}_{\sigma} \left[\sup_{q \in \mathcal{Q}} \left| \frac{1}{n} \sum_{i=1}^n \sigma_i q(x_i) \right| \right], \quad (53)$$

where σ_i are Rademacher variables (i. e., taking the values $\{-1, +1\}$ equiprobably). The corresponding population quantity is defined by taking the expectation over X , i. e., $\mathcal{R}_n(\mathcal{Q}) = \mathbb{E}_X[\hat{\mathcal{R}}_n(\mathcal{Q})] = \mathbb{E}_{X, \sigma} \left[\sup_{q \in \mathcal{Q}} \left| \frac{1}{n} \sum_{i=1}^n \sigma_i q(x_i) \right| \right]$.

Appendix B. Feedforward Neural Networks

The class of feedforward neural network \mathcal{N} is defined by recursion:

$$\mathcal{N} = \{f_d : f_1(x) = \mathbf{W}_1^\top x, \quad f_i(x) = \mathbf{W}_i^\top \sigma(f_{i-1}(x)), \quad i = 2, \dots, d\}, \quad (54)$$

for $d \in \mathbb{N}_{\geq 1}$, matrices $\{\mathbf{W}_i\}_{i=1}^d$ of appropriate dimensions, activation function σ , which applies element-wise, and d is the depth of the neural network.

Then, we define the function classes for the representation, Φ , confounded hypotheses, \mathcal{H} , and bias functions, \mathcal{B} as follows:

$$\begin{aligned} \Phi = \{ & \phi \in \mathcal{N}; \|\mathbf{W}_k\|_{1, \infty} \leq \Omega_k \text{ for } k \in \{1, \dots, K-1\}, \\ & \max(\|\mathbf{W}_K\|_{1, \infty}, \|\mathbf{W}_K\|_{2 \rightarrow \infty}) \leq \Omega, \\ & \text{s.t. } \sigma_r(\mathbb{E}[\phi(X^{\text{Conf}})\phi(X^{\text{Conf}})^\top]) \geq \Omega(1)\}, \end{aligned} \quad (55)$$

$$\mathcal{H} = \{h \in \mathcal{N}; \|\mathbf{W}_d\|_{1, \infty} \leq \Omega_d \text{ for } d \in \{1, \dots, D\}\}, \quad (56)$$

$$\mathcal{B} = \{\delta \in \mathcal{N}; \|\mathbf{W}_b\|_{1, \infty} \leq \Omega_b \text{ for } b \in \{1, \dots, B\}\}, \quad (57)$$

where for a matrix $\mathbf{W} \in \mathbb{R}^{p \times q}$, we let $\|\mathbf{W}\|_{1, \infty} = \max_i \sum_j |\mathbf{W}_{ij}|$ and $\|\mathbf{W}\|_{2 \rightarrow \infty}$ the induced ∞ -to-2 operator norm.

Figure 12 illustrates the neural network architecture of our two-step procedure, which is used in Section 5.

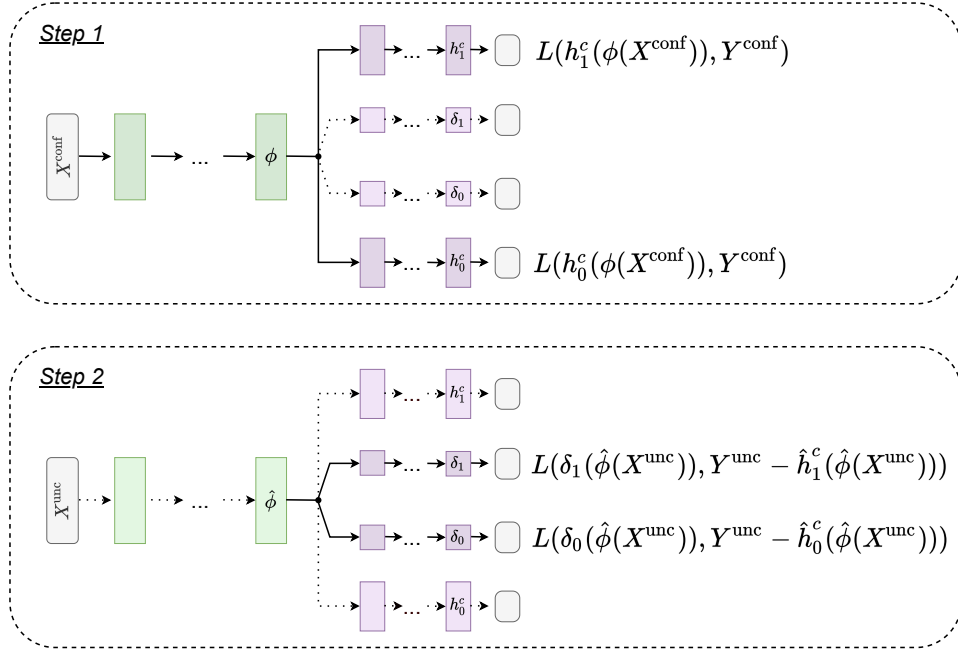


Figure 12: Illustration of our two-step procedure using neural networks. In Step 1, the observational data is used to learn a representation, $\hat{\phi}$, and confounded hypotheses, $\hat{\mathbf{h}}^c$. In Step 2, the randomized data, together with the $\hat{\phi}$ and $\hat{\mathbf{h}}^c$ form the first step, is used to learn the bias, $\hat{\boldsymbol{\delta}}$, in the confounded hypotheses due to unobserved confounding.

Appendix C. Proofs in Section 5

C.1 Proof of Theorem 2

In this section, we prove Theorem 2. To do so, we first prove two lemmas that are needed for the proof. Then, we prove a version of Theorem 2 for arbitrary function classes Φ , \mathcal{H} , and \mathcal{B} . Finally, we can then prove Theorem 2 for feedforward neural networks.

Lemma 16 *Let $\phi \in \Phi$ and $\mathbf{h} \in \mathcal{H}^{\otimes 2}$. Then, for $\hat{\epsilon}_{\text{Unc}}(\boldsymbol{\delta}, \mathbf{h}, \phi)$ as in (13) and*

$$\epsilon(\boldsymbol{\delta}, \mathbf{h}, \phi) = \sum_{t=0}^1 \left[((h_t + \delta_t) \circ \phi(X^{\text{Conf}}) - Y(t)) \right], \quad (58)$$

we have that, if Assumption 3 holds,

$$\sup_{\boldsymbol{\delta} \in \mathcal{B}^{\otimes 2}} |\epsilon(\boldsymbol{\delta}, \mathbf{h}, \phi) - \hat{\epsilon}_{\text{Unc}}(\boldsymbol{\delta}, \mathbf{h}, \phi)| \leq 8Ld_{\infty}(p_{\phi}^{\text{Conf}} | p_{\phi}^{\text{Unc}}) \mathcal{G}_{n^{\text{Unc}}}(\mathcal{B}) + 4d_{\infty}(p_{\phi}^{\text{Conf}} | p_{\phi}^{\text{Unc}}) B \sqrt{\frac{\log(1/p)}{n^{\text{Unc}}}}, \quad (59)$$

with probability at least $1 - p$.

Proof

The proof relies on a modified version of Theorem 4.10 in (Wainwright, 2019) and uses a modification of the bounded differences inequality and a standard symmetrization argument. For ease of notation, we use $l_{\mathbf{h},\phi}(\boldsymbol{\delta}, x, y, t) = ((\mathbf{h}_t + \delta_t) \circ \phi(x) - y)^2$.

Then, note that for, any $\boldsymbol{\delta} \in \mathcal{B}^{\otimes 2}$, $\mathbf{h} \in \mathcal{H}^{\otimes 2}$, and $\phi \in \Phi$,

$$\epsilon(\boldsymbol{\delta}, \mathbf{h}, \phi) = \sum_{t=0}^1 \mathbb{E} \left[((\mathbf{h}_t + \delta_t) \circ \phi(X^{\text{Conf}}) - Y(t))^2 \right] \quad (60)$$

$$= \sum_{t=0}^1 \mathbb{P}(T^{\text{Unc}} = t) \mathbb{E} \left[\mathbb{E} [((\mathbf{h}_t + \delta_t) \circ \phi(X^{\text{Conf}}) - Y^{\text{Unc}})^2 \mid T^{\text{Unc}} = t, X^{\text{Conf}}] \right] \quad (61)$$

$$= \mathbb{E} \left[\mathbb{E} [((\mathbf{h}_{T^{\text{Unc}}} + \delta_{T^{\text{Unc}}}) \circ \phi(X^{\text{Conf}}) - Y^{\text{Unc}})^2 \mid T^{\text{Unc}}, X^{\text{Conf}}] \right] \quad (62)$$

$$= \mathbb{E} \left[((\mathbf{h}_{T^{\text{Unc}}} + \delta_{T^{\text{Unc}}}) \circ \phi(X^{\text{Conf}}) - Y^{\text{Unc}})^2 \right] \quad (63)$$

$$= \mathbb{E} [l_{\mathbf{h},\phi}(\boldsymbol{\delta}, X^{\text{Conf}}, Y^{\text{Unc}}, T^{\text{Unc}})]. \quad (64)$$

This yields

$$\sup_{\boldsymbol{\delta} \in \mathcal{B}^{\otimes 2}} |\epsilon(\boldsymbol{\delta}, \mathbf{h}, \phi) - \hat{\epsilon}_{\text{Unc}}(\boldsymbol{\delta}, \mathbf{h}, \phi)| \quad (65)$$

$$= \sup_{\boldsymbol{\delta} \in \mathcal{B}^{\otimes 2}} \left| \frac{1}{n^{\text{Unc}}} \sum_{i=1}^{n^{\text{Unc}}} l_{\mathbf{h},\phi}(\boldsymbol{\delta}, x_i^{\text{Unc}}, y_i^{\text{Unc}}, t_i^{\text{Unc}}) - \mathbb{E} [l_{\mathbf{h},\phi}(\boldsymbol{\delta}, X^{\text{Conf}}, Y^{\text{Unc}}, T^{\text{Unc}})] \right|. \quad (66)$$

We further simplify notation using $\bar{l}_{\mathbf{h},\phi}(\boldsymbol{\delta}, x_i^{\text{Unc}}, y_i^{\text{Unc}}, t_i^{\text{Unc}}) = l_{\mathbf{h},\phi}(\boldsymbol{\delta}, x_i^{\text{Unc}}, y_i^{\text{Unc}}, t_i^{\text{Unc}}) - \mathbb{E} [l_{\mathbf{h},\phi}(\boldsymbol{\delta}, X^{\text{Conf}}, Y^{\text{Unc}}, T^{\text{Unc}})]$. Then, the above can be written as

$$\sup_{\boldsymbol{\delta} \in \mathcal{B}^{\otimes 2}} \left| \frac{1}{n^{\text{Unc}}} \sum_{i=1}^{n^{\text{Unc}}} \bar{l}_{\mathbf{h},\phi}(\boldsymbol{\delta}, x_i^{\text{Unc}}, y_i^{\text{Unc}}, t_i^{\text{Unc}}) \right|. \quad (67)$$

Thinking of the samples as fixed for the moment, we consider the function

$$G(d_1, \dots, d_{n^{\text{Unc}}}) := \sup_{\boldsymbol{\delta} \in \mathcal{B}^{\otimes 2}} \left| \frac{1}{n^{\text{Unc}}} \sum_{i=1}^{n^{\text{Unc}}} \bar{l}_{\mathbf{h},\phi}(\boldsymbol{\delta}, x_i^{\text{Unc}}, y_i^{\text{Unc}}, t_i^{\text{Unc}}) \right|, \quad (68)$$

where $d_i = (x_i^{\text{Unc}}, y_i^{\text{Unc}}, t_i^{\text{Unc}})$. We prove that G is Lipschitz such that we can apply the bounded difference inequality (see Corollary 2.21 in Wainwright (2019)). Since the function G is invariant to permutation of its coordinates, it suffices to bound the difference when the first coordinate d_1 is perturbed. For this, we define the sample vector $(w_1, \dots, w_{n^{\text{Unc}}})$ such that $w_i = d_i$ for $i \neq 1$. Then, we seek a bound for the difference $|G(d_1, \dots, d_{n^{\text{Unc}}}) - G(w_1, \dots, w_{n^{\text{Unc}}})|$. For any $\mathbf{h} \in \mathcal{H}^{\otimes 2}$, $\phi \in \Phi$, $\boldsymbol{\delta}, \mathbf{f} \in \mathcal{B}^{\otimes 2}$, and $\bar{l}_{\mathbf{h},\phi}(\boldsymbol{\delta}, x_i^{\text{Unc}}, y_i^{\text{Unc}}, t_i^{\text{Unc}})$, we have

that

$$\left| \frac{1}{n^{\text{Unc}}} \sum_{i=1}^{n^{\text{Unc}}} \bar{l}_{\mathbf{h},\phi}(\boldsymbol{\delta}, d_i) \right| - \sup_{\mathbf{f} \in \mathcal{B}^{\otimes 2}} \left| \frac{1}{n^{\text{Unc}}} \sum_{i=1}^{n^{\text{Unc}}} \bar{l}_{\mathbf{h},\phi}(\mathbf{f}, w_i) \right| \quad (69)$$

$$\leq \left| \frac{1}{n^{\text{Unc}}} \sum_{i=1}^{n^{\text{Unc}}} \bar{l}_{\mathbf{h},\phi}(\boldsymbol{\delta}, d_i) \right| - \left| \frac{1}{n^{\text{Unc}}} \sum_{i=1}^{n^{\text{Unc}}} \bar{l}_{\mathbf{h},\phi}(\boldsymbol{\delta}, w_i) \right| \quad (70)$$

$$\leq \frac{1}{n^{\text{Unc}}} \left| \bar{l}_{\mathbf{h},\phi}(\boldsymbol{\delta}, d_1) - \bar{l}_{\mathbf{h},\phi}(\boldsymbol{\delta}, w_1) \right| = \frac{1}{n^{\text{Unc}}} |l_{\mathbf{h},\phi}(\mathbf{h}, d_1) - l_{\mathbf{h},\phi}(\mathbf{h}, w_1)| \quad (71)$$

$$\leq \frac{2B}{n^{\text{Unc}}}, \quad (72)$$

where the last inequality follows from the boundedness of the squared loss. Since the above holds for any function $\boldsymbol{\delta} \in \mathcal{B}^{\otimes 2}$, we can take the supremum over $\boldsymbol{\delta} \in \mathcal{B}^{\otimes 2}$ on each sides. This yields $G(d_1, \dots, d_{n^{\text{Unc}}}) - G(w_1, \dots, w_{n^{\text{Unc}}}) \leq \frac{2B}{n^{\text{Unc}}}$. Since the same argument can be applied with $(d_1, \dots, d_{n^{\text{Unc}}})$ and $(w_1, \dots, w_{n^{\text{Unc}}})$ reversed, we conclude that $|G(d_1, \dots, d_{n^{\text{Unc}}}) - G(w_1, \dots, w_{n^{\text{Unc}}})| \leq \frac{2B}{n^{\text{Unc}}}$. Hence, we can apply the bounded differences inequality (see Corollary 2.21 in (Wainwright, 2019)), which yields

$$\sup_{\boldsymbol{\delta} \in \mathcal{B}^{\otimes 2}} \left| \frac{1}{n^{\text{Unc}}} \sum_{i=1}^{n^{\text{Unc}}} \bar{l}_{\mathbf{h},\phi}(\boldsymbol{\delta}, x_i^{\text{Unc}}, y_i^{\text{Unc}}, t_i^{\text{Unc}}) \right| - \mathbb{E} \left[\sup_{\boldsymbol{\delta} \in \mathcal{B}^{\otimes 2}} \left| \frac{1}{n^{\text{Unc}}} \sum_{i=1}^{n^{\text{Unc}}} \bar{l}_{\mathbf{h},\phi}(\boldsymbol{\delta}, x_i^{\text{Unc}}, y_i^{\text{Unc}}, t_i^{\text{Unc}}) \right| \right] \quad (73)$$

$$\leq B \sqrt{\frac{2 \log(1/p)}{n^{\text{Unc}}}}, \quad (74)$$

with probability at least $1 - p$.

We have now proven that, when \mathcal{B} is uniformly bounded, then the random variable $\sup_{\boldsymbol{\delta} \in \mathcal{B}^{\otimes 2}} \left| \frac{1}{n^{\text{Unc}}} \sum_{i=1}^{n^{\text{Unc}}} \bar{l}_{\mathbf{h},\phi}(\boldsymbol{\delta}, x_i^{\text{Unc}}, y_i^{\text{Unc}}, t_i^{\text{Unc}}) \right|$ is sharply concentrated around its expected value. It remains to upper bound $\mathbb{E} \left[\sup_{\boldsymbol{\delta} \in \mathcal{B}^{\otimes 2}} \left| \frac{1}{n^{\text{Unc}}} \sum_{i=1}^{n^{\text{Unc}}} \bar{l}_{\mathbf{h},\phi}(\boldsymbol{\delta}, x_i^{\text{Unc}}, y_i^{\text{Unc}}, t_i^{\text{Unc}}) \right| \right]$. We show that this quantity is upper bounded using classical symmetrization arguments.

For this, let $\{(X_1^{\text{Unc}}, Y_1^{\text{Unc}}, T_1^{\text{Unc}}), \dots, (X_{n^{\text{Unc}}}^{\text{Unc}'}, Y_{n^{\text{Unc}}}^{\text{Unc}'}, T_{n^{\text{Unc}}}^{\text{Unc}'})\}$ and $\{(X_1^{\text{Conf}}, Y_1^{\text{Unc}'}, T_1^{\text{Unc}'})$, $\dots, (X_{n^{\text{Unc}}}^{\text{Conf}}, Y_{n^{\text{Unc}}}^{\text{Unc}'}, T_{n^{\text{Unc}}}^{\text{Unc}'})\}$ be a second *i.i.d.* sequence independent of the first.

Further, let $w_\phi(z) = \frac{p_\phi^{\text{Conf}}(z)}{p_\phi^{\text{Unc}}(z)}$ and Ψ be the inverse of ϕ . Then, together with Lemma 27, this yields

$$\mathbb{E} \left[\sup_{\delta \in \mathcal{B}^{\otimes 2}} \left| \frac{1}{n^{\text{Unc}}} \sum_{i=1}^{n^{\text{Unc}}} \bar{l}_{\mathbf{h},\phi}(\delta, x_i^{\text{Unc}}, y_i^{\text{Unc}}, t_i^{\text{Unc}}) \right| \right] \quad (75)$$

$$= \mathbb{E} \left[\sup_{\delta \in \mathcal{B}^{\otimes 2}} \left| \frac{1}{n^{\text{Unc}}} \sum_{i=1}^{n^{\text{Unc}}} l_{\mathbf{h},\phi}(\delta, x_i^{\text{Unc}}, y_i^{\text{Unc}}, t_i^{\text{Unc}}) - \mathbb{E}[l_{\mathbf{h},\phi}(\delta, X_i^{\text{Conf}}, Y_i^{\text{Unc},'}, T_i^{\text{Unc},'})] \right| \right] \quad (76)$$

$$= \mathbb{E} \left[\sup_{\delta \in \mathcal{B}^{\otimes 2}} \left| \frac{1}{n^{\text{Unc}}} \sum_{i=1}^{n^{\text{Unc}}} l_{\mathbf{h},\phi}(\delta, \phi(\Psi(z_i^{\text{Unc}})), y_i^{\text{Unc}}, t_i^{\text{Unc}}) - \underbrace{\mathbb{E}[l_{\mathbf{h},\phi}(\delta, \phi(\Psi(Z_i^{\text{Conf}})), Y_i^{\text{Unc},'}, T_i^{\text{Unc},'})]}_{=\mathbb{E}[w(\phi(\Psi(Z_i^{\text{Unc}})))l_{\mathbf{h},\phi}(\delta, \phi(\Psi(Z_i^{\text{Unc}})), Y_i^{\text{Unc},'}, T_i^{\text{Unc},'})]} \right| \right] \quad (77)$$

$$= \mathbb{E} \left[\sup_{\delta \in \mathcal{B}^{\otimes 2}} \left| \frac{1}{n^{\text{Unc}}} \sum_{i=1}^{n^{\text{Unc}}} l_{\mathbf{h},\phi}(\delta, z_i^{\text{Unc}}, y_i^{\text{Unc}}, t_i^{\text{Unc}}) - \underbrace{\mathbb{E}[w(\phi(\Psi(Z_i^{\text{Unc}})))l_{\mathbf{h},\phi}(\delta, \phi(\Psi(Z_i^{\text{Unc}})), Y_i^{\text{Unc},'}, T_i^{\text{Unc},'})]}_{=\mathbb{E}[w(Z_i^{\text{Unc}})l_{\mathbf{h},\phi}(\delta, Z_i^{\text{Unc}}, Y_i^{\text{Unc},'}, T_i^{\text{Unc},'})]} \right| \right] \quad (78)$$

$$= \mathbb{E} \left[\sup_{\delta \in \mathcal{B}^{\otimes 2}} \left| \mathbb{E} \left[\frac{1}{n^{\text{Unc}}} \sum_{i=1}^{n^{\text{Unc}}} l_{\mathbf{h},\phi}(\delta, z_i^{\text{Unc}}, y_i^{\text{Unc}}, t_i^{\text{Unc},'}) - w(z_i^{\text{Unc}})l_{\mathbf{h},\phi}(\delta, z_i^{\text{Unc}}, y_i^{\text{Unc},'}, t_i^{\text{Unc},'}) \right] \right| \right] \quad (79)$$

$$\leq \mathbb{E} \left[\sup_{\delta \in \mathcal{B}^{\otimes 2}} \left| \frac{1}{n^{\text{Unc}}} \sum_{i=1}^{n^{\text{Unc}}} l_{\mathbf{h},\phi}(\delta, z_i^{\text{Unc}}, y_i^{\text{Unc}}, t_i^{\text{Unc}}) - w(z_i^{\text{Conf}})l_{\mathbf{h},\phi}(\delta, z_i^{\text{Unc}}, y_i^{\text{Unc},'}, t_i^{\text{Unc},'}) \right| \right]. \quad (80)$$

Let $(\sigma_1, \dots, \sigma_{n^{\text{Unc}}})$ be *i.i.d.* Rademacher variables, independent of other random variables. Then, the random vector with entries $\sigma_i(l_{\mathbf{h},\phi}(\delta, z_i^{\text{Unc}}, y_i^{\text{Unc}}, t_i^{\text{Unc}}) - w(z_i^{\text{Unc}})l_{\mathbf{h},\phi}(\delta, z_i^{\text{Unc}}, y_i^{\text{Unc},'}, t_i^{\text{Unc},'}))$ has the same joint distribution as the random vector with entries $l_{\mathbf{h},\phi}(\delta, z_i^{\text{Unc}}, y_i^{\text{Unc}}, t_i^{\text{Unc}}) - w(z_i^{\text{Conf}})l_{\mathbf{h},\phi}(\delta, z_i^{\text{Unc}}, y_i^{\text{Unc},'}, t_i^{\text{Unc},'})$. Thus,

$$\mathbb{E} \left[\sup_{\delta \in \mathcal{B}^{\otimes 2}} \left| \frac{1}{n^{\text{Unc}}} \sum_{i=1}^{n^{\text{Unc}}} l_{\mathbf{h},\phi}(\delta, z_i^{\text{Unc}}, y_i^{\text{Unc}}, t_i^{\text{Unc}}) - w(z_i^{\text{Unc}})l_{\mathbf{h},\phi}(\delta, z_i^{\text{Unc}}, y_i^{\text{Unc},'}, t_i^{\text{Unc},'}) \right| \right] \quad (81)$$

$$\leq \mathbb{E}_\sigma \left[\sup_{\delta \in \mathcal{B}^{\otimes 2}} \left| \frac{1}{n^{\text{Unc}}} \sum_{i=1}^{n^{\text{Unc}}} \sigma_i(l_{\mathbf{h},\phi}(\delta, z_i^{\text{Unc}}, y_i^{\text{Unc}}, t_i^{\text{Unc}}) - w(z_i^{\text{Unc}})l_{\mathbf{h},\phi}(\delta, z_i^{\text{Unc}}, y_i^{\text{Unc},'}, t_i^{\text{Unc},'})) \right| \right] \quad (82)$$

$$\leq 2d_\infty(p_\phi^{\text{Conf}} | p_\phi^{\text{Unc}}) \mathbb{E}_\sigma \left[\sup_{\delta \in \mathcal{B}^{\otimes 2}} \left| \frac{1}{n^{\text{Unc}}} \sum_{i=1}^{n^{\text{Unc}}} \sigma_i l_{\mathbf{h},\phi}(\delta, z_i^{\text{Unc}}, y_i^{\text{Unc}}, t_i^{\text{Unc}}) \right| \right] \quad (83)$$

$$= 2d_\infty(p_\phi^{\text{Conf}} | p_\phi^{\text{Unc}}) \mathcal{R}_{n^{\text{Unc}}}(l(\mathcal{B}^{\otimes 2})), \quad (84)$$

using $w_\phi(z) = \frac{p_\phi^{\text{Conf}}(z)}{p_\phi^{\text{Unc}}(z)} \leq \sup_z \frac{p_\phi^{\text{Conf}}(z)}{p_\phi^{\text{Unc}}(z)} = d_\infty(p_\phi^{\text{Conf}} | p_\phi^{\text{Unc}})$.

Since the term $\mathcal{R}_{n^{\text{Unc}}}(l(\mathcal{B}^{\otimes 2}))$ includes the loss function, we have to further decompose it. Since the square loss is uniformly bounded by B , we can center the square loss via $l_{\mathbf{h},\phi}^i(\boldsymbol{\delta}, x_i, y_i, t_i) = ((\mathbf{h}_{t_i} + \delta_{t_i}) \circ \phi(x_i) - y_i)^2 - (\mathbf{h}_{t_i} \circ \phi(x_i) - y_i)^2$. Then, using that $(y_i - \mathbf{h}_{t_i} \circ \phi(x_i))^2 = l_{\mathbf{h},\phi}(\boldsymbol{\delta}, x, y, t)$ with $\delta_t(z) = \mathbf{0}$ and, therefore, $(y - \mathbf{h}_t \circ \phi(x))^2 \leq B$ and using the constant-shift property of Rademacher complexity (Wainwright (2019); Exercise 4.7c) yields

$$\mathbb{E}_\sigma \left[\sup_{\boldsymbol{\delta} \in \mathcal{B}^{\otimes 2}} \frac{1}{n^{\text{Unc}}} \sum_{i=1}^{n^{\text{Unc}}} \sigma_i l_{\mathbf{h},\phi}(\boldsymbol{\delta}, z_i^{\text{Unc}}, y_i^{\text{Unc}}, t_i^{\text{Unc}}) \right] \quad (85)$$

$$\leq \mathbb{E}_\sigma \left[\sup_{\boldsymbol{\delta} \in \mathcal{B}^{\otimes 2}} \frac{1}{n^{\text{Unc}}} \sum_{i=1}^{n^{\text{Unc}}} \sigma_i l_{\mathbf{h},\phi}^i(\boldsymbol{\delta}, z_i^{\text{Unc}}, y_i^{\text{Unc}}, t_i^{\text{Unc}}) \right] + \frac{B}{\sqrt{n^{\text{Unc}}}}. \quad (86)$$

Since the loss is L -Lipschitz and, now, also centered, we can apply contraction principle (Ledoux and Talagrand (2013); Theorem 4.12), which yields

$$E_\sigma \left[\sup_{\boldsymbol{\delta} \in \mathcal{B}^{\otimes 2}} \frac{1}{n^{\text{Unc}}} \sum_{i=1}^{n^{\text{Unc}}} \sigma_i l_{\mathbf{h},\phi}^i(\boldsymbol{\delta}, z_i^{\text{Unc}}, y_i^{\text{Unc}}, t_i^{\text{Unc}}) \right] \leq 2L\mathcal{R}_{n^{\text{Unc}}}(\mathcal{B}^{\otimes 2}). \quad (87)$$

Finally, note that $\mathcal{R}_{n^{\text{Unc}}}(\mathcal{B}^{\otimes 2}) = \mathcal{R}_{n^{\text{Unc}}}(\mathcal{B})$, since in (87), the supremum is over $\delta_1 \in \mathcal{B}$ if $t_i = 1$ and over $\delta_0 \in \mathcal{B}$ if $t_i = 0$. Hence, the complexity is equivalent to the supremum over \mathcal{B} . Putting everything together, we obtain

$$\sup_{\boldsymbol{\delta} \in \mathcal{B}^{\otimes 2}} |\epsilon(\boldsymbol{\delta}, \mathbf{h}, \phi) - \hat{\epsilon}_{\text{Unc}}(\boldsymbol{\delta}, \mathbf{h}, \phi)| = \sup_{\boldsymbol{\delta} \in \mathcal{B}^{\otimes 2}} \left| \frac{1}{n^{\text{Unc}}} \sum_{i=1}^{n^{\text{Unc}}} \bar{l}_{\mathbf{h},\phi}(\boldsymbol{\delta}, x_i^{\text{Unc}}, y_i^{\text{Unc}}, t_i^{\text{Unc}}) \right| \quad (88)$$

$$\leq \mathbb{E} \left[\sup_{\boldsymbol{\delta} \in \mathcal{B}^{\otimes 2}} \left| \frac{1}{n^{\text{Unc}}} \sum_{i=1}^{n^{\text{Unc}}} \bar{l}_{\mathbf{h},\phi}(\boldsymbol{\delta}, x_i^{\text{Unc}}, y_i^{\text{Unc}}, t_i^{\text{Unc}}) \right| \right] + B\sqrt{\frac{2\log(1/p)}{n^{\text{Unc}}}} \quad (89)$$

$$\leq 2d_\infty(p_\phi^{\text{Conf}} | p_\phi^{\text{Unc}})\mathcal{R}_{n^{\text{Unc}}}(l(\mathcal{B}^{\otimes 2})) + B\sqrt{\frac{2\log(1/p)}{n^{\text{Unc}}}} \quad (90)$$

$$\leq 2d_\infty(p_\phi^{\text{Conf}} | p_\phi^{\text{Unc}})(2L\mathcal{R}_{n^{\text{Unc}}}(\mathcal{B}) + \frac{B}{\sqrt{n^{\text{Unc}}}}) + B\sqrt{\frac{2\log(1/p)}{n^{\text{Unc}}}} \quad (91)$$

$$\leq 4Ld_\infty(p_\phi^{\text{Conf}} | p_\phi^{\text{Unc}})\mathcal{R}_{n^{\text{Unc}}}(\mathcal{B}) + 2d_\infty(p_\phi^{\text{Conf}} | p_\phi^{\text{Unc}})B\sqrt{\frac{2\log(1/p)}{n^{\text{Unc}}}} \quad (92)$$

The Rademacher complexity can be upper bounded by the Gaussian complexity (Ledoux and Talagrand (2013); p. 97): $\mathbb{E}[\hat{\mathcal{R}}_{Z^{\text{Unc}}}(\mathcal{B})] \leq \sqrt{\frac{\pi}{2}}\mathbb{E}[\hat{\mathcal{G}}_{Z^{\text{Unc}}}(\mathcal{B})]$. Combining this with the result above yields

$$\sup_{\boldsymbol{\delta} \in \mathcal{B}^{\otimes 2}} |\epsilon(\boldsymbol{\delta}, \mathbf{h}, \phi) - \hat{\epsilon}_{\text{Unc}}(\boldsymbol{\delta}, \mathbf{h}, \phi)| \quad (93)$$

$$\leq 4Ld_\infty(p_\phi^{\text{Conf}} | p_\phi^{\text{Unc}})\sqrt{\frac{\pi}{2}}\mathcal{G}_{n^{\text{Unc}}}(\mathcal{B}) + 2d_\infty(p_\phi^{\text{Conf}} | p_\phi^{\text{Unc}})B\sqrt{\frac{2\log(1/p)}{n^{\text{Unc}}}} \quad (94)$$

with probability at least $1 - p$.

■

Lemma 17 *Let $\hat{\mathbf{h}}, \hat{\phi} = \arg \min_{\mathbf{h} \in \mathcal{H}^{\otimes 2}, \phi \in \Phi} \hat{\epsilon}_{\text{Conf}}(\mathbf{h}, \phi)$ and $\tilde{\mathbf{h}} = \arg \min_{\mathbf{h} \in \mathcal{H}^{\otimes 2}} \epsilon_{\text{Conf}}(\mathbf{h}, \hat{\phi})$. Then, under the assumptions of Theorem 2, with probability at least $1 - p$,*

$$\begin{aligned} \epsilon_{\text{Conf}}(\hat{\mathbf{h}}^c, \hat{\phi}) - \epsilon_{\text{Conf}}(\mathbf{h}^c, \phi^*) &\leq 2048L \left(\frac{D\mathcal{X}}{(n^{\text{Conf}})^2} + \log(n^{\text{Conf}})(L(\mathcal{H})\mathcal{G}_{n^{\text{Conf}}}(\Phi) + \bar{\mathcal{G}}_{n^{\text{Conf}}}(\mathcal{H})) \right) \\ &\quad + 8B \sqrt{\frac{\log(1/p)}{n^{\text{Conf}}}}. \end{aligned} \quad (95)$$

Proof It follows that,

$$\epsilon_{\text{Conf}}(\hat{\mathbf{h}}^c, \hat{\phi}) - \epsilon_{\text{Conf}}(\mathbf{h}^c, \phi^*) \quad (96)$$

$$\begin{aligned} &= \epsilon_{\text{Conf}}(\hat{\mathbf{h}}^c, \hat{\phi}) - \hat{\epsilon}_{\text{Conf}}(\hat{\mathbf{h}}^c, \hat{\phi}) + \underbrace{\hat{\epsilon}_{\text{Conf}}(\hat{\mathbf{h}}^c, \hat{\phi}) - \hat{\epsilon}_{\text{Conf}}(\mathbf{h}^c, \phi^*)}_{\leq 0} + \hat{\epsilon}_{\text{Conf}}(\mathbf{h}^c, \phi^*) - \epsilon_{\text{Conf}}(\mathbf{h}^c, \phi^*) \end{aligned} \quad (97)$$

$$\leq 2 \sup_{\mathbf{h} \in \mathcal{H}^{\otimes 2}, \phi \in \Phi} |\epsilon_{\text{Conf}}(\mathbf{h}, \phi) - \hat{\epsilon}_{\text{Conf}}(\mathbf{h}, \phi)| \quad (98)$$

$$\leq 8LR_{n^{\text{Conf}}}(\mathcal{H}(\Phi)) + \frac{8B\sqrt{2\log(1/p)}}{\sqrt{n^{\text{Conf}}}}, \quad (99)$$

with probability at least $1 - p$. The first inequality follows by the same symmetrization argument as in the proof of Lemma 16 (although without the distributional discrepancy).

The Rademacher complexity can be upper bounded by the Gaussian complexity (Ledoux and Talagrand (2013), p. 97): $\mathbb{E}[\hat{\mathcal{R}}_{X^{\text{Conf}}}(\mathcal{H}(\Phi))] \leq \sqrt{\frac{\pi}{2}} \mathbb{E}[\hat{\mathcal{G}}_{X^{\text{Conf}}}(\mathcal{H}(\Phi))]$. For the last step we use the chain rule for Gaussian complexity from Theorem 7 in Tripuraneni et al. (2020). This yields

$$\hat{\mathcal{G}}_{X^{\text{Conf}}}(\mathcal{H}(\Phi)) \leq 128 \left(\frac{2D\mathcal{X}}{(n^{\text{Conf}})^2} + C(\mathcal{H}(\Phi)) \log(n^{\text{Conf}}) \right), \quad (100)$$

where $C(\mathcal{H}(\Phi)) = L(\mathcal{H})\hat{\mathcal{G}}_{X^{\text{Conf}}}(\Phi) + \max_{\bar{Z} \in \mathcal{Z}} \hat{\mathcal{G}}_{\bar{Z}}(\mathcal{H})$ and $\mathcal{Z} = \{(\phi(x_1), \dots, \phi(x_{n^{\text{Conf}}})) ; \phi \in \Phi\}$. Combining this with the result above and taking expectations yields

$$\epsilon_{\text{Conf}}(\hat{\mathbf{h}}^c, \hat{\phi}) - \epsilon_{\text{Conf}}(\mathbf{h}^c, \phi^*) \leq 2048L \left(\frac{D\mathcal{X}}{(n^{\text{Conf}})^2} + \log(n^{\text{Conf}})(L(\mathcal{H})\mathcal{G}_{n^{\text{Conf}}}(\Phi) + \bar{\mathcal{G}}_{n^{\text{Conf}}}(\mathcal{H})) \right) \quad (101)$$

$$+ 8B \sqrt{\frac{2\log(1/p)}{n^{\text{Conf}}}}, \quad (102)$$

with probability $1 - p$. ■

We are now equipped to prove a version Theorem 2 for an arbitrary representation function class Φ , hypothesis function class \mathcal{H} , and bias function class \mathcal{B} .

For this, we assume the following standard, mild regularity conditions on the loss function $l(\cdot, \cdot)$, the hypothesis class \mathcal{H} , and the function class of representations Φ . Note that these assumptions hold true for neural networks, which we prove later.

Assumption A1 (Regularity Conditions.) We assume the following regularity conditions hold:

1. The loss-function $l(x, y) = (x - y)^2$ is B -bounded and $l(\cdot, y)$ is L -Lipschitz for all $y \in \mathbb{R}$.
2. The function h_t is $L(\mathcal{H})$ -Lipschitz with respect to the l_2 distance, for any $h_t \in \mathcal{H}$.
3. The composition function $h_t \circ \phi$ is bounded, i. e., $\sup_{x \in \mathbb{R}^d} |h_t \circ \phi(x)| \leq D_X$ for any $h_t \in \mathcal{H}$ and $\phi \in \Phi$.

Theorem 18 Let $(\hat{\mathbf{h}}^c, \hat{\phi})$ be the empirical loss minimizer of $\hat{\epsilon}_{\text{Conf}}(\cdot, \cdot)$ from (10) over function classes Φ and \mathcal{H} , and let δ be the empirical loss minimizer of $\hat{\epsilon}_{\text{Unc}}(\cdot, \hat{\mathbf{h}}^c, \hat{\phi})$ from (12) over a function class \mathcal{B} . Further, let $\hat{\tau}_{\text{CorNet}}$ be the resulting CATE estimator from (15). Then, if Assumption 3, Assumption A1, and Condition 1 hold true, we have that, with probability at least $1 - p$,

$$\begin{aligned} \epsilon_{\text{PEHE}}(\hat{\tau}_{\text{Cor}}) \leq & \tilde{O} \left(L(\mathcal{H}) \mathcal{G}_{n^{\text{Conf}}}(\Phi) + \bar{\mathcal{G}}_{n^{\text{Conf}}}(\mathcal{H}) + d_{\infty}(p_{\phi}^{\text{Conf}} | p_{\phi}^{\text{Unc}}) \mathcal{G}_{n^{\text{Unc}}}(\mathcal{B}) \right. \\ & \left. + \frac{D_X}{(n^{\text{Conf}})^2} + \frac{B}{L} \left(\sqrt{\frac{2 \log(1/p)}{n^{\text{Conf}}}} + d_{\infty}(p_{\phi}^{\text{Conf}} | p_{\phi}^{\text{Unc}}) \sqrt{\frac{2 \log(1/p)}{n^{\text{Unc}}}} \right) \right), \end{aligned} \quad (103)$$

where $\mathcal{G}_{n^{\text{Conf}}}(\Phi)$, $\bar{\mathcal{G}}_{n^{\text{Conf}}}(\mathcal{H})$, and $\mathcal{G}_{n^{\text{Unc}}}(\mathcal{B})$ are the Gaussian complexities and worst-case Gaussian complexities of the corresponding functions classes. Moreover, $d_{\infty}(p_{\phi}^{\text{Conf}} | p_{\phi}^{\text{Unc}})$ is the exponential in base 2 of the Rényi divergence.

Proof First,

$$\epsilon_{\text{PEHE}}(\hat{\tau}_{\text{Cor}}) = \mathbb{E}[(\hat{\tau}(X^{\text{Conf}}) - \tau(X^{\text{Conf}}))^2] \quad (104)$$

$$= \mathbb{E}[(\hat{\mathbf{h}}_1^c + \hat{\delta}_1) \circ \hat{\phi}(X^{\text{Conf}}) - ((\hat{\mathbf{h}}_0^c + \hat{\delta}_0) \circ \hat{\phi}(X^{\text{Conf}}) \quad (105)$$

$$- ((\mathbf{h}_1^c + \delta_1) \circ \phi^*(X^{\text{Conf}}) - (\mathbf{h}_0^c + \delta_0) \circ \phi^*(X^{\text{Conf}}))]^2] \quad (106)$$

$$\leq 2\mathbb{E}[(\hat{\mathbf{h}}_1^c + \hat{\delta}_1) \circ \hat{\phi}(X^{\text{Conf}}) - (\mathbf{h}_1^c + \delta_1) \circ \phi^*(X^{\text{Conf}})]^2 \quad (107)$$

$$+ ((\mathbf{h}_0^c + \delta_0) \circ \phi^*(X^{\text{Conf}}) - (\hat{\mathbf{h}}_0^c + \hat{\delta}_0) \circ \hat{\phi}(X^{\text{Conf}})]^2] \quad (108)$$

$$= 2 \sum_{t=0}^1 \mathbb{E}[(\hat{\mathbf{h}}_t^c + \hat{\delta}_t) \circ \hat{\phi}(X^{\text{Conf}}) - (\mathbf{h}_t^c + \delta_t) \circ \phi^*(X^{\text{Conf}})]^2] \quad (109)$$

$$= 2 \sum_{t=0}^1 \mathbb{E}[(\hat{\mathbf{h}}_t^c + \hat{\delta}_t) \circ \hat{\phi}(X^{\text{Conf}}) - Y(t)]^2 - ((\mathbf{h}_t^c + \delta_t) \circ \phi^*(X^{\text{Conf}}) - Y(t)]^2] \quad (110)$$

$$= 2 \left(\sum_{t=0}^1 \mathbb{E}[(\hat{\mathbf{h}}_t^c + \hat{\delta}_t) \circ \hat{\phi}(X^{\text{Conf}}) - Y(t)]^2 \right) - \sum_{t=0}^1 \mathbb{E}[(\mathbf{h}_t^c + \delta_t) \circ \phi^*(X^{\text{Conf}}) - Y(t)]^2 \quad (111)$$

$$= 2(\epsilon(\hat{\boldsymbol{\delta}}, \hat{\mathbf{h}}^c, \hat{\phi}) - \epsilon(\boldsymbol{\delta}, \mathbf{h}^c, \phi^*)), \quad (112)$$

where the inequality follows with $(x + y)^2 \leq 2(x^2 + y^2)$ and the fourth equality follows with Lemma 26.

Let $\hat{\mathbf{h}}^c, \hat{\phi} = \arg \min_{\mathbf{h} \in \mathcal{H}^{\otimes 2}, \phi \in \Phi} \hat{\epsilon}_{\text{Conf}}(\mathbf{h}, \phi)$, and $\tilde{\boldsymbol{\delta}} = \arg \min_{\boldsymbol{\delta} \in \mathcal{B}^{\otimes 2}} \epsilon(\boldsymbol{\delta}, \hat{\mathbf{h}}^c, \hat{\phi})$, and $\hat{\boldsymbol{\delta}} = \arg \min_{\boldsymbol{\delta} \in \mathcal{B}^{\otimes 2}} \hat{\epsilon}_{\text{Unc}}(\boldsymbol{\delta}, \hat{\mathbf{h}}^c, \hat{\phi})$. Then, we have that

$$\epsilon(\hat{\boldsymbol{\delta}}, \hat{\mathbf{h}}^c, \hat{\phi}) - \epsilon(\boldsymbol{\delta}, \mathbf{h}^c, \phi^*) = \underbrace{\epsilon(\hat{\boldsymbol{\delta}}, \hat{\mathbf{h}}^c, \hat{\phi}) - \epsilon(\tilde{\boldsymbol{\delta}}, \hat{\mathbf{h}}^c, \hat{\phi})}_{=(\text{I})} + \underbrace{\epsilon(\tilde{\boldsymbol{\delta}}, \hat{\mathbf{h}}^c, \hat{\phi}) - \epsilon(\boldsymbol{\delta}, \mathbf{h}^c, \phi^*)}_{=(\text{II})}. \quad (113)$$

For the first term (I), we obtain

$$\begin{aligned} (\text{I}) &= \underbrace{\epsilon(\hat{\boldsymbol{\delta}}, \hat{\mathbf{h}}^c, \hat{\phi}) - \hat{\epsilon}_{\text{Unc}}(\hat{\boldsymbol{\delta}}, \hat{\mathbf{h}}^c, \hat{\phi})}_{=(i)} + \underbrace{\hat{\epsilon}_{\text{Unc}}(\hat{\boldsymbol{\delta}}, \hat{\mathbf{h}}^c, \hat{\phi}) - \hat{\epsilon}_{\text{Unc}}(\tilde{\boldsymbol{\delta}}, \hat{\mathbf{h}}^c, \hat{\phi})}_{\leq 0} \\ &\quad + \underbrace{\hat{\epsilon}_{\text{Unc}}(\tilde{\boldsymbol{\delta}}, \hat{\mathbf{h}}^c, \hat{\phi}) - \epsilon(\tilde{\boldsymbol{\delta}}, \hat{\mathbf{h}}^c, \hat{\phi})}_{=(ii)}, \end{aligned} \quad (114)$$

where the middle term is negative, since $\hat{\boldsymbol{\delta}} = \arg \min_{\boldsymbol{\delta} \in \mathcal{B}^{\otimes 2}} \hat{\epsilon}_{\text{Unc}}(\boldsymbol{\delta}, \hat{\mathbf{h}}^c, \hat{\phi})$ and $\tilde{\boldsymbol{\delta}} = \arg \min_{\boldsymbol{\delta} \in \mathcal{B}^{\otimes 2}} \epsilon(\boldsymbol{\delta}, \hat{\mathbf{h}}^c, \hat{\phi})$. Further, (i), (ii) $\leq \sup_{\boldsymbol{\delta} \in \mathcal{B}^{\otimes 2}} |\epsilon(\boldsymbol{\delta}, \hat{\mathbf{h}}^c, \hat{\phi}) - \hat{\epsilon}_{\text{Unc}}(\boldsymbol{\delta}, \hat{\mathbf{h}}^c, \hat{\phi})|$.

From Lemma 16, we know that, with probability at least $1 - p$,

$$\begin{aligned} \sup_{\boldsymbol{\delta} \in \mathcal{B}^{\otimes 2}} |\epsilon(\boldsymbol{\delta}, \hat{\mathbf{h}}^c, \hat{\phi}) - \hat{\epsilon}_{\text{Unc}}(\boldsymbol{\delta}, \hat{\mathbf{h}}^c, \hat{\phi})| &\leq 8Ld_{\infty}(p_{\phi}^{\text{Conf}} | p_{\phi}^{\text{Unc}}) \mathcal{G}_{n^{\text{Unc}}}(\mathcal{B}) \\ &\quad + 4d_{\infty}(p_{\phi}^{\text{Conf}} | p_{\phi}^{\text{Unc}}) B \sqrt{\frac{\log(1/p)}{n^{\text{Unc}}}}. \end{aligned} \quad (115)$$

Moreover, for the second term (II), we obtain

$$(II) = \inf_{\delta' \in \mathcal{B}^{\otimes 2}} \epsilon(\delta', \hat{\mathbf{h}}^c, \hat{\phi}) - \epsilon(\delta, \mathbf{h}^c, \phi^*) \quad (116)$$

$$= \inf_{\delta' \in \mathcal{B}^{\otimes 2}} \sum_{t=0}^1 \mathbb{E} [((\hat{\mathbf{h}}_t^c + \delta'_t) \circ \hat{\phi}(X^{\text{Conf}}) - Y(t))^2 - ((\mathbf{h}_t^c + \delta_t) \circ \phi^*(X^{\text{Conf}}) - Y(t))^2] \quad (117)$$

$$= \inf_{\delta' \in \mathcal{B}^{\otimes 2}} \sum_{t=0}^1 \mathbb{E} [((\hat{\mathbf{h}}_t^c + \delta'_t) \circ \hat{\phi}(X^{\text{Conf}}) - (\mathbf{h}_t^c + \delta_t) \circ \phi^*(X^{\text{Conf}}))^2] \quad (118)$$

$$\leq 2 \inf_{\delta' \in \mathcal{B}^{\otimes 2}} \sum_{t=0}^1 \mathbb{E} [(\hat{\mathbf{h}}_t^c \circ \hat{\phi}(X^{\text{Conf}}) - \mathbf{h}_t^c \circ \phi^*(X^{\text{Conf}}))^2 + (\delta'_t \circ \hat{\phi}(X^{\text{Conf}}) - \delta_t \circ \phi^*(X^{\text{Conf}}))^2] \quad (119)$$

$$= 2 \sum_{t=0}^1 \mathbb{E} [(\hat{\mathbf{h}}_t^c \circ \hat{\phi}(X^{\text{Conf}}) - \mathbf{h}_t^c \circ \phi^*(X^{\text{Conf}}))^2] + 2 d_{\mathcal{B}, \delta}(\hat{\phi}; \phi^*) \quad (120)$$

$$= 2 \sum_{t=0}^1 \mathbb{E} [(\hat{\mathbf{h}}_t^c \circ \hat{\phi}(X^{\text{Conf}}) - Y^{\text{Conf}})^2 - (\mathbf{h}_t^c \circ \phi^*(X^{\text{Conf}}) - Y^{\text{Conf}})^2] + 2 d_{\mathcal{B}, \delta}(\hat{\phi}; \phi^*) \quad (121)$$

$$= 2(\epsilon_{\text{Conf}}(\hat{\mathbf{h}}^c, \hat{\phi}) - \epsilon_{\text{Conf}}(\mathbf{h}^c, \phi^*)) + 2 d_{\mathcal{B}, \delta}(\hat{\phi}; \phi^*), \quad (122)$$

where the third equality follows with Lemma 26. Using Condition 1, $d_{\mathcal{B}, \delta}(\hat{\phi}; \phi^*) \leq \gamma d_{\mathcal{H}, \mathbf{h}^c}(\hat{\phi}; \phi^*)$, and, for $\tilde{\mathbf{h}}^c = \arg \min_{\mathbf{h} \in \mathcal{H}^{\otimes 2}} \epsilon_{\text{Conf}}(\mathbf{h}, \hat{\phi})$,

$$d_{\mathcal{H}, \mathbf{h}^c}(\hat{\phi}; \phi^*) = \underbrace{\epsilon_{\text{Conf}}(\tilde{\mathbf{h}}^c, \hat{\phi}) - \epsilon_{\text{Conf}}(\hat{\mathbf{h}}^c, \hat{\phi})}_{\leq 0} + \epsilon_{\text{Conf}}(\hat{\mathbf{h}}^c, \hat{\phi}) - \epsilon_{\text{Conf}}(\mathbf{h}^c, \phi^*) \quad (123)$$

$$\leq \epsilon_{\text{Conf}}(\hat{\mathbf{h}}^c, \hat{\phi}) - \epsilon_{\text{Conf}}(\mathbf{h}^c, \phi^*) \quad (124)$$

yields that (122) $\leq (2 + 2\gamma)(\epsilon_{\text{Conf}}(\hat{\mathbf{h}}^c, \hat{\phi}) - \epsilon_{\text{Conf}}(\mathbf{h}^c, \phi^*))$. Then, using Lemma 17, we have that, with probability at least $1 - p$,

$$\begin{aligned} \epsilon_{\text{Conf}}(\hat{\mathbf{h}}^c, \hat{\phi}) - \epsilon_{\text{Conf}}(\mathbf{h}^c, \phi^*) &\leq 2048L \left(\frac{D\mathcal{X}}{(n^{\text{Conf}})^2} + \log(n^{\text{Conf}})(L(\mathcal{H})\mathcal{G}_{n^{\text{Conf}}}(\Phi) + \bar{\mathcal{G}}_{n^{\text{Conf}}}(\mathcal{H})) \right) \\ &\quad + 8B \sqrt{\frac{2 \log(1/p)}{n^{\text{Conf}}}}. \end{aligned} \quad (125)$$

Finally, this yields, with probability at least $1 - p$,

$$\epsilon_{\text{PEHE}}(\hat{\tau}_{\text{Cor}}) \leq 2((2 + 2\gamma)2048L \left(\frac{D\mathcal{X}}{(n^{\text{Conf}})^2} + \log(n^{\text{Conf}})(L(\mathcal{H})\mathcal{G}_{n^{\text{Conf}}}(\Phi) + \bar{\mathcal{G}}_{n^{\text{Conf}}}(\mathcal{H})) \right) \quad (126)$$

$$+ 8B\sqrt{\frac{2\log(1/p)}{n^{\text{Conf}}}} + 8Ld_\infty(p_\phi^{\text{Conf}} | p_\phi^{\text{Unc}})\mathcal{G}_{n^{\text{Unc}}}(\mathcal{B}) + 4d_\infty(p_\phi^{\text{Conf}} | p_\phi^{\text{Unc}})B\sqrt{\frac{2\log(1/p)}{n^{\text{Unc}}}} \quad (127)$$

$$\leq \tilde{O}\left(L(\mathcal{H})\mathcal{G}_{n^{\text{Conf}}}(\Phi) + \bar{\mathcal{G}}_{n^{\text{Conf}}}(\mathcal{H}) + d_\infty(p_\phi^{\text{Conf}} | p_\phi^{\text{Unc}})\mathcal{G}_{n^{\text{Unc}}}(\mathcal{B}) \quad (128)$$

$$+ \frac{D\mathcal{X}}{(n^{\text{Conf}})^2} + \frac{B}{L} \left(\sqrt{\frac{2\log(1/p)}{n^{\text{Conf}}}} + d_\infty(p_\phi^{\text{Conf}} | p_\phi^{\text{Unc}})\sqrt{\frac{2\log(1/p)}{n^{\text{Unc}}}} \right). \quad (129)$$

■

We have proven the statement now for general function classes. Since we use neural networks for representation functions and hypotheses in the statement in the main paper, we prove the statement now using neural networks as defined in Appendix B.

Proof of Theorem 2. For the proof, we build upon the error bound for general function classes as in Appendix C.1. We first prove upper bounds for the Gaussian complexities in Theorem 18. Then, we prove that Assumption A1 holds true for neural networks.

In order to find an upper bound for the Gaussian complexity of a neural network, we make use of Theorem 2 from Golowich et al. (2018):

Let \mathcal{N} be the class of real-valued neural networks as defined in Appendix B of depth K over a domain \mathcal{X} with $\|x_i\| \leq D$ for $i \in \{1, \dots, m\}$. Let $\|\mathbf{W}_k\|_{1,\infty} \leq \Omega_k$ for all $k \in \{1, \dots, K\}$ and let the activation function σ be a 1-Lipschitz function with $\sigma(0) = 0$, which is applied element-wise. Then,

$$\hat{\mathcal{R}}_m(\mathcal{N}) \leq \frac{2D\sqrt{K+1+\log(d)}\Omega\prod_{k=1}^{K-1}\Omega_k}{\sqrt{m}}. \quad (130)$$

We proceed to upper bound the Gaussian complexities.

Upper bound for $\hat{\mathcal{G}}_X(\Phi)$: First, we derive an upper bound on the Gaussian complexity of the representation class Φ :

$$\hat{\mathcal{G}}_{X^{\text{Conf}}}(\Phi) = \mathbb{E}_{\mathbf{g}} \left[\sup_{\phi \in \Phi} \frac{1}{n^{\text{Conf}}} \sum_{k=1}^{d_\phi} \sum_{i=1}^{n^{\text{Conf}}} g_{ki} \phi_k(x_i) \right] \leq \sum_{k=1}^{d_\phi} \hat{\mathcal{G}}_{X^{\text{Conf}}}(\Phi_k) \quad (131)$$

$$\leq 2\log(n^{\text{Conf}}) \sum_{k=1}^{d_\phi} \hat{\mathcal{R}}_{n^{\text{Conf}}}(\Phi_k) \leq 2\log(n^{\text{Conf}}) \frac{\mathcal{C}_\Phi}{\sqrt{n^{\text{Conf}}}}, \quad (132)$$

where $\mathcal{C}_\Phi = 2d_\phi D\sqrt{K+1+\log(d)}\Omega\prod_{k=1}^{K-1}\Omega_k$. We use the upper bound of the Rademacher complexity of neural networks as above (Golowich et al., 2018) and $\hat{\mathcal{G}}_{X^{\text{Conf}}}(\mathcal{F}) \leq 2\sqrt{\log(N)}\hat{\mathcal{R}}_{n^{\text{Conf}}}(\mathcal{F})$

for an arbitrary function class \mathcal{F} (Ledoux and Talagrand, 2013). Taking the expectation is trivial, since the upper bound does not depend on the data.

Upper bound for $\bar{\mathcal{G}}_{n^{\text{Conf}}}(\mathcal{H})$: We upper bound on the worst-case Gaussian complexity of \mathcal{H} follows similar to the above for $r = 1$:

$$\bar{\mathcal{G}}_{n^{\text{Conf}}}(\mathcal{H}) = \max_{Z \in \mathcal{Z}} \hat{\mathcal{G}}_{\bar{Z}}(\mathcal{H}) \leq 2 \log(n^{\text{Conf}}) \frac{\mathcal{C}_{\mathcal{H}}}{\sqrt{n^{\text{Conf}}}}, \quad (133)$$

where, similar to the above, $\mathcal{C}_{\mathcal{H}} = 2\|\phi(x)\| \sqrt{D+1+\log(d_{\phi})} \prod_{d=1}^D \Omega_d$, where $\|\phi(x)\| \leq \Omega$ with Lemma 19.

Upper bound for $\hat{\mathcal{G}}_Z(\mathcal{B})$: Finally, we upper bound the Gaussian complexity in the second step similar to the above for $d = 1$ and $z_i^{\text{Unc}} = \hat{\phi}(x_i^{\text{Unc}})$:

$$\hat{\mathcal{G}}_{Z^{\text{Unc}}}(\mathcal{B}) = \mathbb{E}_{\mathbf{g}} \left[\sup_{\delta \in \mathcal{B}} \frac{1}{n^{\text{Unc}}} \sum_{i=1}^{n^{\text{Unc}}} g_i \delta(z_i^{\text{Unc}}) \right] \leq 2 \log(n^{\text{Unc}}) \hat{\mathcal{R}}_{n^{\text{Unc}}}(\mathcal{B}) \leq 2 \log(n^{\text{Unc}}) \frac{\mathcal{C}_{\mathcal{B}}}{\sqrt{n^{\text{Unc}}}}, \quad (134)$$

where, similar to the above, $\mathcal{C}_{\mathcal{B}} = 2\Omega \sqrt{B+1+\log(d_{\phi})} \prod_{b=1}^B \Omega_b$.

Next, we verify that Assumption A1 for Theorem 18 holds true for neural networks. Using Lemma 19, the boundedness parameter is

$$D_{\mathcal{X}} \leq \mathcal{O}(\Omega_D). \quad (135)$$

For the square loss, we have that $\nabla_a(a-y)^2 = 2(a-y) = \mathcal{O}(n+|a|)$ and $n = \mathcal{O}(1)$. Moreover, either $|a| \leq |h \circ \phi(x)| \leq \Omega_D$ or $|a| \leq |\delta \circ \phi(x)| \leq \Omega_B$. Hence, the square loss is Lipschitz with $L = \mathcal{O}(\max(\Omega_D, \Omega_B))$. Furthermore, by the analogous argument, the square loss is bounded by $B = \mathcal{O}(\max(\Omega_D, \Omega_B)^2)$.

Moreover, by Lemma 20, the hypothesis class \mathcal{H} is Lipschitz with $L(\mathcal{H}) \leq \mathcal{O}(\Omega_D)$.

Putting this together with the result from Theorem 18 yields

$$\epsilon_{\text{PEHE}}(\hat{\tau}_{\text{Cor}}) \leq \tilde{\mathcal{O}} \left(\Omega_D \frac{\mathcal{C}_{\Phi}}{\sqrt{n^{\text{Conf}}}} + \frac{\mathcal{C}_{\mathcal{H}}}{\sqrt{n^{\text{Conf}}}} + d_{\infty}(p_{\phi}^{\text{Conf}} | p_{\phi}^{\text{Unc}}) \frac{\mathcal{C}_{\mathcal{B}}}{\sqrt{n^{\text{Unc}}}} \right) \quad (136)$$

$$+ \frac{\Omega_D}{(n^{\text{Conf}})^2} + \max(\Omega_D, \Omega_B) \left(\sqrt{\frac{\log(1/p)}{n^{\text{Conf}}}} + d_{\infty}(p_{\phi}^{\text{Conf}} | p_{\phi}^{\text{Unc}}) \sqrt{\frac{\log(1/p)}{n^{\text{Unc}}}} \right) \quad (137)$$

$$\leq \tilde{\mathcal{O}} \left(\frac{\mathcal{C}_{\Phi} + \mathcal{C}_{\mathcal{H}}}{\sqrt{n^{\text{Conf}}}} + \frac{d_{\infty}(p_{\phi}^{\text{Conf}} | p_{\phi}^{\text{Unc}}) \mathcal{C}_{\mathcal{B}}}{\sqrt{n^{\text{Unc}}}} + \frac{1}{(n^{\text{Conf}})^2} \right) \quad (138)$$

$$+ \left(\sqrt{\frac{\log(1/p)}{n^{\text{Conf}}}} + d_{\infty}(p_{\phi}^{\text{Conf}} | p_{\phi}^{\text{Unc}}) \sqrt{\frac{\log(1/p)}{n^{\text{Unc}}}} \right) \quad (139)$$

$$\leq \tilde{\mathcal{O}} \left(\frac{\mathcal{C}_{\Phi} + \mathcal{C}_{\mathcal{H}}}{\sqrt{n^{\text{Conf}}}} + \frac{d_{\infty}(p_{\phi}^{\text{Conf}} | p_{\phi}^{\text{Unc}}) \mathcal{C}_{\mathcal{B}}}{\sqrt{n^{\text{Unc}}}} \right), \quad (140)$$

for p large enough, which concludes the proof of Theorem 2. ■

Lemma 19 *Let ϕ and h be feedforward neural networks as defined in Appendix B with bounded data $\|x\| \leq D$. Then,*

$$D_{\mathcal{X}} \leq \prod_{d=1}^D \Omega_d \prod_{k=1}^{K-1} \Omega_k \Omega_D. \quad (141)$$

Moreover, if σ is the tanh activation function, i. e., $\sigma(x) = \frac{e^x - e^{-x}}{e^x + e^{-x}}$, which is centered and 1-Lipschitz, then we obtain

$$\|\phi(x)\| \leq \|\mathbf{W}_K\|_{\infty \rightarrow 2}, \quad (142)$$

$$D_{\mathcal{X}} \leq \Omega_D, \quad (143)$$

which does not require to bound the input data x .

Proof We proceed iteratively and, for this purpose, let ϕ_k and h_d denote the vector-valued output of the k^{th} and d^{th} layer for $k \in [K]$ and $d \in [D]$ for the neural networks ϕ and h , respectively. Then,

$$D_{\mathcal{X}} \lesssim \sup_{h \in \mathcal{H}, \phi \in \Phi, x} \|h_t \circ \phi(x)\|^2, \quad (144)$$

and

$$\|h_t \circ \phi(x)\|^2 = \|h_D\|^2 = \|\mathbf{W}_D \sigma(h_{D-1})\|_2^2 \leq \|\mathbf{W}_D\|_2^2 \|\sigma(h_{D-1})\|_2^2 \quad (145)$$

$$\leq \|\mathbf{W}_D\|_2^2 \|h_{D-1}\|_2^2 \quad (146)$$

where the second inequality holds, since σ is element-wise 1-Lipschitz and centered. Applying this argument recursively until $h_0 = \phi(x)$, yields

$$\|h_D\|^2 \leq \prod_{d=1}^D \|\mathbf{W}_d\|_2^2 \|\phi(x)\|_2^2. \quad (147)$$

Then, with a similar argument for the neural network ϕ ,

$$\|\phi(x)\|_2^2 = \|\phi_K(x)\|_2^2 = \|\mathbf{W}_K \sigma(\phi_{K-1}(x))\|_2^2 \leq \|\mathbf{W}_K\|_2^2 \|\sigma(\phi_{K-1}(x))\|_2^2 \leq \|\mathbf{W}_K\|_2^2 \quad (148)$$

$$\|\mathbf{W}_{K-1} \phi_{K-2}(x)\|_2^2 \leq \|\mathbf{W}_K\|_2^2 \|\mathbf{W}_{K-1}\|_2^2 \|\phi_{K-2}(x)\|_2^2, \quad (149)$$

again, using that σ is element-wise 1-Lipschitz and centered. Recursively applying this argument until $\phi_0 = x$ yields the conclusion after taking square roots and noting that $\|\mathbf{W}_d\| \leq \Omega_d$, $\|\mathbf{W}_k\| \leq \Omega_k$, and $\|x\| \leq D$.

We further consider $\sigma(\cdot)$ to be the tanh activation, which is 1-Lipschitz and centered, as in the statement. Then, by noting that $\|\phi_{K-1}\|_{1, \infty} \leq 1$, we obtain

$$\|\phi(x)\|_2^2 = \|\phi_K\|_2^2 = \|\mathbf{W}_K \sigma(\phi_{K-1})\|_2^2 \leq \|\mathbf{W}_K\|_{\infty \rightarrow 2}^2 \leq \Omega^2, \quad (150)$$

which, after taking square roots, concludes the proof.

For the last claim, we consider again that $\sigma(\cdot)$ to be the tanh activation, which is 1-Lipschitz and centered. Then, by noting that $\|h_{D-1}\|_{1, \infty} \leq 1$, we obtain

$$\|h_t \circ \phi(x)\|^2 = \|h_D\|^2 \leq \|\mathbf{W}_D\|_2^2 \|h_{D-1}\|_2^2 \leq \Omega_D^2. \quad (151)$$

■

Lemma 20 *The function class \mathcal{H} as in Appendix B is $L(\mathcal{H})$ -Lipschitz with*

$$L(\mathcal{H}) = \prod_{d=1}^D \Omega_d. \quad (152)$$

Moreover, if σ is the tanh activation function, i. e., $\sigma(x) = \frac{e^x - e^{-x}}{e^x + e^{-x}}$, which is centered and 1-Lipschitz, then $L(\mathcal{H}) = \alpha\Omega$.

Proof

$$\|\mathbf{h}_t(z) - \mathbf{h}_t(z')\|_2^2 = \|\mathbf{W}_D \sigma(\mathbf{h}_{D-1}(z)) - \mathbf{W}_D \sigma(\mathbf{h}_{D-1}(z'))\|_2^2 \quad (153)$$

$$\leq \|\mathbf{W}_D\|_2^2 \|\sigma(\mathbf{h}_{D-1}(z)) - \sigma(\mathbf{h}_{D-1}(z'))\|_2^2 \leq \|\mathbf{W}_D\|_2^2 \|\mathbf{h}_{D-1}(z) - \mathbf{h}_{D-1}(z')\|_2^2, \quad (154)$$

where the last inequality holds, since $\sigma(\cdot)$ is 1-Lipschitz. Recursively applying the argument yields

$$\|\mathbf{h}_t(z) - \mathbf{h}_t(z')\|_2^2 \leq \prod_{d=1}^D \|\mathbf{W}_d\|_2^2 \|z - z'\|_2^2, \quad (155)$$

which yields the conclusion after taking square roots and noting that $\|\mathbf{W}_d\|_2 \leq \Omega_d$ for $d \in \{1, \dots, D\}$.

If we further consider σ to be the tanh activation as in the statement, then, by an analogous argument as in the proof of Lemma 19, it yields that \mathbf{h} is Lipschitz with $L(\mathcal{H}) = \Omega_D$. ■

C.2 Proof of Theorem 4

The proof relies on similar procedures as the proof of Theorem 2. In particular, we again use a modification of the bounded differences inequality and a standard symmetrization argument. For ease of notation, we use $l_\phi(\mathbf{h}, x, y, t) = (\mathbf{h}_t \circ \phi(x) - y)^2$. Then, similar to the proof of Theorem 2, we obtain

$$\epsilon_{\text{PEHE}}(\hat{\tau}_{\text{Unc}}) \leq 2(\epsilon(\hat{\mathbf{h}}^u, \hat{\phi}) - \epsilon(\mathbf{h}^u, \phi^*)), \quad (156)$$

where for any $\mathbf{h} \in \mathcal{H}^{\otimes 2}$ and $\phi \in \Phi$,

$$\epsilon(\mathbf{h}, \phi) = \sum_{t=0}^1 \mathbb{E}[(\mathbf{h}_t \circ \phi(X^{\text{Conf}}) - Y(t))^2] \quad (157)$$

$$= \sum_{t=0}^1 \mathbb{P}(T^{\text{Unc}} = t) \mathbb{E}[\mathbb{E}[(\mathbf{h}_t \circ \phi(X^{\text{Conf}}) - Y^{\text{Unc}})^2 \mid T^{\text{Unc}} = t, X^{\text{Conf}}]] \quad (158)$$

$$= \mathbb{E}[\mathbb{E}[(\mathbf{h}_{T^{\text{Unc}}} \circ \phi(X^{\text{Conf}}) - Y^{\text{Unc}})^2 \mid T^{\text{Unc}}, X^{\text{Conf}}]] \quad (159)$$

$$= \mathbb{E}[(\mathbf{h}_{T^{\text{Unc}}} \circ \phi(X^{\text{Conf}}) - Y^{\text{Unc}})^2] \quad (160)$$

$$= \mathbb{E}[l_\phi(\mathbf{h}, X^{\text{Conf}}, Y^{\text{Unc}}, T^{\text{Unc}})]. \quad (161)$$

Let $\hat{\mathbf{h}}^u, \hat{\phi} = \arg \min_{\mathbf{h} \in \mathcal{H}^{\otimes 2}, \phi \in \Phi} \hat{\epsilon}_{\text{Unc}}(\mathbf{h}, \phi)$. Then, with probability at least $1 - p$,

$$\epsilon(\hat{\mathbf{h}}^u, \hat{\phi}) - \epsilon(\mathbf{h}^u, \phi^*) \quad (162)$$

$$= \epsilon(\hat{\mathbf{h}}^u, \hat{\phi}) - \hat{\epsilon}_{\text{Unc}}(\hat{\mathbf{h}}^u, \hat{\phi}) + \underbrace{\hat{\epsilon}_{\text{Unc}}(\hat{\mathbf{h}}^u, \hat{\phi}) - \hat{\epsilon}_{\text{Unc}}(\mathbf{h}^u, \phi^*)}_{\leq 0} + \hat{\epsilon}_{\text{Unc}}(\mathbf{h}^u, \phi^*) - \epsilon(\mathbf{h}^u, \phi^*) \quad (163)$$

$$\leq 2 \sup_{\mathbf{h} \in \mathcal{H}^{\otimes 2}, \phi \in \Phi} |\epsilon(\mathbf{h}, \phi) - \hat{\epsilon}_{\text{Unc}}(\mathbf{h}, \phi)| \quad (164)$$

$$\leq 8L\bar{d}_{\infty}(p_{\phi}^{\text{Conf}} | p_{\phi}^{\text{Unc}}) \mathcal{G}_{n^{\text{Unc}}}(\mathcal{H}(\Phi)) + 4\bar{d}_{\infty}(p_{\phi}^{\text{Conf}} | p_{\phi}^{\text{Unc}}) B \sqrt{\frac{2 \log(1/p)}{n^{\text{Unc}}}}, \quad (165)$$

where the first inequality follows, since the middle term is negative due to $\hat{\mathbf{h}}^u, \hat{\phi} = \arg \min_{\mathbf{h} \in \mathcal{H}^{\otimes 2}, \phi \in \Phi} \hat{\epsilon}_{\text{Unc}}(\mathbf{h}, \phi)$. The second inequality follows by an identical argument as in the proof of Lemma 16. Moreover, $\bar{d}_{\infty}(p_{\phi}^{\text{Conf}} | p_{\phi}^{\text{Unc}}) = \sup_{\phi \in \Phi} d_{\infty}(p_{\phi}^{\text{Conf}} | p_{\phi}^{\text{Unc}})$. The term $\bar{d}_{\infty}(p_{\phi}^{\text{Conf}} | p_{\phi}^{\text{Unc}})$ arises, since, in order to pull it out, we have to take the supremum over the function class Φ in (164). Again, using the chain rule for Gaussian complexities, similar to the proof of Lemma 17, yields

$$\hat{\mathcal{G}}_X(\mathcal{H}(\Phi)) \leq 128 \left(\frac{2D_X}{n^{\text{Unc}^2}} + C(\mathcal{H}(\Phi)) \log(n^{\text{Unc}}) \right), \quad (166)$$

where $C(\mathcal{H}(\Phi)) = L(\mathcal{H})\hat{\mathcal{G}}_X(\Phi) + \max_{Z \in \mathcal{Z}} \hat{\mathcal{G}}_Z(\mathcal{H})$. The remainder of the proof is identical to the proof of Theorem 18 for general function classes and the proof of Theorem 2 for the complexities of neural networks. \blacksquare

C.3 Proof of Theorem 5

First, using Lemma 26, it follows that

$$\epsilon_{\text{PEHE}}(\hat{\tau}_{\text{Conf}}) = \mathbb{E}[(\hat{\tau}_{\text{Conf}}(X^{\text{Conf}}) - \tau(X^{\text{Conf}}))^2] \quad (167)$$

$$= \mathbb{E}[(\hat{\mathbf{h}}_1^c \circ \hat{\phi}(X^{\text{Conf}}) - \hat{\mathbf{h}}_0^c \circ \hat{\phi}(X^{\text{Conf}}) - (\mathbf{h}_1^c + \delta_1) \circ \phi^*(X^{\text{Conf}}) \quad (168)$$

$$+ (\mathbf{h}_0^c + \delta_0) \circ \phi^*(X^{\text{Conf}}))^2] \quad (169)$$

$$= \mathbb{E}[(\hat{\mathbf{h}}_1^c \circ \hat{\phi}(X^{\text{Conf}}) - \mathbf{h}_1^c \circ \phi(X^{\text{Conf}}) + \mathbf{h}_0^c \circ \phi^*(X^{\text{Conf}}) - \hat{\mathbf{h}}_0^c \circ \hat{\phi}(X^{\text{Conf}}) \quad (170)$$

$$+ (\delta_0 - \delta_1) \circ \phi^*(X^{\text{Conf}}))^2] \quad (171)$$

$$\leq 2\mathbb{E}_{X^{\text{Conf}}}[(\hat{\mathbf{h}}_1^c \circ \hat{\phi}(X^{\text{Conf}}) - \mathbf{h}_1^c \circ \phi(X^{\text{Conf}}) + \mathbf{h}_0^c \circ \phi^*(X^{\text{Conf}}) - \hat{\mathbf{h}}_0^c \circ \hat{\phi}(X^{\text{Conf}}))^2] \quad (172)$$

$$+ ((\delta_0 - \delta_1) \circ \phi^*(X^{\text{Conf}}))^2] \quad (173)$$

$$= 4 \sum_{t=0}^1 \mathbb{E}[(\hat{\mathbf{h}}_t^c \circ \hat{\phi}(X^{\text{Conf}}) - \mathbf{h}_t^c \circ \phi^*(X^{\text{Conf}}))^2] + 2\mathbb{E}[(\delta_0 - \delta_1) \circ \phi^*(X^{\text{Conf}}))^2] \quad (174)$$

$$\leq 4 \sum_{t=0}^1 \mathbb{E}[(\hat{\mathbf{h}}_t^c \circ \hat{\phi}(X^{\text{Conf}}) - Y^{\text{Conf}})^2 - (Y^{\text{Conf}} - \mathbf{h}_t^c \circ \phi^*(X^{\text{Conf}}))^2 | T = t] \quad (175)$$

$$+ 2\mathbb{E}[(\delta_0 - \delta_1) \circ \phi^*(X^{\text{Conf}}))^2] \quad (176)$$

$$= 4(\epsilon_{\text{Conf}}(\hat{\mathbf{h}}^c, \hat{\phi}) - \epsilon_{\text{Conf}}(\mathbf{h}^c, \phi^*)) + 2\Delta, \quad (177)$$

where $\Delta = \mathbb{E} \left[((\delta_0 - \delta_1) \circ \phi^*(X^{\text{Conf}}))^2 \right]$. Then, we can use the same upper bound for $\epsilon_{\text{Conf}}(\hat{\mathbf{h}}^c, \hat{\phi}) - \epsilon_{\text{Conf}}(\mathbf{h}^c, \phi^*)$ as in the proof of Theorem 2. This yields the claim. \blacksquare

C.4 Proof of Theorem 7

The proof of Theorem 7 is a immediate implication of Theorem 4 and Theorem 5. This can be seen as follows:

$$\epsilon_{\text{PEHE}}(\hat{\tau}_{\text{Avg}}(\lambda)) = \mathbb{E}[(\hat{\tau}_{\text{Avg}}(\lambda)(X^{\text{Conf}}) - \tau(X^{\text{Conf}}))^2] \quad (178)$$

$$= \mathbb{E}[(1 - \lambda)\hat{\tau}_{\text{Unc}}(X^{\text{Conf}}) + \lambda\hat{\tau}_{\text{Conf}}(X^{\text{Conf}}) - \tau(X^{\text{Conf}})]^2 \quad (179)$$

$$= \mathbb{E}[(1 - \lambda)\hat{\tau}_{\text{Unc}}(X^{\text{Conf}}) + \lambda\hat{\tau}_{\text{Conf}}(X^{\text{Conf}}) - (\lambda\tau(X^{\text{Conf}}) + (1 - \lambda)\tau(X^{\text{Conf}}))]^2 \quad (180)$$

$$= 2(1 - \lambda)\mathbb{E}[(\hat{\tau}_{\text{Unc}}(X^{\text{Conf}}) - \tau(X^{\text{Conf}}))^2] + 2\lambda\mathbb{E}[(\hat{\tau}_{\text{Conf}}(X^{\text{Conf}}) - \tau(X^{\text{Conf}}))^2] \quad (181)$$

$$= 2(1 - \lambda)\epsilon_{\text{PEHE}}(\hat{\tau}_{\text{Unc}}) + 2\lambda\epsilon_{\text{PEHE}}(\hat{\tau}_{\text{Conf}}). \quad (182)$$

Hence, using the bounds for $\epsilon_{\text{PEHE}}(\hat{\tau}_{\text{Unc}})$ and $\epsilon_{\text{PEHE}}(\hat{\tau}_{\text{Conf}})$ yields the claim. \blacksquare

C.5 Proof of Theorem 9

First, we define $\lambda = \frac{n^{\text{Conf}}}{\lambda n^{\text{Unc}} + n^{\text{Conf}}}$. This implies that $1 - \lambda = \frac{\lambda n^{\text{Unc}}}{\lambda n^{\text{Unc}} + n^{\text{Conf}}}$. Then, the weighted empirical risk is given by

$$\hat{\epsilon}_{\text{Weight}}(\mathbf{h}, \phi) = (1 - \lambda) \frac{1}{n^{\text{Unc}}} \sum_{i=1}^{n^{\text{Unc}}} (\mathbf{h}_{t_i^{\text{Unc}}} \circ \phi(x_i^{\text{Unc}}) - y_i^{\text{Unc}})^2 \quad (183)$$

$$+ \lambda \frac{1}{n^{\text{Conf}}} \sum_{i=1}^{n^{\text{Conf}}} (\mathbf{h}_{t_i^{\text{Conf}}} \circ \phi(x_i^{\text{Conf}}) - y_i^{\text{Conf}})^2. \quad (184)$$

Further, we can write

$$\epsilon_{\text{PEHE}}(\hat{\tau}_{\text{Weight}}) = \mathbb{E}[(\hat{\tau}_{\text{Weight}}(\lambda)(X^{\text{Conf}}) - \tau(X^{\text{Conf}}))^2] \quad (185)$$

$$= (1 - \lambda) \underbrace{\mathbb{E}[(\hat{\tau}_{\text{Weight}}(\lambda)(X^{\text{Conf}}) - \tau(X^{\text{Conf}}))^2]}_{=(\text{I})} + \lambda \underbrace{\mathbb{E}[(\hat{\tau}_{\text{Weight}}(\lambda)(X^{\text{Conf}}) - \tau(X^{\text{Conf}}))^2]}_{=(\text{II})}. \quad (186)$$

Then, using the same the same argument as in the proof of Theorem 4 and Theorem 5, yields the following upper bounds,

$$(\text{I}) \leq 2(\epsilon(\hat{\mathbf{h}}, \hat{\phi}) - \epsilon(\mathbf{h}^u, \phi^*)), \quad (187)$$

$$(\text{II}) \leq 4(\epsilon_{\text{Conf}}(\hat{\mathbf{h}}, \hat{\phi}) - \epsilon_{\text{Conf}}(\mathbf{h}^c, \phi^*)) + 2\Delta \quad (188)$$

where $\hat{\mathbf{h}}$ and $\hat{\phi}$ are the estimators from (29). Then, we claim follows by using the results from Theorem 4 and Theorem 5. \blacksquare

Appendix D. Impact of Selection Bias in Observational Data

In the main paper, we have considered the case in which there is no selection bias in the observational data. Selection bias is present if the covariate distributions $p_{t=1}^{\text{Conf}}(x) =$

$p^{\text{Conf}}(x | t = 1)$ and $p_{t=0}^{\text{Conf}}(x) = p^{\text{Conf}}(x | t = 0)$ differ. This can be due to covariate-dependent treatment assignment. There is a large body of research addressing the selection bias in observational data (e. g., Shalit et al., 2017; Johansson et al., 2018; Yao et al., 2018; Zhang et al., 2020), which is orthogonal to our work. However, since selection bias may occur in practice, we discuss this case briefly here. In particular, we show how Theorem 2 changes in the presence of selection bias. Based on this, algorithmic designs can be easily adjusted in order to counteract selection bias.

In presence of selection bias, the error bound of τ_{Cor} is given by the following result.

Theorem 21 *Let $(\hat{\mathbf{h}}^c, \hat{\phi})$ be the empirical loss minimizer of $\hat{\epsilon}_{\text{Conf}}(\cdot, \cdot)$ from (10) over the function classes Φ and \mathcal{H} , and let δ be the empirical loss minimizer of $\hat{\epsilon}_{\text{Unc}}(\cdot, \hat{\mathbf{h}}^c, \hat{\phi})$ from (12) over the function class \mathcal{B} . Further, let $\hat{\tau}_{\text{Cor}}$ be the resulting CATE estimator from (15). Then, if Assumption 3 and Condition 1 hold true, we have that, with probability at least $1 - p$*

$$\epsilon_{\text{PEHE}}(\hat{\tau}_{\text{Cor}}) \leq \tilde{\mathcal{O}}\left(\bar{d}_{\infty}(p_{\phi,t=1}^{\text{Conf}} | p_{\phi,t=0}^{\text{Conf}}) \frac{\mathcal{C}_{\Phi} + \mathcal{C}_{\mathcal{H}}}{\sqrt{n^{\text{Conf}}}} + \frac{d_{\infty}(p_{\phi}^{\text{Conf}} | p_{\phi}^{\text{Unc}}) \mathcal{C}_{\mathcal{B}}}{\sqrt{n^{\text{Unc}}}}\right), \quad (189)$$

where \mathcal{C}_{Φ} , $\mathcal{C}_{\mathcal{H}}$, and $\mathcal{C}_{\mathcal{B}}$ are constants depending on the complexity of the neural networks. Moreover, $p_{\phi,t}^{\text{Conf}}$, p_{ϕ}^{Conf} , and p_{ϕ}^{Unc} denote the push-forwards through ϕ of the corresponding covariate distributions.

Proof The proof of Theorem 21 differs from the proof of Theorem 2 only in Lemma 17, which is the upper bound on $d_{\mathcal{H}, \mathbf{h}^c}(\hat{\phi}; \phi^*)$. We only need to prove that, in presence of selection bias, the upper bound for $d_{\mathcal{H}, \mathbf{h}^c}(\hat{\phi}; \phi^*)$ is given by:

$$d_{\mathcal{H}, \mathbf{h}^c}(\hat{\phi}; \phi^*) \leq 4096L \left(\frac{D_{\mathcal{X}}}{(n^{\text{Conf}})^2} + \bar{d}_{\infty}(p_{\phi,t=1}^{\text{Conf}} | p_{\phi,t=0}^{\text{Conf}}) \log(n^{\text{Conf}}) (L(\mathcal{H}) \frac{\mathcal{G}_{n^{\text{Conf}}}(\Phi)}{n^{\text{Conf}}} + \frac{\bar{\mathcal{G}}_{n^{\text{Conf}}}(\mathcal{H})}{n^{\text{Conf}}}) \right) \quad (190)$$

$$+ 8B \sqrt{\frac{\log(1/p)}{n^{\text{Conf}}}}, \quad (191)$$

where $\bar{d}_{\infty}(p_{\phi,t=1}^{\text{Conf}} | p_{\phi,t=0}^{\text{Conf}}) = \sup_{\phi \in \Phi} d_{\infty}(p_{\phi,t=1}^{\text{Conf}} | p_{\phi,t=0}^{\text{Conf}})$ and $p_{\phi,t=1}^{\text{Conf}}(z)$ is the push-forward of $p^{\text{Conf}}(x | t = 1)$ through ϕ and similar for $p_{\phi,t=0}^{\text{Conf}}$. For this, we assume w.l.o.g. that $\sup_z p_{\phi,t=1}^{\text{Conf}}(z) > \sup_z p_{\phi,t=0}^{\text{Conf}}(z)$. Otherwise, the term $\bar{d}_{\infty}(p_{\phi,t=1}^{\text{Conf}} | p_{\phi,t=0}^{\text{Conf}})$ in the statement changes to $\bar{d}_{\infty}(p_{\phi,t=0}^{\text{Conf}} | p_{\phi,t=1}^{\text{Conf}})$. This is due to the fact that the Renyi divergence is asymmetric.

Similar to the proof of Lemma 17,

$$d_{\mathcal{H}, \mathbf{h}^c}(\hat{\phi}; \phi^*) \leq 2 \sup_{\mathbf{h} \in \mathcal{H}^{\otimes 2}, \phi \in \Phi} |\epsilon_{\text{Conf}}(\mathbf{h}, \phi) - \hat{\epsilon}_{\text{Conf}}(\mathbf{h}, \phi)|. \quad (192)$$

We intend to proceed similar to the proof of Lemma 16, where we use a change of probability measure and change of variable (to push-forward the covariate distribution into the representation space). For this, we again use the Radon-Nikodym derivative $w_{\phi}(z)$ for the change of probability measure. However, here, we face two different covariate distributions that we need to change. That is, we need to change from $p_{\phi,t=1}^{\text{Conf}}$ to p_{ϕ}^{Conf} and from $p_{\phi,t=0}^{\text{Conf}}$ to p_{ϕ}^{Conf} .

Hence, we use the Radon-Nikodym derivative $w_\phi(z) = \frac{T \cdot p_{\phi,t=1}^{\text{Conf}}(z) + (1-T) \cdot p_{\phi,t=0}^{\text{Conf}}}{p_\phi^{\text{Conf}}(z)}$. Further, note that $p_\phi^{\text{Conf}}(z) = q \cdot p_{\phi,t=1}^{\text{Conf}}(z) + (1-q) \cdot p_{\phi,t=0}^{\text{Conf}}(z)$, where $q = \mathbb{P}(T = 1)$. Then,

$$w_\phi(z) = \frac{T \cdot p_{\phi,t=1}^{\text{Conf}}(z) + (1-T) \cdot p_{\phi,t=0}^{\text{Conf}}}{q \cdot p_{\phi,t=1}^{\text{Conf}}(z) + (1-q) \cdot p_{\phi,t=0}^{\text{Conf}}(z)}, \quad (193)$$

and, hence, since $T \in \{0, 1\}$ and $\sup_z p_{\phi,t=1}^{\text{Conf}}(z) > \sup_z p_{\phi,t=0}^{\text{Conf}}(z)$, this yields $\sup_z w_\phi(z) < \sup_z \frac{p_{\phi,t=1}^{\text{Conf}}(z)}{p_{\phi,t=0}^{\text{Conf}}(z)}$. Then, similar to the proof of Lemma 16,

$$2 \sup_{\mathbf{h} \in \mathcal{H}^{\otimes 2}, \phi \in \Phi} |\epsilon_{\text{Conf}}(\mathbf{h}, \phi) - \hat{\epsilon}_{\text{Conf}}(\mathbf{h}, \phi)| \quad (194)$$

$$\leq 4L \sup_{\phi \in \Phi} d_\infty(p_{\phi,t=1}^{\text{Conf}} | p_{\phi,t=0}^{\text{Conf}}) \mathcal{R}_{n^{\text{Unc}}}(\mathcal{H}(\Phi)) + 4 \sup_{\phi \in \Phi} d_\infty(p_{\phi,t=1}^{\text{Conf}} | p_{\phi,t=0}^{\text{Conf}}) B \sqrt{\frac{2 \log(1/\delta)}{n^{\text{Unc}}}} \quad (195)$$

$$= 4L \bar{d}_\infty(p_{\phi,t=1}^{\text{Conf}} | p_{\phi,t=0}^{\text{Conf}}) \mathcal{R}_{n^{\text{Unc}}}(\mathcal{H}(\Phi)) + 4 \bar{d}_\infty(p_{\phi,t=1}^{\text{Conf}} | p_{\phi,t=0}^{\text{Conf}}) B \sqrt{\frac{2 \log(1/\delta)}{n^{\text{Unc}}}}. \quad (196)$$

We then proceed similar to the proof of Lemma 17 and use the chain rule of Gaussian complexities and upper bound the Gaussian complexities for the neural networks as in Appendix C.1. \blacksquare

From this result, we can see that, besides the impact of the distributional discrepancy between $d_\infty(p_\phi^{\text{Conf}} | p_\phi^{\text{Unc}})$, another factor impacts the error as well: the distributional discrepancy between the covariate distributions of the treatment and control group, $d_\infty(p_{\phi,t=1}^{\text{Conf}} | p_{\phi,t=0}^{\text{Conf}})$. The impact of this factor is similar to the impact of the distributional discrepancy between $d_\infty(p_\phi^{\text{Conf}} | p_\phi^{\text{Unc}})$. Namely, it does not introduce bias, but slows down the convergence of the error. The most common approach to address the discrepancy in the representation space due to selection bias is balancing, which was discussed in many works on treatment effect estimation using observational data (e. g., Johansson et al., 2016; Shalit et al., 2017; Zhang et al., 2020) and domain adaptation (Ganin and Lempitsky, 2015; Ganin et al., 2016). Further, we can also see from the above result that, in the case in which n^{Conf} is large, the constant factor due to selection bias, $d_\infty(p_{\phi,t=1}^{\text{Conf}} | p_{\phi,t=0}^{\text{Conf}})$, may not play an important role. Hence, in observational data, it may not be necessary to address the selection bias. Nevertheless, our procedure can be easily adjusted for this case if required.

D.1 Proof of Proposition 11

The proof of Proposition 11 follows by straightforward algebraic manipulation. For Condition 1, which compares τ_{Cor} and τ_{Unc} , the following yields the claim:

$$\frac{\mathcal{C}_\Phi + \mathcal{C}_\mathcal{H}}{\sqrt{n^{\text{Conf}}}} + \frac{d_\infty(p_\phi^{\text{Conf}} | p_\phi^{\text{Unc}})\mathcal{C}_\mathcal{B}}{\sqrt{n^{\text{Unc}}}} < \bar{d}_\infty(p_\phi^{\text{Conf}} | p_\phi^{\text{Unc}}) \frac{\mathcal{C}_\Phi + \mathcal{C}_\mathcal{H}}{\sqrt{n^{\text{Unc}}}} \quad (197)$$

$$\frac{\mathcal{C}_\Phi + \mathcal{C}_\mathcal{H}}{\sqrt{n^{\text{Conf}}}} < \frac{\bar{d}_\infty(p_\phi^{\text{Conf}} | p_\phi^{\text{Unc}})(\mathcal{C}_\Phi + \mathcal{C}_\mathcal{H}) - d_\infty(p_\phi^{\text{Conf}} | p_\phi^{\text{Unc}})\mathcal{C}_\mathcal{B}}{\sqrt{n^{\text{Unc}}}} \quad (198)$$

$$\frac{\mathcal{C}_\Phi + \mathcal{C}_\mathcal{H}}{\bar{d}_\infty(p_\phi^{\text{Conf}} | p_\phi^{\text{Unc}})(\mathcal{C}_\Phi + \mathcal{C}_\mathcal{H}) - d_\infty(p_\phi^{\text{Conf}} | p_\phi^{\text{Unc}})\mathcal{C}_\mathcal{B}} < \sqrt{\frac{n^{\text{Conf}}}{n^{\text{Unc}}}}. \quad (199)$$

For Condition 2, which compares τ_{Cor} and τ_{Conf} , similar to the above, the following yields the claim:

$$\frac{\mathcal{C}_\Phi + \mathcal{C}_\mathcal{H}}{\sqrt{n^{\text{Conf}}}} + \frac{d_\infty(p_\phi^{\text{Conf}} | p_\phi^{\text{Unc}})\mathcal{C}_\mathcal{B}}{\sqrt{n^{\text{Unc}}}} < \frac{\mathcal{C}_\Phi + \mathcal{C}_\mathcal{H}}{\sqrt{n^{\text{Conf}}}} + 2\Delta \quad (200)$$

$$\frac{d_\infty(p_\phi^{\text{Conf}} | p_\phi^{\text{Unc}})\mathcal{C}_\mathcal{B}}{\sqrt{n^{\text{Unc}}}} < 2\Delta. \quad (201)$$

Appendix E. Theoretical Properties for CorNet

In this section, we give variants of the results in Theorem 2 for our algorithm CorNet.

In particular, \mathcal{H} and \mathcal{B} are given by

$$\mathcal{H} = \{h \mid h(z, t) = \mathbf{w}_t^\top z, \mathbf{w}_t \in \mathbb{R}^{d_\phi}, \|\mathbf{w}_t\|_2 \leq \alpha\}, \quad (202)$$

$$\mathcal{B} = \{\delta \mid \delta(z, t) = \boldsymbol{\delta}_t^\top z, \boldsymbol{\delta}_t \in \mathbb{R}^{d_\phi}, \|\boldsymbol{\delta}_t\|_1 \leq \beta\}, \quad (203)$$

where d_ϕ denotes the dimension of the representation space.

E.1 Finite Sample Learning Bound

The following error bound holds.

Corollary 22 *Let $(\hat{\mathbf{h}}^c, \hat{\phi})$ be the empirical loss minimizer of $\hat{\epsilon}_{\text{Conf}}(\cdot, \cdot)$ from (10) over the function classes Φ as in (55) and \mathcal{H} as in (202), and let $\hat{\boldsymbol{\delta}}$ be the empirical loss minimizer of $\hat{\epsilon}_{\text{Unc}}(\cdot, \hat{\mathbf{h}}^c, \hat{\phi})$ from (12) over the function class \mathcal{B} as in (203). Further, let $\hat{\tau}_{\text{Cor}}$ be the resulting CATE estimator from (15). Then, if Assumption 3 holds true, we have that, with probability at least $1 - p$,*

$$\epsilon_{\text{PEHE}}(\hat{\tau}_{\text{Cor}}) \leq \tilde{\mathcal{O}}\left(\frac{\mathcal{C}_\Phi + \alpha}{\sqrt{n^{\text{Conf}}}} + \frac{d_\infty(p_{\hat{\phi}}^{\text{Conf}} | p_{\hat{\phi}}^{\text{Unc}})\beta\sqrt{2\log d_\phi}}{\sqrt{n^{\text{Unc}}}}\right) \quad (204)$$

Proof We continue the proof of Appendix C.1 in Equation (133). The term for the representation function remains the same as we still consider neural networks for Φ . We continue with bounded the Rademacher complexity of \mathcal{H} and \mathcal{B} .

Then, using that $z = \phi(x)$ and $\|\phi(x)\| \leq \Omega$ (by Lemma 19),

$$\hat{\mathcal{G}}_Z(\mathcal{H}) \leq 2 \log(n^{\text{Conf}}) \hat{\mathcal{R}}_Z(\mathcal{H}) \leq 2 \log(n^{\text{Conf}}) \frac{\alpha}{\sqrt{n^{\text{Conf}}}} \sqrt{\mathbb{E} \left[\sum_{i=1}^{n^{\text{Conf}}} \|z_i\|_2^2 \right]} \quad (205)$$

$$\leq 2 \log(n^{\text{Conf}}) \frac{\alpha}{\sqrt{n^{\text{Conf}}}} \Omega \quad (206)$$

$$\hat{\mathcal{G}}_Z(\mathcal{B}) \leq 2 \log(n^{\text{Unc}}) \hat{\mathcal{R}}_Z(\mathcal{B}) \leq 2 \log(n^{\text{Unc}}) \frac{\beta \sqrt{2 \log d_\phi}}{\sqrt{n^{\text{Unc}}}} \sup_j \sqrt{\sum_{i=1}^{n^{\text{Unc}}} (z_i)_j^2} \quad (207)$$

$$\leq 2 \log(n^{\text{Unc}}) \frac{\beta \sqrt{2 \log d_\phi}}{\sqrt{n^{\text{Unc}}}} \Omega, \quad (208)$$

where we use bounds on the Rademacher complexity for linear functions (see for instance Kakade et al. (2009)). This yields

$$\bar{\mathcal{G}}_{n^{\text{Conf}}}(\mathcal{H}) = \max_{Z \in \mathcal{Z}} \hat{\mathcal{G}}_Z(\mathcal{H}) \leq 2 \log(n^{\text{Conf}}) \frac{\alpha}{\sqrt{n^{\text{Conf}}}} \Omega, \quad (209)$$

$$\hat{\mathcal{G}}_Z(\mathcal{B}) \leq 2 \log(n^{\text{Unc}}) \frac{\beta \sqrt{2 \log d_\phi}}{\sqrt{n^{\text{Unc}}}} \Omega, \quad (210)$$

which concludes the proof. \blacksquare

E.2 Improvement Condition

In this section, we derive conditions for when combining observational data and randomized data is beneficial for our algorithm proposed in Algorithm 1. In particular, we compare the error bounds our estimator against the baseline estimators which only use randomized or observational data. Based on this, we derive conditions for when our algorithm improves upon the baselines estimators and when we should rely on one of the baseline estimators.

First, we derive finite sample bounds for the estimator which only uses randomized data and, then, for the estimator which only uses observational data, similarly to Theorem 4 and Theorem 5.

E.2.1 ESTIMATOR ON RANDOMIZED DATA

Similarly to the results in Theorem 4, we derive the following finite sample error bound for τ_{Unc} in 5.3.1.

Theorem 23 (*Estimation on randomized data*) *Let $(\hat{\mathbf{h}}, \hat{\phi})$ be the empirical loss minimizer from (19) over the function classes Φ as in (55) and \mathcal{H} as in (202) and $\hat{\tau}_{\text{Unc}}$ from (21). Then, we have that with probability at least $1 - p$,*

$$\epsilon_{\text{PEHE}}(\hat{\tau}_{\text{Unc}}) \leq \tilde{O} \left(\bar{d}_\infty(p_\phi^{\text{Conf}} | p_\phi^{\text{Unc}}) \frac{\mathcal{C}_\Phi + \alpha}{\sqrt{n^{\text{Unc}}}} \right), \quad (211)$$

where \mathcal{C}_Φ is a constant depending on the complexity of the neural networks and $\bar{d}_\infty(p_\phi^{\text{Conf}} | p_\phi^{\text{Unc}}) = \sup_{\phi \in \Phi} d_\infty(p_\phi^{\text{Conf}} | p_\phi^{\text{Unc}})$.

Proof Similar to the proof of Theorem 4, but using that $\bar{\mathcal{G}}_{n^{\text{Conf}}}(\mathcal{H}) = \max_{\bar{Z} \in \mathcal{Z}} \hat{\mathcal{G}}_{\bar{Z}}(\mathcal{H}) \leq 2 \log(n^{\text{Conf}}) \frac{\alpha}{\sqrt{n^{\text{Conf}}}} \Omega$. \blacksquare

E.2.2 ESTIMATOR ON OBSERVATIONAL DATA

Similarly to the results in Lemma 17, we derive the following finite sample error bound for τ_{Conf} in 5.3.2.

Theorem 24 *Let $(\hat{\mathbf{h}}^c, \hat{\phi})$ be the empirical loss minimizer over the function classes Φ as in (55) and \mathcal{H} as in (202) from (10) and $\hat{\tau}_{\text{Conf}}$ as in (23). Then, we have that, with probability at least $1 - p$,*

$$\epsilon_{\text{PEHE}}(\hat{\tau}_{\text{Conf}}) \leq \tilde{O}\left(\frac{\mathcal{C}_{\Phi} + \alpha}{\sqrt{n^{\text{Conf}}}}\right) + 2\Delta, \quad (212)$$

where $\Delta = \mathbb{E}[\|(\boldsymbol{\delta}_1 - \boldsymbol{\delta}_0) \circ \phi(X^{\text{Conf}})\|^2]$ is the bias due to unobserved confounding and \mathcal{C}_{Φ} is the same as in Theorem 2.

Proof Similar to the proof of Lemma 17, but, again, using that $\bar{\mathcal{G}}_{n^{\text{Conf}}}(\mathcal{H}) = \max_{Z \in \mathcal{Z}} \hat{\mathcal{G}}_Z(\mathcal{H}) \leq 2 \log(n^{\text{Conf}}) \frac{\alpha}{\sqrt{n^{\text{Conf}}}} \Omega$. \blacksquare

E.3 Condition

Similar to Proposition 11, we derive the same conditions for our algorithm proposed in Algorithm 1.

Proposition 25 *If the following conditions hold true,*

$$\frac{\mathcal{C}_{\Phi} + \alpha}{\bar{d}_{\infty}(p_{\phi}^{\text{Conf}} | p_{\phi}^{\text{Unc}})(\mathcal{C}_{\Phi} + \alpha) - d_{\infty}(p_{\phi}^{\text{Conf}} | p_{\phi}^{\text{Unc}})\beta\sqrt{2\log d_{\phi}}} < \sqrt{\frac{n^{\text{Conf}}}{n^{\text{Unc}}}}, \quad (213)$$

$$\frac{d_{\infty}(p_{\phi}^{\text{Conf}} | p_{\phi}^{\text{Unc}})\beta\sqrt{2\log d_{\phi}}}{\sqrt{n^{\text{Unc}}}} < 2\Delta, \quad (214)$$

then the error of our estimator $\hat{\tau}_{\text{Cor}}$ can be substantially lower than the error of the baseline estimators, which only use either observational or randomized data.

Proof Similar to Appendix D.1, where we use $\bar{\mathcal{G}}_{n^{\text{Conf}}}(\mathcal{H}) = \max_{Z \in \mathcal{Z}} \hat{\mathcal{G}}_Z(\mathcal{H}) \leq 2 \log(n^{\text{Conf}}) \frac{\alpha}{\sqrt{n^{\text{Conf}}}} \Omega$ and $\hat{\mathcal{G}}_Z(\mathcal{B}) \leq 2 \log(n^{\text{Unc}}) \frac{\beta\sqrt{2\log d_{\phi}}}{\sqrt{n^{\text{Unc}}}} \Omega$. \blacksquare

E.4 Proof of Proposition 12

We use a modified version of Lemma 6 in (Tripuraneni et al., 2020). For two representation functions $\hat{\phi}$ and ϕ^* , we define the population covariance as

$$\Sigma(\hat{\phi}, \phi^*) = \begin{pmatrix} \mathbb{E}[\hat{\phi}(X^{\text{Conf}})\hat{\phi}(X^{\text{Conf}})^\top] & \mathbb{E}[\hat{\phi}(X^{\text{Conf}})\phi^*(X^{\text{Conf}})^\top] \\ \mathbb{E}[\phi^*(X^{\text{Conf}})\hat{\phi}(X^{\text{Conf}})^\top] & \mathbb{E}[\phi^*(X^{\text{Conf}})\phi^*(X^{\text{Conf}})^\top] \end{pmatrix} = \begin{pmatrix} \Sigma_{\hat{\phi}, \hat{\phi}} & \Sigma_{\hat{\phi}, \phi^*} \\ \Sigma_{\phi^*, \hat{\phi}} & \Sigma_{\phi^*, \phi^*} \end{pmatrix}. \quad (215)$$

We further define the generalized Schur complement as

$$\Sigma_{sc} = \Sigma_{\phi^*, \phi^*} - \Sigma_{\phi^*, \hat{\phi}} \Sigma_{\hat{\phi}, \hat{\phi}}^{-1} \Sigma_{\hat{\phi}, \phi^*}. \quad (216)$$

Then,

$$d_{\mathcal{B}, \delta}(\hat{\phi}; \phi^*) = \inf_{\delta' \in \mathbb{R}^{d_{\phi \otimes 2}}} \sum_{t=0}^1 \mathbb{E}[(\hat{\phi}(X^{\text{Conf}})\delta'_t - \phi^*(X^{\text{Conf}})\delta_t)^2] \quad (217)$$

$$= \inf_{\delta' \in \mathbb{R}^{d_{\phi \otimes 2}}} \sum_{t=0}^1 (\delta'_t, -\delta_t) \Sigma(\hat{\phi}, \phi^*) (\delta'_t, -\delta_t)^\top \quad (218)$$

$$= \inf_{\delta' \in \mathbb{R}^{d_{\phi \otimes 2}}} \sum_{t=0}^1 (\delta'_t, \delta_t) \Sigma(\hat{\phi}, \phi^*) (\delta'_t, \delta_t)^\top \quad (219)$$

$$= \sum_{t=0}^1 \delta_t \Sigma_{sc} \delta_t^\top, \quad (220)$$

where the last equality follows, since the infimum is a partial minimization of a convex quadratic form (see, for example, Boyd et al. (2004), Example 3.15). Finally, we can use the variational characterization of the singular values and that $\|\delta_t\|_1 \leq \alpha$ implies that $\|\delta_t\|_2 \leq \alpha$, which yields

$$\sum_{t=0}^1 \delta_t \Sigma_{sc} \delta_t^\top \leq \sup_{\delta \in \mathbb{R}^{d_{\phi \otimes 2}}, \|\delta_t\|_1 \leq \alpha} \sum_{t=0}^1 \delta_t \Sigma_{sc} \delta_t^\top \leq \sup_{\delta \in \mathbb{R}^{d_{\phi \otimes 2}}, \|\delta_t\|_2 \leq \alpha} \sum_{t=0}^1 \delta_t \Sigma_{sc} \delta_t^\top = 2\alpha \sigma_1(\Sigma_{sc}), \quad (221)$$

where $\sigma_1(\Sigma_{sc})$ denotes the largest singular value of the generalized Schur complement. Hence,

$$d_{\mathcal{B}, \delta}(\hat{\phi}; \phi^*) \leq 2\alpha \sigma_1(\Sigma_{sc}). \quad (222)$$

We proceed similarly for

$$d_{\mathcal{H}, \mathbf{w}^c}(\hat{\phi}; \phi^*) = \inf_{\mathbf{w}' \in \mathbb{R}^{d_{\phi \otimes 2}}} \sum_{t=0}^1 \mathbb{E}[(\hat{\phi}(X^{\text{Conf}})\mathbf{w}'_t - \phi^*(X^{\text{Conf}})(\mathbf{w}^c_t))^2] = \sum_{t=0}^1 \mathbf{w}^c_t \Sigma_{sc} (\mathbf{w}^c_t)^\top \quad (223)$$

$$= 2\text{Tr}(\Sigma_{sc} \frac{(\mathbf{w}^c)^\top \mathbf{w}^c}{2}). \quad (224)$$

Then, using a corollary of the Von-Neumann trace inequality yields

$$\mathrm{Tr}(\boldsymbol{\Sigma}_{sc} \frac{(\mathbf{w}^c)^\top \mathbf{w}^c}{2}) \geq \sum_{i=1}^{d_\phi} \sigma_i(\boldsymbol{\Sigma}_{sc}) \sigma_{d_\phi-i+1}(\frac{(\mathbf{w}^c)^\top \mathbf{w}^c}{2}) \geq \mathrm{Tr}(\boldsymbol{\Sigma}_{sc}) \sigma_{d_\phi}(\frac{(\mathbf{w}^c)^\top \mathbf{w}^c}{2}) \quad (225)$$

$$\geq \sigma_1(\boldsymbol{\Sigma}_{sc}) \sigma_{d_\phi}(\frac{(\mathbf{w}^c)^\top \mathbf{w}^c}{2}). \quad (226)$$

Hence,

$$d_{\mathcal{B},\delta}(\hat{\phi}; \phi^*) \leq 2\alpha \sigma_1(\boldsymbol{\Sigma}_{sc}) \leq \frac{\alpha}{\sigma_{d_\phi}(\frac{(\mathbf{w}^c)^\top \mathbf{w}^c}{2})} d_{\mathcal{H},\mathbf{w}^c}(\hat{\phi}; \phi^*). \quad (227)$$

Appendix F. Auxiliary Lemmas

Lemma 26 *For random variables X and Y and some appropriate function f , we have that*

$$\mathbb{E}[(f(X) - Y)^2] = \mathbb{E}[(f(X) - \mathbb{E}[Y | X])^2] + \mathbb{E}[(\mathbb{E}[Y | X] - Y)^2]. \quad (228)$$

Proof

$$\mathbb{E}[(f(X) - Y)^2] = \mathbb{E}[(f(X) - \mathbb{E}[Y | X] + \mathbb{E}[Y | X] - Y)^2] \quad (229)$$

$$= \mathbb{E}[(f(X) - \mathbb{E}[Y | X])^2] + \mathbb{E}[(\mathbb{E}[Y | X] - Y)^2] + \underbrace{\mathbb{E}[(f(X) - \mathbb{E}[Y | X])(\mathbb{E}[Y | X] - Y)]}_{=0} \quad (230)$$

$$= \mathbb{E}[(f(X) - \mathbb{E}[Y | X])^2] + \mathbb{E}[(\mathbb{E}[Y | X] - Y)^2]. \quad (231)$$

■

Lemma 27 *Let $\Psi : \mathcal{Z} \rightarrow \mathcal{X}$ be the inverse of $\phi : \mathcal{X} \rightarrow \mathcal{Z}$. Then, for some function f , random variable $X \sim p$, and $Z = \phi(X)$ with p_ϕ being the push-forward of p through ϕ , the following holds true*

$$\mathbb{E}_{X \sim p}[f(X)] = \mathbb{E}_{Z \sim p_\phi}[f(\Psi(Z))]. \quad (232)$$

Proof

$$\mathbb{E}_{X \sim p}[f(X)] = \int_{\mathcal{X}} f(x)p(x)dx = \int_{\mathcal{Z}} f(\Psi(z))p_\phi(z)dz = \mathbb{E}_{Z \sim p_\phi}[f(\Psi(Z))] \quad (233)$$

■

Appendix G. Details on Optimization of H -Divergence

Let $\phi : \mathbb{R}^d \rightarrow \mathbb{R}^{d_\phi}$ be a representation and $c : \mathbb{R}^{d_\phi} \rightarrow \{0, 1\}$ be a classifier, which predicts, for a given sample x , it is an interpolated or observational sample. Then, the H -divergence can be written as

$$\hat{d}_H(\tilde{\mathcal{U}}, \mathcal{U}^{\text{Conf}}) = 2 \left(1 - \min_c \left(\frac{1}{m} \sum_{i=1}^m \mathbf{1}_{\{0\}}(c(\phi(\tilde{x}_i))) + \frac{1}{n^{\text{Conf}}} \sum_{i=1}^{n^{\text{Conf}}} \mathbf{1}_{\{1\}}(c(\phi(x_i^{\text{Conf}}))) \right) \right) \quad (234)$$

Intuitively, if the distributional discrepancy is large, the classifier could easily distinguish the observational from interpolated samples. As a consequence, the prediction errors would be small and the H -divergence large. Since we aim at reducing the distributional discrepancy between observational and interpolated data, $\hat{d}_H(\tilde{\mathcal{U}}, \mathcal{U}^{\text{Conf}})$ is minimized. This enforces the representation, ϕ , to learn a representation space in which observational and randomized data are balanced. This is achieved by solving the following optimization problem:

$$\arg \min_{\phi \in \Phi} \hat{d}_H(\tilde{\mathcal{U}}, \mathcal{U}^{\text{Conf}}) = \arg \max_{\phi \in \Phi} \min_c \left(\frac{1}{m} \sum_{i=1}^m \mathbf{1}_{\{0\}}(c(\phi(\tilde{x}_i))) + \frac{1}{n^{\text{Conf}}} \sum_{i=1}^{n^{\text{Conf}}} \mathbf{1}_{\{1\}}(c(\phi(x_i^{\text{Conf}}))) \right). \quad (235)$$

We optimize the max-min problem in (235) using adversarial learning. In particular, we use a gradient reverse layer (GRL) which automatically reverse the gradient after the classifier. As such, we can directly minimize the classification loss of the classifier c (Ganin and Lempitsky, 2015). Hence, this renders, as mentioned in the main paper, step 1 in Algorithm 1 as

$$\arg \min_{\phi \in \Phi, \mathbf{w}^c \in \mathbb{R}^{d_\phi \otimes 2}} \frac{1}{n^{\text{Conf}}} \sum_{i=1}^{n^{\text{Conf}}} (\phi(x_i^{\text{Conf}}) \mathbf{w}_{t_i^{\text{Conf}}}^c - y_i^{\text{Conf}})^2 + \lambda_d \hat{d}_H(\tilde{\mathcal{U}}, \mathcal{U}^{\text{Conf}}), \quad (236)$$

where λ_d trades off the predictive accuracy and the distributional discrepancy. Therefore, augmented distribution alignment can be easily incorporated by appending a classifier with the gradient reversal layer (GRL), and adding the proposed interpolated samples during mini-batch data preparation.

Appendix H. Details on Real-World Data

Tennessee Student/Teacher Achievement Ratio (STAR) experiment: The Tennessee Student/Teacher Achievement Ratio (STAR) experiment is a randomized experiment, which started in 1985 with the objective to study the effect of class size (i. e., treatment) on students' standardized test scores (i. e., outcome). In the first school year, students (as well as teachers) were randomly assigned to class size conditions, which were tried to keep the same for the duration of the experiment. This dataset was also used in Kallus et al. (2018) for removing bias due to unmeasured confounding in observational data.

Our setup follows the one in Kallus et al. (2018). As such, we focus on two conditions (i. e., treatments): small classes (i. e., 13–17 pupils) and regular classes (i. e., 22–25 pupils). We take as treatment the students class size condition at first grade, which yields 4,509

students. The student outcome Y is measured as the sum of listening, reading, and math standardized test scores at the end of the first grade. In addition to class-size (i. e., treatment) and test scores (i. e., outcome), we use the following covariates for each student: gender, race, birth month, birthday, birth year, free lunch given or not, rural or not, and teacher ID. We remove students with missing outcomes or covariates, which yields a randomized samples of 4,139 students: 1,774 students assigned to treatment (i. e., small class, $T = 1$) and 2,365 students assigned to control (i. e., regular class, $T = 0$).

AIDS Clinical Trial Group (ACTG) study 175: The AIDS Clinical Trial Group (ACTG) study 175 is a clinical trial with the goal of comparing four treatments randomly to 2,139 subjects with human immunodeficiency virus type 1 (HIV-1), whose CD4 counts were 200–500 cells/mm³ (Hammer et al., 1996). The trial compared zidovudine (ZDV) monotherapy, the didanosine (ddI) monotherapy, the ZDV combined with ddI, and the ZDV combined with zalcitabine (ZAL). The ACTG study was used in Hatt et al. (2021) for learning policies that generalize to the target population. Even though this is a different problem, the study is particularly suited for evaluating our method since HIV-positive females tend to be underrepresented in clinical trials, which makes these studies not representative of the target population (i. e., the HIV-positive population) (Gandhi et al., 2005; Greenblatt, 2011).

The outcome Y is defined as the difference between the cluster of differentiation 4 (CD4) cell counts at the beginning of the study and the CD4 counts after 20 ± 5 weeks. The average treatment effects on the male and female subgroups are -8.97 and -1.39 , respectively (Hatt et al., 2021), which suggests a large discrepancy in the treatment effects between both subgroups. We consider two treatment arms: one treatment arm for both zidovudine (ZDV) and zalcitabine (ZAL) ($T = 1$) vs. one treatment arm for ZDV only ($T = 0$). In total, we consider 1,056 patients and 12 covariates. There are 5 continuous covariates: age (year), weight (kg, coded as wtkg), CD4 count (cells/mm³) at baseline, Karnofsky score (scale of 0–100, coded as karnof), CD8 count (mm³) at baseline. They are centered and scaled before further analysis. In addition, there are 7 binary variables: gender (1 = male, 0 = female), homosexual activity (homo, 1 = yes, 0 = no), race (1 = nonwhite, 0 = white), history of intravenous drug use (drug, 1 = yes, 0 = no), symptomatic status (symptom, 1 = symptomatic, 0 = asymptomatic), antiretroviral history (str2, 1 = experienced, 0 = naive) and hemophilia (hemo, 1 = yes, 0 = no).

The National Supported Work: The National Supported Work (NSW) Demonstration was a transitional, subsidized work experience program that operated for 4 years at 15 locations throughout the United States. The program first provided trainees with work in a sheltered training environment and then assisted them in finding regular jobs. From April 1975 to August 1977, the NSW program operated in 10 locations as a randomized experiment with some program applicants being randomly assigned to a control group that was not allowed to participate in the program. The randomized sample includes 6616 treatment and control observations for which data were gathered through a retrospective baseline interview and four follow-up interviews. These interviews cover the two years prior to random assignment and up to 36 months thereafter.

For our experiments, we consider one randomized dataset from [LaLonde \(1986\)](#)²³. Following [Smith and Todd \(2005\)](#), we combine randomized samples of 465 subjects (297 treated, 425 control) with the 2,490 PSID controls to create an observational dataset. The dataset consists of 297 treatment group (i. e., $T = 1$) observations and 2,915 control group (i. e., $T = 0$) observations. The presence of the experimental subgroup allows us to estimate the “ground truth” treatment effect (see explanation below). The study includes 8 covariates: age, level of education, ethnicity (split into two covariates), marital status, and educational degree.

Appendix I. Discussion of the Baseline in [Kallus et al. \(2018\)](#)

In this section, we discuss the poor performance of the baselines based on [Kallus et al. \(2018\)](#) in Section 7. For this, we briefly summarize the method proposed by ([Kallus et al., 2018](#)). First, a function \hat{f} is estimated using the observational data, i. e., $\{(x_i^{\text{Conf}}, t_i^{\text{Conf}}, y_i^{\text{Conf}})\}_{i=1}^{n^{\text{Conf}}}$. For the propensity score $e^{\text{Unc}}(x) = \mathbb{P}(T = 1 | X^{\text{Unc}} = x)$, let $q(x_i^{\text{Unc}}) = \frac{t_i^{\text{Unc}}}{e^{\text{Unc}}(x_i^{\text{Unc}})} - \frac{1-t_i^{\text{Unc}}}{1-e^{\text{Unc}}(x_i^{\text{Unc}})}$ be a signed re-weighting function. Then, we use this re-weighting function to estimate the following:

$$\hat{\theta} = \arg \min_{\theta \in \mathbb{R}^d} \frac{1}{n^{\text{Unc}}} \sum_{i=1}^{n^{\text{Unc}}} \left(q(x_i^{\text{Unc}}) y_i^{\text{Unc}} - f(x_i^{\text{Unc}}) - \theta^\top x_i^{\text{Unc}} \right)^2. \quad (237)$$

Finally, the proposed estimator for the CATE is given by

$$\hat{\tau}(x) = f(x) + \hat{\theta}^\top x. \quad (238)$$

The re-weighting is justified, since $\mathbb{E}[q(X^{\text{Unc}})Y^{\text{Unc}} | X^{\text{Unc}}] = \tau(X^{\text{Unc}})$ (see Lemma 1 in [Kallus et al. \(2018\)](#)). Learning a biased function and then the difference is common in transfer learning, where it is called “offset approach” (eg, [Wang et al., 2014](#)). Moreover, in order to extrapolate and learn from few randomized samples, [Kallus et al. \(2018\)](#) assume that the bias is linear in the covariates (hence, the linear regression in the second step yielding $\hat{\theta}$). This linearity for extrapolation has been used before for extrapolating survival functions from clinical trials using external data (e. g., [Jackson et al., 2017](#)).

As discussed in Remark 15, the poor performance of these baselines originates from the re-weighting of the outcomes, which is well-known to yield high-variance estimates. This is particularly pronounced in a setting with small sample size. We can see this by increasing n^{Unc} , which we did in Figure 11. In this case, the performance of the three baselines improves. However, it remains inferior to the naïve approach τ_{Unc} , which improves as well by increasing n^{Unc} . In addition, the three baselines remain inferior to our method in any setting.

In order to show that the poor performance originates from re-weighting with the inverse propensity score, we propose two modifications for these methods: (1) using the estimated propensity score instead of the true one and (2) targeting the outcomes rather than the CATE directly.

23. The study by [LaLonde \(1986\)](#) is a widely used dataset in the causal inference literature and is also known as the “Jobs” dataset (e. g., [Shalit et al., 2017](#); [Hatt and Feuerriegel, 2021a](#))

For (1), it has been observed that it is often more beneficial to use an estimated propensity score for re-weighting than the true propensity score (Kennedy, 2016). Based on this observation, we estimate the propensity score using a logistic regression and, then, re-weight the outcome identically to the algorithm in Kallus et al. (2018). For (2), in order to avoid re-weighting, we target the outcome functions directly, rather than targeting the CATE as in Kallus et al. (2018). In particular, we fit a function, $\hat{f}(x, t)$, on the confounded data $\{(x_i^{\text{Conf}}, y_i^{\text{Conf}}, t_i^{\text{Conf}})\}_{i=1}^{n^{\text{Conf}}}$, i. e.,

$$\hat{f} = \arg \min_f \frac{1}{n^{\text{Conf}}} \sum_{i=1}^{n^{\text{Conf}}} \left(y_i^{\text{Conf}} - f(x_i^{\text{Conf}}, t_i^{\text{Conf}}) \right)^2. \quad (239)$$

Then, in the second step, similar to Kallus et al. (2018), we remove the confounding bias assuming that it is linear. However, we remove it from the outcome function directly instead of the CATE, i. e., for $n_1^{\text{Unc}} = |\{i \in \{1, \dots, n^{\text{Unc}}\} : t_i^{\text{Unc}} = 1\}|$ and $n_0^{\text{Unc}} = |\{i \in \{1, \dots, n^{\text{Unc}}\} : t_i^{\text{Unc}} = 0\}|$,

$$\hat{\theta}_1 = \arg \min_{\theta_1} \frac{1}{n_1^{\text{Unc}}} \sum_{i=1}^{n_1^{\text{Unc}}} \left(y_i^{\text{Unc}} - f(x_i^{\text{Unc}}, 1) - \theta_1^\top x_i^{\text{Unc}} \right)^2, \quad (240)$$

and

$$\hat{\theta}_0 = \arg \min_{\theta_0} \frac{1}{n_0^{\text{Unc}}} \sum_{i=1}^{n_0^{\text{Unc}}} \left(y_i^{\text{Unc}} - f(x_i^{\text{Unc}}, 0) - \theta_0^\top x_i^{\text{Unc}} \right)^2, \quad (241)$$

where θ_1 and θ_0 are the linear regression vectors for each of the outcomes. The CATE is then estimated by $\hat{\tau}(x) = \hat{f}(x, 1) - \hat{\theta}_1^\top x - (\hat{f}(x, 0) - \hat{\theta}_0^\top x) = \hat{f}(x, 1) - \hat{f}(x, 0) + (\hat{\theta}_0 - \hat{\theta}_1)^\top x$.

In Table 5, we present the results for these two modifications to the original method proposed in Kallus et al. (2018). We observe that both modifications improves the performance by a substantial margin. First, using the estimated propensity score (2-step ridge^{prop}, 2-step RF^{prop}, and 2-step NN^{prop}) improves over the original methods. However, the performance remains poorly compared to the other approaches presented in Section 7. Second, removing the bias in the outcome functions directly (2-step ridge^{out}, 2-step RF^{out}, and 2-step NN^{out}), yields a much larger improvement, placing it on par with the naïve approaches, τ_{Unc} and τ_{Conf} . However, the performance remains substantially inferior to our methods.

Appendix J. Sensitivity of Ablation Study with respect to n^{Conf} and n^{Unc}

In this section, we study the sensitivity of the ablation study in Section 7.2.8 for different numbers of n^{Conf} and n^{Unc} . In the ablation study, we chose an explicit size of the observational and randomized dataset. We chose n^{Conf} to be the maximum available samples for the observational dataset after the processing described in Section 7.2.3. In particular, this yields $n^{\text{Conf}} \in \{643, 552, 482\}$ for the datasets STAR, ACTG, and NSW. Moreover, we chose $n^{\text{Unc}} = 2d$, where d is the number of covariates. We did so, since the randomized datasets is usually data-scarce. Here, we study the robustness of our results from the ablation study in Section 7.2.8 when n^{Conf} and n^{Unc} change.

Table 5: Results for the modifications of the baselines proposed in Kallus et al. (2018) on the real-world datasets STAR, ACTG, and NSW. Results are obtained via 10 runs. Lower is better.

Results: Modifications of baselines from Kallus et al. (2018)				
		$\sqrt{\epsilon_{\text{PEHE}}}$ (Mean \pm Std)		
Estimator \ Dataset	STAR	ACTG	NSW	
2-step ridge	3.01 \pm 0.01	1.51 \pm 0.01	2.82 \pm 0.02	
2-step RF	3.14 \pm 0.03	1.58 \pm 0.07	3.10 \pm 0.12	
2-step NN	3.03 \pm 0.02	1.60 \pm 0.02	2.82 \pm 0.02	
2-step ridge ^{prop}	1.97 \pm 0.01	1.59 \pm 0.01	2.77 \pm 0.03	
2-step RF ^{prop}	2.14 \pm 0.01	1.36 \pm 0.01	3.08 \pm 0.03	
2-step NN ^{prop}	1.98 \pm 0.03	1.68 \pm 0.02	2.79 \pm 0.03	
2-step ridge ^{out}	1.85 \pm 0.01	0.92 \pm 0.01	0.16 \pm 0.02	
2-step RF ^{out}	2.08 \pm 0.01	1.17 \pm 0.02	0.97 \pm 0.04	
2-step NN ^{out}	1.90 \pm 0.03	0.84 \pm 0.03	0.12 \pm 0.04	

Sensitivity in n^{Conf} : We conduct an ablation study on the different components of our method across different numbers of observational samples used, i. e., we vary n^{Conf} . In particular, we choose $n^{\text{Conf}} \in \{300, 400, 500, 600, 643\}$ for STAR, $n^{\text{Conf}} \in \{200, 300, 400, 500, 552\}$ for ACTG, and $n^{\text{Conf}} \in \{100, 200, 300, 400, 482\}$ for NSW. The results are presented in Figure 13 (top). We observe similar behavior as in the ablation study in Section 7.2.8: τ_{CorNet^+} consistently improves upon τ_{CorNet} across all numbers of observational and randomized samples for the datasets STAR and ACTG, but not on NSW. The reason for this seems to be that the bias function is not sparse on NSW.

Sensitivity in n^{Unc} : We conduct an ablation study on the different components of our method across different numbers of randomized samples used, i. e., we vary n^{Unc} . In particular, we choose $n^{\text{Unc}} \in \{1 \cdot d, 2 \cdot d, 3 \cdot d, 4 \cdot d, 6 \cdot d, 8 \cdot d\}$ for STAR, ACTG, and NSW. The results are presented in Figure 13 (bottom). We observe similar behavior as in the ablation study in Section 7.2.8: τ_{CorNet^+} consistently improves upon τ_{CorNet} across all numbers of observational and randomized samples for the datasets STAR and ACTG and the differences between the methods becomes smaller, the more randomized samples we acquire. On NSW, the results are less clear. Although τ_{CorNet} and τ_{CorNet^+} consistently achieve low error, depending on the number of randomized samples, τ_{CorNet} is superior to τ_{CorNet^+} or vice versa. We attribute this behavior to the non-sparse bias function, which leads to greater variability of the estimates.

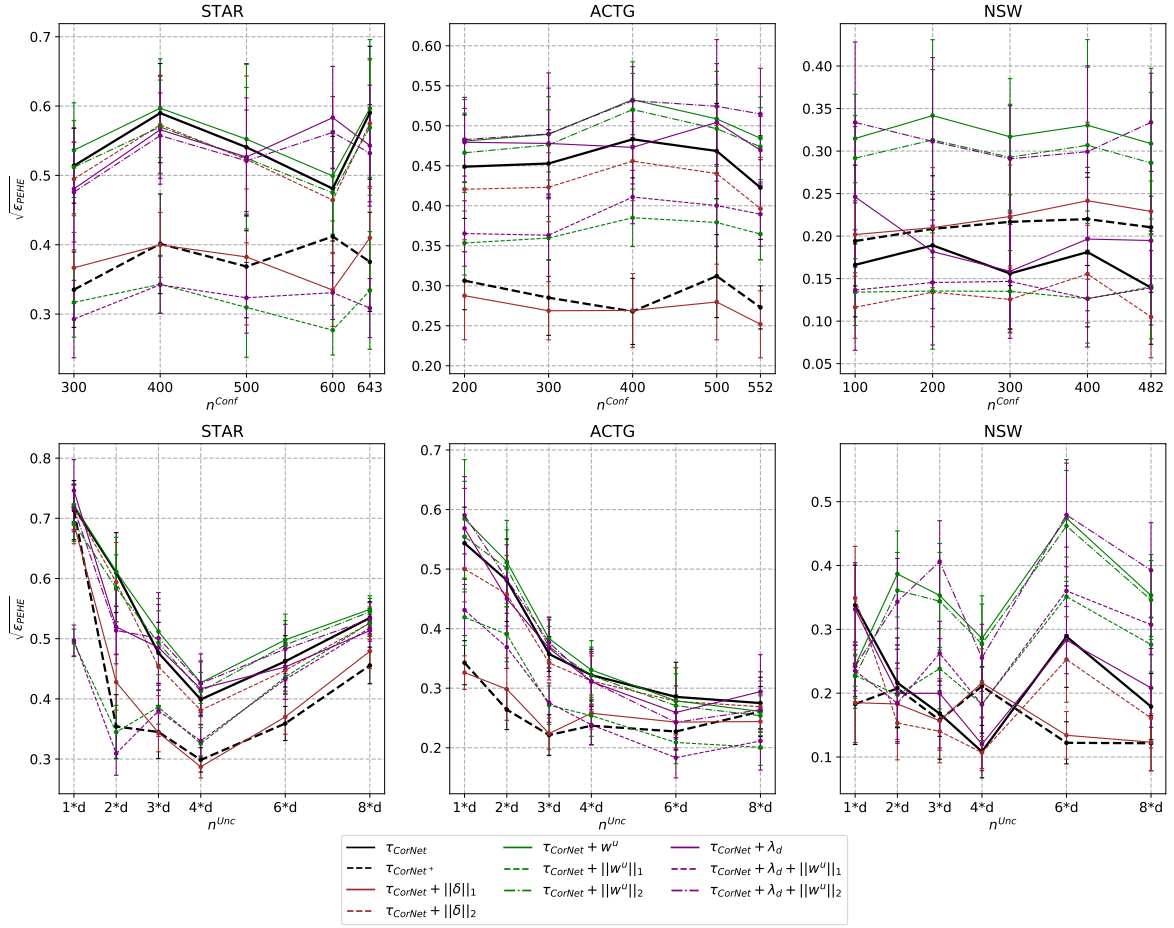


Figure 13: Sensitivity study on ablation study for different numbers of n^{Conf} (top) and n^{Unc} (bottom) across all real-world datasets STAR, ACTG, and NSW. The findings are consistent across all number of observational (i. e., n^{Conf}) and randomized samples (i. e., n^{Unc}).

Appendix K. Variants and Extensions of CorNet

In this section, we study multi-task variants of our method as follows. (i) We simply estimate the representation function, ϕ , and all four hypotheses, $\mathbf{h}^c = (h_1^c, h_0^c)$ and $\mathbf{h}^u = (h_1^u, h_0^u)$, in one step. We denote this 1-step multi-task learning (MTL) variant as τ_{MTL} . (ii) In addition this, we consider a 2-step MTL variant, which uses the representation, $\hat{\phi}$, and confounded hypotheses, $\hat{\mathbf{h}}^c$, from τ_{MTL} and, in a second step, estimate the bias function with a L_1 -regularization. This resembles our method. (iii) We also study the 2-step MTL variant that uses balancing and (iv) the 2-step MTL variant with L_1 -regularization and balancing.

The results are presented in Table 6. We observe that the multi-task learning variant, τ_{MTL} , performs inferior to our method. Notably, it yields much higher variance than our method. This is, again, due to the small sample size of randomized data, which is not controlled for, since the method is learned in one step. The 2-step multi-task learning variants, which also learn the bias function in a second step and also apply L_1 -regularization and balancing do not improve upon our methods. Similarly to the sensitivity study for n^{Conf}

and n^{Unc} in Section 7.2.7 and Appendix J, we run such a sensitivity study for the multi-task learning variants. The findings are consistent across different numbers of observational and randomized samples. The results can be found in Appendix K.1.

Table 6: Results for the multi-task learning variant study on the real-world datasets STAR, ACTG, and NSW. “2-step”, L_1 , and λ_d indicate whether a 2-step procedure, L_1 -regularization, or balancing was used. Results obtained via 10 runs. Lower is better.

Estimator					$\sqrt{\hat{\epsilon}_{\text{PEHE}}}$ (Mean \pm Std)		
		2-step	L_1	λ_d	STAR	ACTG	JOBS
τ_{MTL}	(i)	✗	✗	✗	1.27 ± 0.21	1.07 ± 0.07	0.48 ± 0.13
	(ii)	✓	✓	✗	0.59 ± 0.06	0.35 ± 0.05	0.13 ± 0.04
	(iii)	✓	✗	✓	1.21 ± 0.25	1.12 ± 0.09	0.47 ± 0.10
	(iv)	✓	✓	✓	1.16 ± 0.18	0.89 ± 0.06	0.14 ± 0.06
	(v) τ_{CorNet}	✓	✗	✗	0.59 ± 0.10	0.42 ± 0.06	0.14 ± 0.07
	(vi) τ_{CorNet^+}	✓	✓	✓	0.38 ± 0.07	0.27 ± 0.03	0.21 ± 0.08

K.1 Sensitivity of Variants and Extensions with respect to n^{Conf} and n^{Unc}

In this section, we study the sensitivity of the variant study in Appendix K for different numbers of n^{Conf} and n^{Unc} . In the variant study, we chose an explicit size of the observational and randomized dataset. We chose n^{Conf} to be the maximum available samples for the observational dataset after the processing described in Section 7.2.3. In particular, this yields $n^{\text{Conf}} \in \{643, 552, 482\}$ for the datasets STAR, ACTG, and NSW. Moreover, we chose $n^{\text{Unc}} = 2d$, where d is the number of covariates. We did so, since the randomized datasets is usually data-scarce. Here, we study the robustness of our results from the variant study in Appendix K when n^{Conf} and n^{Unc} change.

Sensitivity in n^{Conf} : We conduct an variant study on the different components of our method across different numbers of observational samples used, i. e., we vary n^{Conf} . In particular, we choose $n^{\text{Conf}} \in \{300, 400, 500, 600, 643\}$ for STAR, $n^{\text{Conf}} \in \{200, 300, 400, 500, 552\}$ for ACTG, and $n^{\text{Conf}} \in \{100, 200, 300, 400, 482\}$ for NSW. The results are presented in Figure 14 (top). We observe similar behavior as in Appendix K: τ_{MTL} consistently performs inferior to our methods across all numbers of observational and randomized samples and across all datasets. Moreover, we find that the 2-step multi-task learning variant with L_1 -regularization achieves similar performance on ACTG and NSW.

Sensitivity in n^{Unc} : We vary n^{Unc} . In particular, we choose $n^{\text{Unc}} \in \{1 \cdot d, 2 \cdot d, 3 \cdot d, 4 \cdot d, 6 \cdot d, 8 \cdot d\}$ for STAR, ACTG, and NSW. The results are presented in Figure 14 (bottom). We observe similar behavior as in Appendix K: τ_{MTL} consistently performs inferior to our methods across all numbers of observational and randomized samples and across all datasets. However, the performance of all variants converges when the number of randomized samples

increases. This is because once we exceed a certain number of randomized samples, the multi-task learning variant stops suffering from the data scarcity of the randomized samples. This behavior is less clear on NSW. Although we do not observe any benefit from the multi-task learning variant, τ_{MTL} , and its covariate balanced extensions, $\tau_{\text{MTL}} + \lambda_d$ and $\tau_{\text{MTL}} + \lambda_d + \|\delta\|_1$, we observe that the extension which re-estimates the bias function (and regularizes it) in a second step, $\tau_{\text{MTL}} + \|\delta\|_1$, seems to have some advantage in some cases, but not consistently. However, it is doubtful how reasonable it is to re-estimate the bias function, if the unconfounded hypotheses are already estimated in the first step.

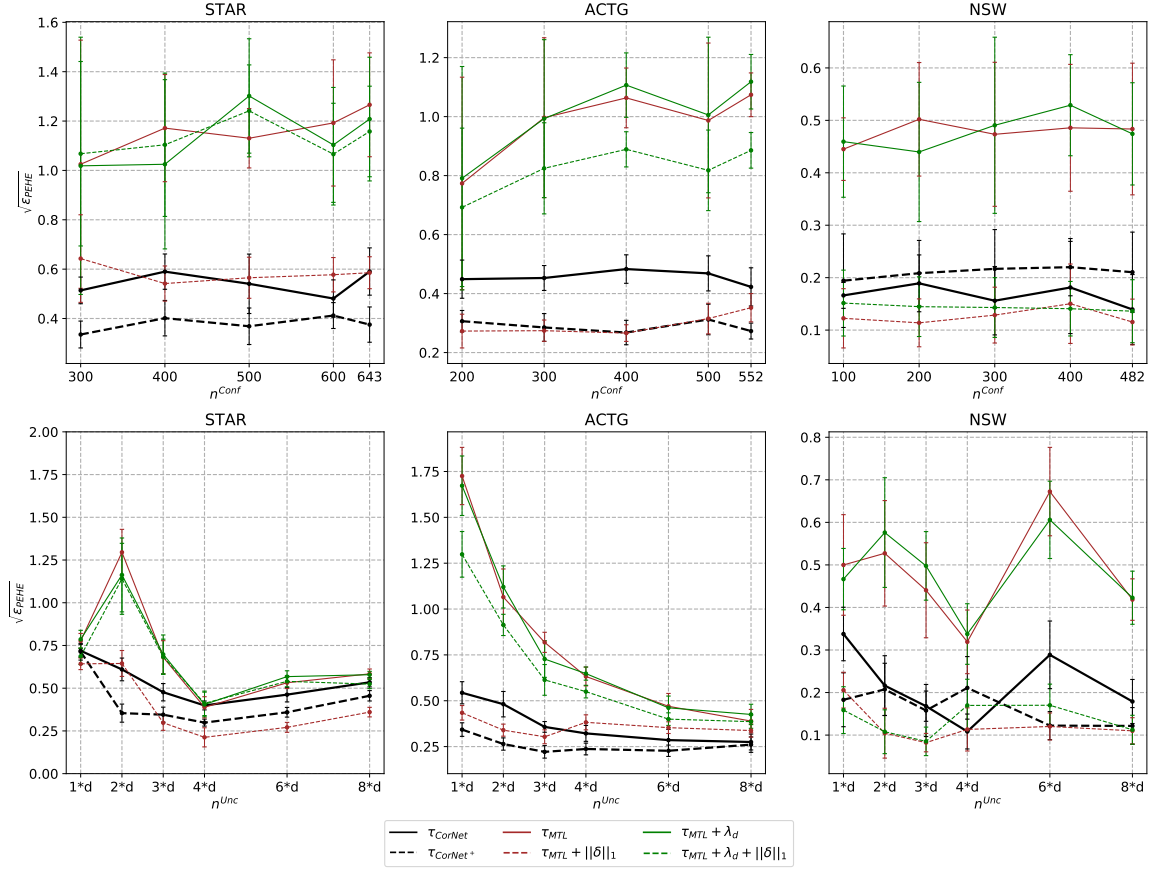


Figure 14: Sensitivity study on the variant study for different numbers of n^{Conf} (top) and n^{Unc} (bottom) across all real-world datasets STAR, ACTG, and NSW. The results are mostly consistent across the number of observational (i. e., n^{Conf}) and randomized samples (i. e., n^{Unc}). For large number of randomized samples, the error of τ_{MTL} and its extensions approach the error of our methods, τ_{Cor} and τ_{CorNet} . This is expected, since once the randomized dataset is not small anymore. While τ_{MTL} and its covariate balanced variants perform consistently inferior than our method, $\tau_{\text{MTL}} + \|\delta\|_1$ shows a slight advantage in some cases.